

***Initial Performance
Assessment to Evaluate
Technical Feasibility of
Direct Disposal of
Electrorefiner Salt Waste
in Salt Repository***

Fuel Cycle Research & Development

*Prepared for
U.S. Department of Energy
Used Fuel Disposition
Joon H. Lee
Yifeng Wang
Sandia National Laboratories
Michael Simpson
Idaho National Laboratory
August 30, 2013
FCRD-UFD-2013-000275*



DISCLAIMER

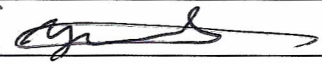
This information was prepared as an account of work sponsored by an agency of the U.S. Government. Neither the U.S. Government nor any agency thereof, nor any of their employees, makes any warranty, expressed or implied, or assumes any legal liability or responsibility for the accuracy, completeness, or usefulness, of any information, apparatus, product, or process disclosed, or represents that its use would not infringe privately owned rights. References herein to any specific commercial product, process, or service by trade name, trade mark, manufacturer, or otherwise, does not necessarily constitute or imply its endorsement, recommendation, or favoring by the U.S. Government or any agency thereof. The views and opinions of authors expressed herein do not necessarily state or reflect those of the U.S. Government or any agency thereof.

APPENDIX E FCT DOCUMENT COVER SHEET ¹

Name/Title of Deliverable/Milestone/Revision No. initial performance assessment to evaluate technical feasibility of direct disposal electrorefiner salt waste in salt repository / M3FT-135N0807084

Work Package Title and Number Natural Systems / FT-135N080708

Work Package WBS Number 1.02.08.07

Responsible Work Package Manager YIFENG WANG / 
(Name/Signature)

Date Submitted

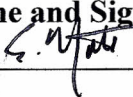
Quality Rigor Level for Deliverable/Milestone ²	<input checked="" type="checkbox"/> QRL-3	<input type="checkbox"/> QRL-2	<input type="checkbox"/> QRL-1 Nuclear Data	<input type="checkbox"/> Lab/Participant QA Program (no additional FCT QA requirements)
--	---	--------------------------------	--	---

This deliverable was prepared in accordance with Sandia National Labs
(Participant/National Laboratory Name)

QA program which meets the requirements of
 DOE Order 414.1 NQA-1-2000 Other

This Deliverable was subjected to:

- | | |
|--|--|
| <input checked="" type="checkbox"/> Technical Review | <input type="checkbox"/> Peer Review |
| Technical Review (TR) | Peer Review (PR) |
| Review Documentation Provided | Review Documentation Provided |
| <input checked="" type="checkbox"/> Signed TR Report or, | <input type="checkbox"/> Signed PR Report or, |
| <input type="checkbox"/> Signed TR Concurrence Sheet or, | <input type="checkbox"/> Signed PR Concurrence Sheet or, |
| <input type="checkbox"/> Signature of TR Reviewer(s) below | <input type="checkbox"/> Signature of PR Reviewer(s) below |

Name and Signature of Reviewers
 Edward Matteo 8/29/13

NOTE 1: Appendix E should be filled out and submitted with the deliverable. Or, if the PICS:NE system permits, completely enter all applicable information in the PICS:NE Deliverable Form. The requirement is to ensure that all applicable information is entered either in the PICS:NE system or by using the FCT Document Cover Sheet.

NOTE 2: In some cases there may be a milestone where an item is being fabricated, maintenance is being performed on a facility, or a document is being issued through a formal document control process where it specifically calls out a formal review of the document. In these cases, documentation (e.g., inspection report, maintenance request, work planning package documentation or the documented review of the issued document through the document control process) of the completion of the activity, along with the Document Cover Sheet, is sufficient to demonstrate achieving the milestone. If QRL 1, 2, or 3 is not assigned, then the Lab / Participant QA Program (no additional FCT QA requirements) box must be checked, and the work is understood to be performed and any deliverable developed in conformance with the respective National Laboratory / Participant, DOE or NNSA-approved QA Program.

THIS PAGE INTENTIONALLY LEFT BLANK

ACKNOWLEDGEMENT

Authors like to acknowledge Ernie Hardin (SNL) for his assistance in the waste package thermal calculations, and James Smith (SNL) for ORIGEN calculations for the decay heat output of electrorefiner (ER) salt wastes. The technical support by Gregory Teske (INL) is greatly appreciated. Authors would also like to express their gratitude for the technical interest and programmatic support by Mike Patterson (INL), Kevin McMahan (SNL) and Peter Swift (SNL).

THIS PAGE INTENTIONALLY LEFT BLANK

SUMMARY

As part of the study to evaluate technical feasibility of direct disposal of electrorefiner (ER) salt waste in a salt repository, an existing performance assessment (PA) model for a generic salt repository was improved substantially with the implementation of the source-term and WP configuration that are specific to the ER salt waste, and the incorporation of the latest understanding and representative geologic settings and features of generic salt disposal system processes.

For the WP configuration and salt waste loading (~120 kg salt waste per waste package (WP)) considered in the PA analysis, the per-WP decay heat output is low that no noticeable thermal perturbations were calculated for the Mark-V ER salt WPs, and moderate temperature increases (up to ~48 °C) only during first 200 years for the Mark-IV ER salt WPs. This low thermal perturbation renders no significant changes to the near-field thermal and geochemical conditions and allows use of the ambient geochemical conditions for the PA analysis. This provides the WP exposure conditions of low overpack corrosion rates, which results in a long WP lifetime, although it was not the intended design function of the WPs in salt repository. The salt waste dissolution in contact with brine, upon WP failure, is rapid; however, most of the released RNs precipitate out as incorporated in the solubility controlling solid phase under geochemically reducing conditions and are released slowly from the solid phase in the near-field over very long time periods.

The initial PA analysis shows the ER salt waste can be disposed of safely without “extensive” treatments in a bedded salt repository (a type of salt formation in this study). The contribution of the ER salt waste to the radionuclide (RN) releases to the biosphere and to the dose rate of an individual is negligibly small. The conclusion is contributed by the major attributes of salt repository: 1) very stable geology, 2) anoxic geochemically reducing condition, 3) very limited brine movement, 4) “self-healing” of salt rock by creep deformation, and 5) sorption of mobilized RNs on geologic materials.

The PA analysis also demonstrated salt repository performance is not sensitive to the waste form durability. Analyses to evaluate the effect of the durability of two ER salt waste types (raw ER salt waste with no treatments, and ER salt incorporated into a borosilicate-like glass) on the long-term repository performance in terms of the mean annual dose by radionuclides at a hypothetical biosphere showed that the dose contributions by both the ER salt waste forms are negligibly small, and there are *practically no differences* in the peak mean annual dose and mean annual dose histories between two ER salt waste types. The PA analysis demonstrated that the waste form durability *is not important* to the disposal performance of a salt repository, as its performance is driven by its key performance attributes listed above, not by the waste form durability. The analysis also demonstrates that high-level nuclear waste can be disposed of safely in a salt repository, with no or minimal treatments of the waste.

The feasibility of the direct disposal concept feasibility in a salt repository, as demonstrated by the PA analysis, is highly attractive relative to the current baseline ceramic waste form process, because of the 13-fold increase in the salt waste mass loading per a unit mass of waste form and expected dramatically reduced cost of completing the Experimental Breeder Reactor (EBR)-II spent fuel treatment project as part of the Spent Fuel Treatment Program at Idaho National Laboratory (INL).

The current study has demonstrated a great potential of utilizing a PA tools to develop guidance for high-level radioactive waste (HLW) management strategy. A great amount of resources and time has been invested to develop highly durable waste forms for the HLW in the DOE complex, and this study and its

outcome, although it is still an initial phase of the evaluation, provides an opportunity to re-consider the current baseline disposal approach, which is based on high performing and highly durable waste forms. This approach can also be applied to develop the management and disposal strategy for other HLW in the DOE complex that needs treatment for final disposal.

CONTENTS

ACKNOWLEDGEMENT	v
SUMMARY	vii
ACRONYMS	xvii
1. INTRODUCTION	1
2. OBJECTIVES.....	2
3. APPROACH.....	2
4. GENERIC SALT REPOSITORY PERFORMANCE ASSESSMENT MODEL	3
4.1 Conceptual Model for Repository Radionuclide Release and Transport.....	4
4.2 ER Salt Waste Inventory	8
4.3 Waste Package Configuration	11
4.4 Waste Package Emplacement	15
4.5 Salt Rock Creep and Waste Encapsulation	16
4.6 Waste Package Thermal Conditions	18
4.7 Waste Package Corrosion Environment.....	20
4.8 Waste Package Degradation.....	22
4.9 ER Salt Waste Dissolution	25
4.10 Brine Flows Analysis	25
4.11 Natural Barrier System Parameters	27
4.12 Radionuclide Solubility.....	28
4.13 Biosphere Model	33
4.14 Performance Assessment Model Implementation.....	35
4.14.1 Near-Field Model Implementation.....	36
4.14.2 Far-Field Model Implementation	37
5. MODEL RESULTS.....	39
5.1 Reference Case Analysis.....	41
5.1.1 Waste Package Failure	41
5.1.2 Salt Waste Form Releases	41
5.1.3 Repository Releases	44
5.1.4 Interbed Releases	45
5.1.5 Repository Shaft Releases.....	47
5.1.6 Biosphere Releases and Dose	48
5.2 Sensitivity Analysis.....	49
5.2.1 Waste Package Overpack Wall Thickness	50
5.2.2 ER Salt Waste Form Degradation	55
5.3 Disturbed Case Analysis	60
6. SUMMARY AND CONCLUSION	63

**Initial Performance Assessment to Evaluate Technical Feasibility of Direct Disposal of
Electrorefiner Salt Waste in Salt Repository**

x

8/30/2013

7.	FUTURE WORK	66
8.	REFERENCES	69

FIGURES

Figure 1. Schematic Showing the Conceptual Model for Radionuclide Release and Transport from Salt Generic Repository.	5
Figure 2. Simplified Cross Section of the Gorleben Salt Dome (Figure 36, Bornemann et al 2008).....	7
Figure 3. A Schematic Showing a Preliminary Conceptual Configuration of Waste Package for Disposal of ER Salt Waste in Salt Repository.....	12
Figure 4. Minimum Wall-thickness to Outer-Diameter Ratio as a Function of Lithostatic Pressure to Prevent Buckling Failure of Carbon Steel and Stainless Steel Overpack.....	14
Figure 5. Minimum Wall Thickness of Carbon Steel and Stainless Steel Overpack as a Function of Lithostatic Pressure to Prevent Buckling Failure of ER Salt WP and Larger WP in Salt Repository.	14
Figure 6. A Schematic Showing the ER Salt WP Emplacement Layout Implemented in the PA Analysis (adopted from Hardin et al 2012).	16
Figure 7. A Schematic Showing Alcove Emplacement of ER Salt WP and Alcove and WP Spacing Implemented in the PA Analysis (adopted from Hardin et al 2012).	16
Figure 8. In-situ Simulated Heater Test for the Thermal Simulation of Drift Emplacement (TSDE) at Asse Mine: (left) simulated canister being backfilled with crushed salt, and (right) simulated canister surrounded by consolidating salt upon excavation for post-test.....	17
Figure 9. Recent UFD Coupled Thermal-Mechanical Model Results for Salt Backfill Consolidation.....	18
Figure 10. Decay Heat Output of Mark-IV and Mark-V ER Salt Waste per MT, Compared to That of Commercial UNF and DHLW.	19
Figure 11. Decay Heat Output of (left) Mark-IV and (right) Mark-V ER Salt Waste Package (120 kg Salt Waste per WP).	19
Figure 12. Temperature Histories of Mark-IV and Mark-V ER Salt Waste Package and Emplacement Alcove Wall.....	20
Figure 13. A Conceptual Schematic Illustrating WP Corrosion Environment in Post-Closure Repository.	21
Figure 14. Long-term Brine Flow Grid Used in Analysis (Clayton et al 2011).....	26
Figure 15. Brine Flow Rate Histories from the Repository and in Underlying Interbed Used in the PA Analysis (Clayton et al 2011).	27
Figure 16. Solubility of Uranium, Plutonium, Americium, Neptunium and Thorium As a Function of Temperature in Near-Field Concentrated Brine Implemented in the PA Analysis (Wang and Lee 2010).	32

Figure 17. A Schematic Illustrating the Model Implementation Configuration of the PA Model for ER Salt Waste Direct Disposal.	36
Figure 18. Model Result of Mean Overpack Corrosion Rate (left) and Mean Overpack Corrosion Depth (right) as a Function of Time for Mark-IV and Mark-V ER Salt Waste Packages.	42
Figure 19. Model Result of Overpack Corrosion Rate (left) and Overpack Corrosion Depth (right) as a Function of Time for Mark-IV and Mark-V ER Salt Waste Package for Realization 82.	42
Figure 20. Model Result of Major RNs in Salt Waste of Mark-IV ER Salt WP: Mean RN Masses (left), and RN Masses for Realization 88 (right).	43
Figure 21. Model Result of Mean ER Salt Dissolution and Mean RN Precipitate Masses in Mark-IV ER Salt WP.	43
Figure 22. Model Result of ER Salt Waste Dissolution and RN Precipitate Masses in Mark-IV ER Salt WP: Realization 88 for LiCl dissolution control (left) and Realization 82 for no LiCl dissolution control (right).	44
Figure 23. Model Result of Mean Mass Flux of RNs from Repository.	45
Figure 24. Model Result of Mean Mass Flux of RNs from Interbed at the Repository Footprint.	46
Figure 25. Model Result of Mean Mass Flux of RNs from Interbed at 1,000 m from the Repository Footprint.	46
Figure 26. Model Result of Mean Mass Flux of RNs from Bottom Third Section of Repository Access Shaft.	47
Figure 27. Model Result of Mean Mass Flux of RNs from Top of Repository Access Shaft.	48
Figure 28. Model result of Mean Mass Flux of RNs from the Overlying Aquifer to the Hypothetical Biosphere Located at the Repository Site Boundary.	49
Figure 29. Model Result of Mean Annual Dose at the Hypothetical Biosphere Located at the Repository Site Boundary.	49
Figure 30. Sensitivity Analysis for Thinner WP Overpack: Model Result of Mean Overpack Corrosion Rate (left) and Mean Overpack Corrosion Depth (right) as a Function of Time for Mark-IV and Mark-V ER Salt Waste Packages.	50
Figure 31. Sensitivity Analysis for Thinner WP Overpack: Model Result of Overpack Corrosion Rate (left) and Overpack Corrosion Depth (right) as a Function of Time for Mark-IV and Mark-V ER Salt Waste Packages for Realization 82.	50
Figure 32. Sensitivity Analysis for Thinner WP Overpack: Model Result of Mean ER Salt Dissolution and Mean RN Precipitate Masses in Mark-IV ER Salt WP.	51
Figure 33. Sensitivity Analysis for Thinner WP Overpack: Model Result of ER Salt Waste Dissolution and RN Precipitate Masses in Mark-IV ER Salt WP: Realization 88	

for LiCl-dissolution control (left) and Realization 82 for no LiCl-dissolution Control (right). 52

Figure 34. Sensitivity Analysis for Thinner WP Overpack: Model Result of Mean Mass Flux of RNs from Repository: Mean total mass flux (top), Mean diffusive mass flux (bottom left), and Mean advective mass flux (bottom right)..... 53

Figure 35. Sensitivity Analysis for Thinner WP Overpack: Model Result of RN Mass Flux in Interbed: Mean total mass flux at the repository boundary (left), and at 1,000 m from repository boundary (right)..... 54

Figure 36. Sensitivity Analysis for Thinner WP Overpack: Model Result of RN Mass Flux in Repository Access Shaft: Mean total mass flux from the bottom a third section (left), and at the shaft top (right)..... 54

Figure 37. Sensitivity Analysis for Thinner WP Overpack: Mean total RN mass flux from overlying aquifer to hypothetical biosphere (left), and Mean annual dose by RNs (right). 55

Figure 38. Sensitivity Analysis for Assumed ER Salt Waste Glass: Model Result of Mean ER Salt Waste Glass Degradation in Mark-IV ER Salt WP..... 56

Figure 39. Sensitivity Analysis for Assumed ER Salt Waste Glass: Model Result of ER Salt Waste Glass Degradation in Mark-IV ER Salt WP: Realization 74 for the lowest degradation rate (left) and Realization 82 for the highest degradation rate (right)..... 57

Figure 40. Sensitivity Analysis for Assumed ER Salt Waste Glass: Model Result of Mean Mass Flux of RNs from Repository: Mean total mass flux (top), Mean diffusive mass flux (bottom left), and Mean advective mass flux (bottom right)..... 58

Figure 41. Sensitivity Analysis for Assumed ER Salt Waste Glass: Model Result of RN Mass Flux in Interbed: Mean total mass flux at the repository boundary (left), and at 1,000 m from repository boundary (right)..... 59

Figure 42. Sensitivity Analysis for Assumed ER Salt Waste Glass: Model Result of RN Mass Flux in Repository Access Shaft: Mean total mass flux from the bottom a third section (left), and at the shaft top (right)..... 59

Figure 43. Sensitivity Analysis for Assumed ER Salt Waste Glass: Mean total RN mass flux from overlying aquifer to hypothetical biosphere (left), and Mean annual dose by RNs (right)..... 60

Figure 44. Human Intrusion Case Model Result of Mean Mass Flux of RNs from the Overlying Aquifer to the Hypothetical Biosphere Located at the Repository Site Boundary..... 62

Figure 45. Human Intrusion Case Model Result of Mean Annual Dose at the Hypothetical Biosphere Located at the Repository Site Boundary..... 62

Figure 46. Comparison of the Effect of Durability of Two ER Salt Waste Types (Raw Salt without Treatment vs. Borosilicate-Like Salt Waste Glass) on Disposal Performance of a Generic Salt Repository in Terms of Mean Annual Dose by Radionuclides at Hypothetical Biosphere..... 65

THIS PAGE INTENTIONALLY LEFT BLANK

TABLES

Table 1. Current Estimated Electrorefiner Salt Composition (mass fractions).....	9
Table 2. Isotopic Inventory for Mark-IV and Mark-V ER Salt Waste Used in the Source-Term Model.....	10
Table 3. Mechanical Properties of Carbon Steel and Stainless Steel Overpack Used in the Minimum Overpack Wall Thickness Analysis.....	13
Table 4. WP Overpack General Corrosion Rate Model and Data Summary.....	23
Table 5. Natural Barrier System Parameters and Their Values Implemented in the PA Analysis.....	28
Table 6. Elemental Solubility of Radionuclides in Near-Field Brine as a Function of Temperature Implemented in the PA analysis.....	30
Table 7. Elemental Solubility of Radionuclides in Far-Field Dilute Brine Implemented in the PA analysis.....	31
Table 8. IAEA ERB 1A Parameters Implemented in the Biosphere Model.....	34
Table 9. Model Parameters for the Near-Field and Interface Block Region Implemented in the PA Analysis.....	37
Table 10. Far-Field Model Parameters for Radionuclide Transport in the Interbed and Repository Access Shaft Implemented in the PA Analysis.....	38
Table 11. Far-Field Model Parameters for Radionuclide Transport in Overlying Carbonate Aquifer.....	40

THIS PAGE INTENTIONALLY LEFT BLANK

ACRONYMS

BRAGFLO	Brine And Gas FLOW
CFR	Code of Federal Regulations
CS	Carbon Steel
DHLW	Defense High-Level (radioactive) Waste
DOE	U.S. Department of Energy
EBR	Experimental Breeder Reactor
EDZ	Excavation Damage Zone
ER	Electrorefiner
ERB	Example Reference Biosphere
FCF	Fuel Conditioning Facility
FY	Fiscal Year
GPa	Gigapascals
HLW	High-Level (radioactive) Waste
IAEA	International Atomic Energy Agency
INL	Idaho National Laboratory
MFC	Materials and Fuels Complex
MPa	Megapascals
MT	Metric Ton
NBS	Natural Barrier System
NUTS	NUclide Transport System
OD	Outer (or Outside) Diameter
PA	Performance Assessment
PWR	Pressurized Water Reactor
RN	Radionuclide
SNL	Sandia National Laboratories
SRP	Salt Repository Project
SS	Stainless Steel

THM	Thermal-Mechanical-Hydrological
TSDE	Thermal Simulation of Drift Emplacement
TSPA	Total System Performance Assessment
UFD	Used Fuel Disposition
UNF	Used Nuclear Fuel
WIPP	Waste Isolation Pilot Plant
WP	Waste Package

INITIAL PERFORMANCE ASSESSMENT TO EVALUATE TECHNICAL FEASIBILITY OF DIRECT DISPOSAL OF ELECTROREFINER SALT WASTE IN SALT REPOSITORY

1. INTRODUCTION

The United States is now re-assessing its nuclear waste disposal policy and also re-evaluating the option of moving away from the current once-through open fuel cycle to a closed fuel cycle. This policy shift creates a unique opportunity for exploring new concepts and ideas that can potentially lead to the development of transformational technologies for an efficient and clean nuclear fuel cycle.

Electrochemical processing (aka “pyroprocessing”) of used nuclear fuel has been considered as a promising technology and is currently being developed and evaluated for potential commercial implementation by several nations. It is considered to have great promise for being applied to managing used nuclear fuel waste and potentially recycling actinides for use in either thermal or fast neutron spectrum reactors. This technology has advantages over aqueous processes. It involves fewer processing steps and is potentially much less expensive than aqueous processing. For this technology to succeed, the path forward for safe disposition of the resulting salt waste must be developed.

A salt repository is one of the four geologic media currently under study by the U.S. DOE Office of Nuclear Energy to support development of a long-term strategy for geologic disposal of commercial used nuclear fuel (UNF) and defense high-level radioactive waste (DHLW). A concept of direct disposal of ER salt waste in a salt repository was first proposed (Wang et al 2011a), and studies have been underway to explore the feasibility of the new proposed disposal concept with no or minimal treatment to the salt waste (Wang et al 2011b, Wang et al 2012). The concept is based on the consideration that brines in a salt repository are already saturated with salt minerals and that ER salt as a waste form would be stable in such environments.

The durability of a waste form is a relative concept and should be evaluated in the context of relevant disposal environments. In this sense, ER salt itself may be an ideal waste form for disposal in a salt repository. Previous calculations for the saturation indexes of a brine from the Waste Isolation Pilot Plant (WIPP) with respect to various salt minerals showed that the brine is at or close to equilibrium with both major and minor minerals in the formation, including halite (NaCl), sylvite (KCl), glaserite [NaK₃(SO₄)₂], anhydrite (CaSO₄), and calcite (CaCO₃) (Wang et al 2012). Typical ER salt waste contains approximately 50% of NaCl and KCl in the mass fractions, with the rest being mostly LiCl (~40 wt.%) and metal chlorides (see Section 4.2). If the rest of salt components are embedded as isolated inclusions in the matrix of NaCl and KCl, the ER salt waste will be highly durable and even thermodynamically stable in a salt repository environment.

Because the direct disposal concept does not require immobilization of the salt waste into a waste form matrix, it has several advantages over the baseline waste treatment for ER salt waste such as currently proposed glass-bonded sodalite waste form (Simpson and Law, 2010). Two major advantages are significantly reduced waste volume and greatly simplified processing processes.

Based on the composition of used fuel from Experimental Breeder Reactor-II (EBR-II) (Simpson and Law, 2010), it has been estimated that direct disposal can reduce waste volume by at least 10 fold as compared with the baseline approach. Increasing the salt waste content in the glass-bonded sodalite is

possible, but the increased chloride content reduces the waste form durability (Simpson and Law, 2010). In direct disposal, however, high chloride concentrations in the ER salt would not pose any problem. Because of the much simplified processing steps for direct disposal, the disposal concept can potentially eliminate the need for all of the complex process steps currently proposed for waste separation and treatment. Since the waste treatment processes should be done remotely in a hot cell, these benefits will result in substantially reduced waste treatment processing cost and time. In addition, because of its plastic creep deformation behavior, the ER salt as a waste form possesses a self-healing capability with regard to any mechanical or radiation damages. More detailed discussions of the proposed concept are provided in the previous reports (Wang et al 2011b; Wang et al 2012).

This report documents the approach, methodology and initial results of the quantitative analyses recently conducted to evaluate the technical feasibility of the direct disposal concept of the ER waste in a salt repository. The current initial analyses utilized the performance assessment (PA) model for a generic salt repository developed for the Used Fuel Disposition (UFD) Campaign (Lee et al 2011, Lee et al 2012, Lee et al 2013).

As the ER salt contains higher fissile material content, the criticality potential during storage, transportation and disposal is another important technical issue that needs to be evaluated. Note that the current analysis did not consider the criticality issue, and it will be evaluated in the next iteration of the feasibility analysis planned in Fiscal Year 2014 (FY 14).

2. OBJECTIVES

Evaluation of the proposed concept of direct disposal of ER salt in a salt repository was initiated in FY 10. In FY 11 and FY 12, work was focused on the experimental studies to evaluate the direct disposal concept feasibility, including laboratory studies of salt waste dissolution behavior in simulated salt repository brines (Wang et al 2011b, Wang et al 2012).

The main objectives of the FY13 study are 1) to conduct quantitative assessment for the feasibility of the ER salt waste direct disposal concept in a salt repository, and 2) to develop and provide the technical basis for the direct disposal concept. Another objective of the current work is to demonstrate application of the PA methodology to aiding in the development and guidance of the treatment and disposal strategy of high-level radioactive waste (HLW) in the DOE complex that needs treatment for permanent disposal. In addition, successful completion of the disposal concept feasibility analysis will provide the basis to demonstrate the integration of the fast reactor technology, the ER fuel treatment process, and the salt repository into a coherent and efficient fuel cycle.

3. APPROACH

The performance assessment (PA) methodology was used 1) to conduct quantitative assessment for the feasibility of the ER salt waste direct disposal concept in a salt repository, and 2) to develop the technical basis for the direct disposal concept. The analysis assumes the ER salt waste is disposed of in a salt repository that is developed for disposal of the primary HLW, that is, commercial UNF and DOE DHLW. This year's initial analysis treats the ER salt waste independent of the primary wastes in the repository. Associated repository parameters such as repository footprint were adjusted accordingly to be consistent with the current approach. Impacts of the presence of the primary heat-generating HLW (commercial UNF and defense HLW) is planned to be included in the FY 14 analysis.

This year's analyses conducted a series of PA calculations to evaluate the disposal concept technical feasibility, and help evaluate, if any, what characteristics of a salt repository could limit the ability to directly dispose of it. The PA calculations were performed using the PA model for a generic salt

repository developed for the UFD campaign (Lee et al 2011, 2012 and 2013). The PA model was improved and updated to include the models and parameters that are specific to the ER salt waste and has incorporated the latest understanding in the processes and models related to the generic salt disposal system.

For the feasibility analysis, Idaho National Laboratory (INL) developed the ER salt waste source-term information, including as the salt waste form characteristics and composition, radioisotope inventory in the waste, disposal WP design and configuration, etc.

A series of sensitivity analyses were performed (and some are undergoing at the time of report writing) to evaluate impact of a range of important repository and disposal parameters on the disposal concept feasibility. The parameters included in this year's initial analysis are rather limited, and those include repository radionuclide (RN) release and transport scenarios, waste package (WP) wall thickness, and surrogate waste form performance. More extensive sensitivity analyses are planned in the FY 14 work scope, and the planned candidate parameters include:

- RN release and transport scenarios
- Salt waste loading in the WP
- WP design (including materials, wall thickness and internal configuration for criticality)
- Near-field environment conditions (temperature, brine flows, geochemistry, etc.)
- Effect of waste form performance
 - Glass-bonded sodalite glass-ceramic waste form (baseline waste form)
 - Tellurite ($\text{TeO}_2 + \text{PbO}$) glass waste form (alternative waste form)
- Transport process parameters (sorption, diffusion, advection, etc.)

The disposal concept feasibility was evaluated in terms of the following repository performance matrix: 1) RN release rate (mass flux) at various subsystem boundaries and 2) dose rate at a "hypothetical" biosphere that is assumed to be located at the repository site boundary. The repository subsystem boundaries include the WP/near-field, repository footprint, far-field boundary and "hypothetical" biosphere.

The following caveats are noted for the current PA model, which are not modeled explicitly in this year's analysis and will be addressed in the future analysis:

- Representation of the coupled thermal-mechanical-hydrological (TMH) processes in the near-field conditions for the ER waste PA.
- Representation of the effect of the above coupled processes on waste package corrosion, corrosion gas pressure buildup, salt creep behavior and brine flows in the repository.
- RN sorption on WP corrosion products in the near-field in contact with concentrated brines at elevated temperatures. The current PA model assumes conservatively no sorption on the corrosion products in the waste emplacement area.

4. GENERIC SALT REPOSITORY PERFORMANCE ASSESSMENT MODEL

A salt repository is one of the four geologic media currently under study to support development of a long-term strategy for geologic disposal of commercial UNF and DHLW. Among many attributes of salt formation, the prominent ones include very stable geology, very limited water movement, geochemically

reducing conditions, and fracture healing and waste encapsulation by creep plastic deformation of salt rock under lithostatic pressure. The immediate goal of the generic salt repository study is to develop the necessary modeling tools to evaluate and improve the understanding of the generic disposal system response and processes relevant to long-term disposal of commercial UNF and DHLW in a salt formation. The PA model for the salt generic disposal system was developed to aid in the study, and the details of the model development and analysis have been documents in the project reports (Wang and Lee 2010, Clayton et al 2011, Vaughn et al 2012) and recent publications (Lee et al 2011, Lee et al 2012, Lee et al 2013).

This section discusses the PA model for a generic salt repository that was used to evaluate the technical feasibility of the direct disposal concept of ER salt waste in salt repository. The section also includes the technical basis of the subsystem component models that were implemented in the PA model. As described below, the PA model is an improved version of the version reported in Vaughn et al (2012) and has incorporated the latest understanding of the processes and parameters that are important to the long-term behavior of a generic salt repository. The current version also has implemented the source-term model that is specific to the ER salt waste. The improvements in the current PA model were made by incorporating the analysis in the recent study on the salt disposal of heat generating HLW (Sevougian et al 2012), and implementing representative geologic settings and features adopted from previous studies for salt repository sites; these sites include the Salt Repository Project (SRP) site in Deaf Smith County in Texas (DOE 1988), Project Salt Vault in a mine near Lyons, Kansas (Bradshaw and McClain 1971), the Waste Isolation Pilot Plant (WIPP) near Carlsbad, New Mexico (Helton et al 1988), and the Gorleben domal salt site in Germany (Bornemann et al 2008, Bräuer et al 2011, Klinge et al 2007, Köthe et al 2007). These studies were utilized to update and reinforce the processes and parameters of subsystem components, and to improve the conceptual model and scenarios for radionuclide release and transport in a generic salt repository.

4.1 Conceptual Model for Repository Radionuclide Release and Transport

This section discusses the conceptual model for the processes and behavior of a generic salt repository that have been implemented in the current PA model. Figure 1 shows a schematic of the geologic setting and the conceptual description for radionuclide release and transport in a generic salt repository. The current conceptual model assumes that repository is located in a bedded salt formation in a saturated, chemically reducing environment. The waste package is assumed to be placed horizontally in an emplacement alcove and backfilled with crushed salt.

Although the salt repository disposal concept generally does not rely on a long-term containment capability of WP, the WP should meet the following design functions: 1) complete containment of the waste and sufficient shielding for the workers for handling and operations during pre-closure period, and 2) mechanical strength to withstand the lithostatic pressure at the depth of repository. In addition, regulations may require the waste retrievability for a period of time after repository closure. Meeting these functions would require a thick-wall overpack for the WP, and the current analysis assumes the WP employs a thick walled overpack made of carbon steel (see Section 4.3 for discussions of WP configuration).

The current analysis assumes that the ER salt WPs are emplaced in the alcoves on the edge of the repository footprint, and the assumption is to purposely avoid issues related to potential impacts of primary heat-generating HLW (commercial UNF and DHLW) in this year's analysis. As discussed above, the potential impact will be included in the FY 14 analysis. The current analysis also assumes that a repository access shaft exists near the area where ER salt WPs are emplaced, and as discussed below,

the access shaft is one of the transport pathways of RNs in the repository. The access shaft is assumed to be 5 m in diameter, which is consistent with other UFD analysis (Hardin et al 2012).

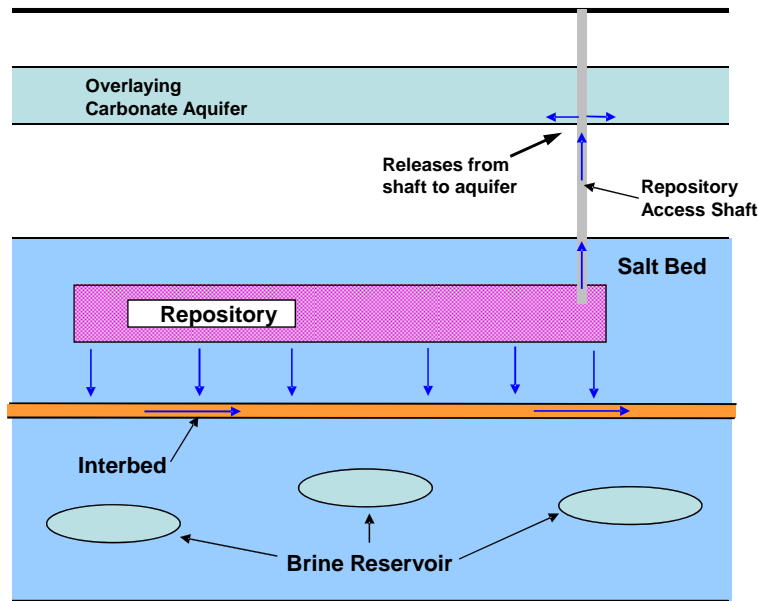


Figure 1. Schematic Showing the Conceptual Model for Radionuclide Release and Transport from Salt Generic Repository.

Over a period of time following the WP emplacement, the space of the disposal alcove would be slowly closed by salt backfill reconsolidation and plastic deformation of the salt rock undergoing creep inward toward the waste emplacement area, both under lithostatic pressure at the repository depth. This would result in close contact of the WP with the salt backfill undergoing reconsolidation, exerting the lithostatic pressure on the WP surface. The creep closure process would result in encapsulation of the WP by salt rock (see Section 4.5 for discussions of salt creep closure).

It is assumed that a horizontal interbed with a significant thickness of relatively more permeable anhydrite exists below the repository, and runs in parallel with the repository horizon to extended distances in all horizontal directions (i.e., the length- and width-wise directions). Horizontally running interbeds are a common geologic feature found in a bedded salt formation (Helton et al 1988). A carbonate aquifer of a significant thickness with extended distances in all horizontal directions is assumed to exist above the repository. Impermeable formations with sufficient thicknesses are assumed to exist below the aquifer separating the aquifer and the repository salt formation and protecting the salt formation from the intrusion of the fresh groundwater in the aquifer.

In the post-closure repository, the waste decay heat would perturb the near field environments (i.e., thermal, hydrological, geochemical and mechanical conditions) from the ambient conditions. It would heat near-field brines (present in small quantities in salt rock formation as pore brine and inclusion brine) to elevated temperatures, and if the thermal loading is high enough, could boil the brines, driving the water away from the waste disposal area and leaving behind salt minerals in the pore space. This would create a dry-out zone around the waste disposal area, and its duration and extent would depend mostly on the waste heat output characteristics, repository thermal loading, release and migration behaviors of inclusion and pore brines, and thermal characteristics of the salt rock. The thermal perturbation and

moisture movement could enhance creep deformation of salt rock and reconsolidation of salt backfill (Jove-Colon et al 2012), therefore could accelerate closure of remaining open space of the waste disposal area (Hansen and Leigh 2011). As the temperature decreases following the peak, brines could start moving toward and into the waste disposal area driven by higher (i.e., near lithostatic) pore pressure in the far field.

Corrosion of the WP and other potential engineered component materials in the disposal area could be enhanced by contact with concentrated brines at elevated temperatures. Another concern is hydrogen gas generated as a result of the corrosion under anoxic and chemically reducing conditions. Hydrogen gas overpressure would build up in the confined space between the WP surface and salt rock undergoing creep deformation and exerting the lithostatic pressure on the WP, and the overpressure could reach near the lithostatic pressure (Clayton et al 2011). The corrosion products forming on the WP surface would be compacted under the lithostatic pressure and continue to build up to a thicker corrosion product layer as corrosion proceeds. As the corrosion products grow thicker, corrosion rates, especially general corrosion rates, would be lowered because the compacted corrosion product layer would act as a barrier to the transport of reacting and product species into and away from the corroding surface of WP. The corrosion attack mode and rate of WP would depend on the package material and environmental conditions including brine chemistry (especially chloride and magnesium concentrations and pH), temperature, hydrogen gas overpressure, stress from the pressure exerted on the WP surface by salt rock undergoing creep, corrosion products buildup, etc.

The corrosion of the WP and other engineered components would consume residual oxygen in the repository and help maintain anoxic conditions in the repository. Anoxic corrosion in geochemically reducing conditions would also consume brines that come in contact with the WP surface as the water reduction would be the major cathodic reaction to support the corrosion (anodic reaction). This would result in the precipitation of dissolved salts of brine in the pores of compact corrosion product layer, reducing the pore space in the corrosion products, which would further lower corrosion rates of the WP by restricting transport of reacting and product species through the corrosion product layer.

The current analysis assume WPs fail mechanically under the lithostatic pressure when WP has corroded to a threshold remaining wall thickness, which, among many factors, would depend primarily on the external (i.e., lithostatic) pressure, WP material properties, uniformity of remaining wall thickness undergoing corrosion, presence of defects, etc. (see Section 4.3 for more discussion). When the waste package fails, corrosion of the waste form canister, waste form, and waste package internal structure materials would occur in addition to the continuing corrosion of remaining waste package materials, which could result in generation of additional hydrogen gases. Combined actions of the corrosion gas generation and decreasing confined space in the disposal area by salt backfill reconsolidation and salt rock creep deformation would result in pressurization in the disposal area; this could significantly affect brine movements and transport of dissolved radionuclides into and away from the disposal areas, under balancing interactions with the pore pressure in the surrounding salt rock (Clayton et al 2012).

The reference case scenario of RN release and transport of the current PA model considers that RNs are released from the repository by a sequence of processes that could occur in a generic salt repository, and the reference case assumes that the repository drift and shaft seals and the underlying interbed are the primary pathways for radionuclide release and transport from the repository. The access shaft seals would include layers of crushed salts and non-salt materials (such as concrete, asphalt, clay, lining materials, etc.). Those non-salt seal materials may prevent complete reconsolidation of the salt seal layer, and the layers of non-salt seal materials would remain more porous than the surrounding intact salt rock formation. Mobilized RNs would be transported upward by pressurized brines in the access shaft as the

brines are pushed away from the repository from the pressurization by the combined effects of corrosion gas generation and salt reconsolidation and creep closure reducing the space in the repository.

Although the movement of brines in the transport pathways is likely very small, the pathway conceptual models are supported by previous analyses for salt repository sites: the interbed release pathway conceptual model is supported by the performance analyses of certain scenarios for the WIPP site (Helton et al 1988), and the drift and shaft seals release pathway conceptual model is consistent with the analyses for certain scenarios of the WIPP (Helton et al 1988) and Gorleben domal salt sites (Buhmann et al 2009, Rübél et al 2009).

While the interbed release pathway conceptual model may be applicable to a repository situated in a bedded salt formation, different conceptual models may be considered for brine flow and radionuclide transport pathways for a repository in a domal salt formation such as the Gorleben repository site (Buhmann et al 2009, Rübél et al 2009). A cross-section of the domal salt Gorleben site with the proposed repository location is shown in Figure 2. The transport pathway conceptual models developed for the domal salt repository include: 1) vertical upward movement of brine toward the overlying aquifer driven by pressurization from the corrosion gas buildup and the reduction in the confined space as a result of salt rock creep deformation; and 2) lateral movement of brine caused by brine exchange driven by the brine density gradient in adjacent salt rock volumes, which could be enhanced by the variations in local heating by the waste decay heat (Buhmann et al 2009, Rübél et al 2009).

The current analysis assumes the radionuclides released from WP are transported to a nearby repository access shaft (assume 5 m in diameter) and to the underlying interbed. The radionuclides are transported upward in the access shaft, released to overlying aquifer from the shaft and transported advectively to a hypothetical biosphere located at the site boundary (5 km down-gradient from the repository footprint). The radionuclides released to underlying interbed remain in the interbed, as there is no hydrogeological feature for brine flow from the interbed to biosphere; the diffusive mass flux from the interbed upward to the overlying aquifer through intact salt rock and other overburden formations would be negligible. The reference case release pathway conceptual models will be improved and updated as the study progresses and additional understanding is gained.

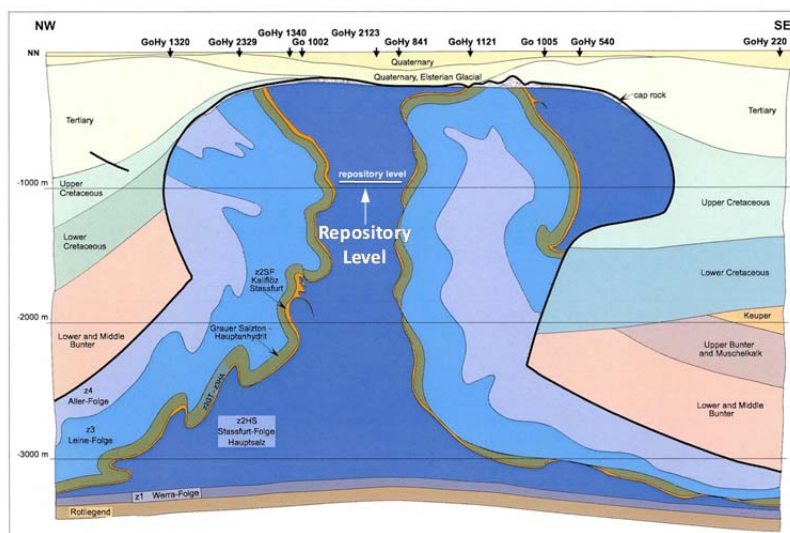


Figure 2. Simplified Cross Section of the Gorleben Salt Dome (Figure 36, Bornemann et al 2008).

4.2 ER Salt Waste Inventory

Electrochemical processing of used nuclear fuel involves operation of one or more cells containing molten salt electrolyte. This process is currently being used at Idaho National Laboratory (INL) to treat used fuel from Experimental Breeder Reactor-II (EBR-II) for final disposal. This operation is being performed in the Fuel Conditioning Facility (FCF) at INL's Materials and Fuels Complex (MFC). Two electrorefiners (ERs) are operating in FCF, each containing a large inventory of molten chloride salt (primarily LiCl-KCl at or near the eutectic composition at $\sim 500^{\circ}\text{C}$) that is used as the electrolyte for electrorefining. The Mark-IV ER is used to process the driver fuel containing highly enriched uranium and low concentration of plutonium, and the Mark-V ER is used to treat the blanket fuel containing depleted uranium and a relatively high concentration of plutonium for breeding. Molten LiCl-KCl salt used for ER has high solubility for metal chlorides as well as high electrical conductivity and stability over a broad range of electrochemical potentials.

In the electrochemical processing, metallic used fuel (or reduced oxide fuel) is loaded into anode baskets of the ER and lowered into a vessel containing molten chloride salt. When electric current is passed, the uranium, transuranic elements, and "active" metal fission products become oxidized and dissolved in the molten salt. Pure uranium is simultaneously recovered at the primary cathode where it deposits as metal. A mixture of uranium and transuranic elements can be periodically recovered from the molten salt using a secondary cathode (Simpson and Law, 2010; Inoue and Koch, 2008).

The ER processing of the fuel results in contamination of the salt via accumulation of fission products and transuranic elements. Active metal species from the spent fuel are converted to chlorides and partition into the salt phase during each electrorefining run, and the contaminated salt contains NaCl (from sodium-bonded fuel), UCl_3 , and numerous fission product and transuranic chlorides. Upon reaching contamination limits, the salt must be removed and either disposed or treated to remove the contaminants and recycled back to the process.

As a result of processing approximately 4.7 metric tons (heavy metal) of EBR-II fuel, the salt electrolyte has become contaminated with fission products and mixed actinides. By the end of operations, it is estimated that the mass of Mark-IV salt waste will be 1,017 kg, and the mass of Mark-V salt waste will be 699 kg. The current estimated salt composition in each ER is given in Table 1. As shown in the table, LiCl-KCl combined makes up about 70 wt.% of the Mark-IV ER salt waste and about 85 wt.% of Mark-V ER salt waste; NaCl is about 10 wt.% and 6 wt.% respectively of the Mark-IV and Mark-V ER salt waste. The three major salt phase, LiCl-KCl-NaCl combined makes up about 80 wt.% of the Mark-IV ER salt, and about 91 wt.% of the Mark-V ER salt. Note that the plutonium contents in the ER salt waste (i.e., about 3 wt.% PuCl_3 in the Mark-IV ER salt and about 6 wt.% PuCl_3 in the Mark-V ER salt) are much higher than commercial UNF and DHLW, which may present technical issues associated with the packaging and other design considerations to mitigate the nuclear criticality issues during storage, transportation and repository disposal. The current PA analysis did not consider the criticality issues in the conceptual WP design and other disposal configurations; the issue will be considered in the next year's analysis (see Section 4.3).

Table 2 lists the isotopic inventory for the radionuclides of the Mark-IV and Mark-V ER salt wastes included in the source-term model. Note the fractional mass of the isotopes listed in the fractional mass column of each ER waste does not add up to one because it lists only those included in the source-term model that are important to the repository performance. Two most abundant isotopes of the both ER salt wastes are Cl-35 and K-39, and their fractional mass inventories are 58 % and 20 % respectively in the Mark-IV ER salt and 61 % and 24 % respectively in the Mark-V ER salt. These isotopes are not listed in the table because they are non-radioactive and are not of interest to the repository performance. Although

it is not radioactive, the source-term model includes Li-7 because dissolution of LiCl is used as the marker for the ER salt waste dissolution in the PA analysis (see Section 4.9 for additional discussions).

Table 1. Current Estimated Electrorefiner Salt Composition (mass fractions).

Salt Compound	Mark-IV ER Salt	Mark-V ER Salt
LiCl	3.181E-01	3.877E-01
KCl	3.881E-01	4.609E-01
NaCl	9.818E-02	5.787E-02
RbCl	1.666E-03	5.898E-05
SrCl ₂	4.983E-03	1.952E-04
YCl ₃	3.505E-03	1.621E-04
CsCl	1.235E-02	6.908E-04
BaCl ₂	7.199E-03	5.254E-04
LaCl ₃	8.517E-03	3.574E-04
CeCl ₃	1.622E-02	6.468E-04
PrCl ₃	8.015E-03	2.936E-04
NdCl ₃	2.730E-02	1.071E-03
PmCl ₃	5.723E-04	2.194E-05
SmCl ₃	5.196E-03	2.865E-04
EuCl ₃	2.418E-04	1.488E-05
GdCl ₃	1.620E-04	1.660E-05
NpCl ₃	1.414E-03	7.278E-05
UCl ₃	6.849E-02	3.163E-02
PuCl ₃	2.982E-02	5.750E-02
AmCl ₃	1.035E-05	1.299E-05

Pu-239 is the most abundant plutonium isotope of the both salt wastes, and its fractional mass inventory is 2 % in the Mark-IV ER salt and 3.9 % in the Mark-V ER salt. As discussed above, the high contents of Pu-239 require further considerations in the storage, transportation and disposal packaging to mitigate potential nuclear criticality issues. The ER salt wastes do not include some noble metal and fission product isotopes that are commonly present in the commercial UNF and DHLW. These are C-14, Nb-93 (Zr-93 decay daughter), Pb-210, Pd-107, Sb-126, Se-79, Sn-126, Tc-99 and Zr-93, and listed in the table as zero inventories. In the ER processing, the isotopes are retained in the anode baskets with the cladding hulls and are incorporated into a separate metallic waste form, which is disposed of as a high-level waste.

Table 2. Isotopic Inventory for Mark-IV and Mark-V ER Salt Waste Used in the Source-Term Model.

Isotope	Half Life (yr)	Mark-IV ER Salt		Mark-V ER Salt	
		Fractional Mass	Isotope mass per WP (g/WP)	Fractional Mass	Isotope mass per WP (g/WP)
²²⁷ Ac	2.18E+01	9.452E-13	1.1342E-07	1.534E-10	1.8410E-05
²⁴¹ Am	4.32E+02	7.138E-06	8.5652E-01	8.983E-06	1.0780E+00
²⁴³ Am	7.37E+03	3.956E-09	4.7477E-04	4.000E-09	4.7999E-04
¹⁴ C	5.71E+03	0.000E+00	0.0000E+00	0.000E+00	0.0000E+00
³⁶ Cl	3.01E+05	8.486E-09	1.0183E-03	1.560E-14	1.8720E-09
²⁴⁵ Cm	8.50E+03	2.331E-12	2.7971E-07	3.107E-10	3.7290E-05
¹³⁵ Cs	2.30E+06	3.448E-03	4.1372E+02	2.055E-04	2.4658E+01
¹³⁷ Cs	3.01E+01	2.847E-03	3.4159E+02	1.478E-04	1.7731E+01
¹²⁹ I	1.70E+07	6.968E-04	8.3621E+01	3.023E-05	3.6275E+00
⁷ Li	N/A	5.187E-02	6.2239E+03	6.349E-02	7.6183E+03
⁹³ Nb	1.36E+01	0.000E+00	0.0000E+00	0.000E+00	0.0000E+00
²³⁷ Np	2.14E+06	9.717E-04	1.1661E+02	5.021E-05	6.0248E+00
²³¹ Pa	3.25E+04	7.259E-09	8.7112E-04	3.306E-10	3.9668E-05
²¹⁰ Pb	2.26E+01	0.000E+00	0.0000E+00	0.000E+00	0.0000E+00
¹⁰⁷ Pd	6.50E+06	0.000E+00	0.0000E+00	0.000E+00	0.0000E+00
²³⁸ Pu	8.77E+01	5.739E-05	6.8872E+00	1.116E-05	1.3389E+00
²³⁹ Pu	2.41E+04	1.993E-02	2.3915E+03	3.900E-02	4.6803E+03
²⁴⁰ Pu	6.54E+03	5.490E-04	6.5876E+01	7.508E-04	9.0096E+01
²⁴¹ Pu	1.44E+01	5.506E-06	6.6073E-01	9.372E-06	1.1246E+00
²⁴² Pu	3.76E+05	2.390E-07	2.8681E-02	1.093E-07	1.3118E-02
²²⁶ Ra	1.60E+03	3.967E-12	4.7609E-07	2.695E-10	3.2335E-05
²²⁸ Ra	6.70E+00	1.907E-18	2.2886E-13	1.821E-10	2.1853E-05
¹²⁶ Sb	3.61E-05	0.000E+00	0.0000E+00	0.000E+00	0.0000E+00
⁷⁹ Se	6.50E+04	0.000E+00	0.0000E+00	0.000E+00	0.0000E+00
¹²⁶ Sn	1.00E+05	0.000E+00	0.0000E+00	0.000E+00	0.0000E+00
⁹⁰ Sr	2.91E+01	1.613E-03	1.9354E+02	6.373E-05	7.6478E+00
⁹⁹ Tc	2.13E+05	0.000E+00	0.0000E+00	0.000E+00	0.0000E+00
²²⁹ Th	7.90E+03	1.965E-11	2.3583E-06	2.370E-10	2.8438E-05
²³⁰ Th	7.54E+03	1.380E-07	1.6560E-02	1.012E-09	1.2143E-04
²³² Th	1.41E+10	8.727E-09	1.0472E-03	3.431E-10	4.1173E-05
²³² U	6.89E+01	6.324E-10	7.5882E-05	1.591E-12	1.9093E-07
²³³ U	1.59E+05	6.550E-09	7.8598E-04	1.358E-10	1.6294E-05
²³⁴ U	2.45E+05	5.601E-06	6.7216E-01	1.133E-07	1.3602E-02

Isotope	Half Life (yr)	Mark-IV ER Salt		Mark-V ER Salt	
		Fractional Mass	Isotope mass per WP (g/WP)	Fractional Mass	Isotope mass per WP (g/WP)
²³⁵ U	7.04E+08	9.262E-03	1.1114E+03	5.343E-05	6.4117E+00
²³⁶ U	2.34E+07	9.491E-04	1.1389E+02	1.704E-06	2.0444E-01
²³⁸ U	4.46E+09	3.686E-02	4.4229E+03	2.179E-02	2.6151E+03
⁹³ Zr	1.53E+06	0.000E+00	0.0000E+00	0.000E+00	0.0000E+00

Note the fractional mass of the isotopes listed in the column does not add up to one because it lists only those included in the source-term model.

4.3 Waste Package Configuration

The waste package configuration considered in this FY feasibility analysis is preliminary in nature and was developed for use in the current PA analysis. The preliminary configuration does not consider all the technical issues that could be important to the safe disposal in a salt repository, such as the potential for criticality in the disposal environment. Additional design analysis is required for improved packaging design to fully support the feasibility analysis, and is planned for the next FY work scope.

In general the salt disposal concept does not rely heavily on robust WP performance, but a reasonable wall thickness and mechanical strength is required for the WP to meet the design functions of 1) handling and shielding to the workers during pre-closure operations, and 2) mechanical strength to withstand the lithostatic pressure on the WP (exerted by salt rock undergoing creep deformation) during pre-closure operations and an early time period (10 to 50 years, see Section 4.5) of the post-closure to prevent premature failure of WP. The lithostatic pressure in a salt repository can be about 15 MPa at a depth of 600 m and about 20 MPa at 800 m. Figure 3 shows a schematic of the preliminary conceptual configuration of waste package for ER salt waste disposal in salt repository. Contaminated molten ER salt is poured directly into and solidified in small cylindrical thin-walled stainless steel (SS) containers. Each container is 25 cm in diameter and 50.5 cm in length, and holds about 40 kg ER salt waste. Three containers are stacked up in a thin-walled cylindrical SS disposal canister with the dimension of 27 cm outer diameter (OD) and 155 cm length. Each canister holds about 120 kg ER salt waste. The canister is inserted in a prefabricated thick-walled cylindrical overpack, and the remaining end is sealed by welding a thick-walled lid of the same overpack material to the overpack cylinder.

As discussed in Section 4.2, the estimated total mass of Mark-IV ER salt waste is 1,017 kg, and the total mass of Mark-V ER salt waste is 699 kg. As each WP holds 120 kg of ER salt waste in the current configuration, nine WPs are needed for the Mark-IV ER salt waste, and six WPs for the Mark-V ER salt waste. A total of 15 ER salt WPs will be disposed in a salt repository based on the current inventory estimate.

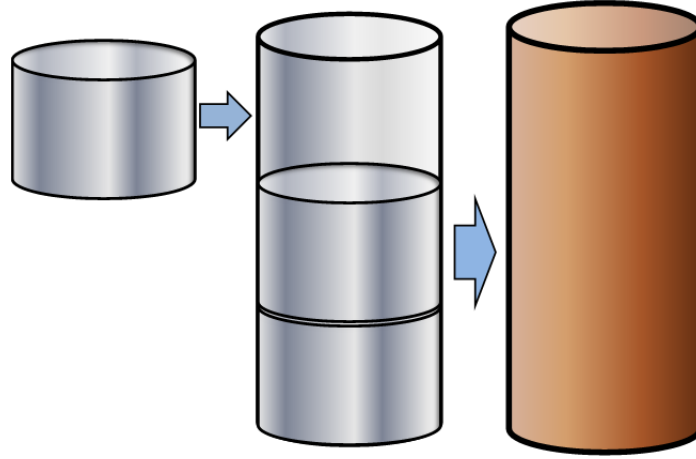


Figure 3. A Schematic Showing a Preliminary Conceptual Configuration of Waste Package for Disposal of ER Salt Waste in Salt Repository.

As part of the ER salt WP configuration analysis, an initial bounding analysis was conducted to estimate the minimum wall thickness of the WP overpack to prevent buckling failure under lithostatic pressure in a salt repository. A simple analytical solution for the critical pressure to cause buckling failure of a cylindrical pipe under external pressure (Yeh and Kyriakides 1986; Fraldi and Guarracino 2011) was used for the analysis. The equation is expressed as

$$P_{CB} = \frac{2E}{(1 - \nu^2)} \left(\frac{t_w}{D_o} \right)^3 \quad (1)$$

where P_{CB} is the critical buckling pressure, E is Young's modulus of elasticity of the pipe material, t_w is the pipe wall thickness, D_o is the outside diameter (OD) of pipe, and ν is Poisson's ratio of the pipe material. The equation applies to a pipe having a set of ideal conditions such as perfect geometry of the pipe, uniform wall thickness (i.e., no wall thickness variations), no preexisting imperfections in the pipe, and uniform external pressure on the pipe. The actual critical buckling pressure can be significantly lower than the calculated value for a pipe having wall thickness or geometry variations (Yeh and Kyriakides 1986; Sakakibara et al 2008; Netto et al 2007; Netto 2009) or for a pipe that has imperfections or damages caused by corrosion (Kara et al 2010; Gong et al 2013). Therefore a thicker pipe wall than the calculated value may be required for real service conditions.

By rearranging the terms in Equation (1), an expression is obtained to calculate the minimum (wall) thickness to (outer) diameter ratio (R_{min}) of the WP overpack that is required to prevent buckling failure, as a function of the external pressure (P_{ext}).

$$\left(\frac{t_w}{D_o} \right)_{min} = R_{min} = \left[P_{ext} \cdot \left(\frac{1 - \nu^2}{2 \cdot E} \right) \right]^{\frac{1}{3}} \quad (2)$$

The thickness to diameter ratio of the overpack should be greater than the calculated minimum ratio to prevent buckling failure for a given external pressure. Substituting the lithostatic pressure for the external

pressure in Equation (2), the minimum thickness to diameter ratio of the overpack with the above-mentioned ideal conditions (i.e., perfect geometry, uniform wall thickness, no preexisting imperfections, and uniform external pressure) can be calculated for a given lithostatic pressure of a salt repository. As $D_o = D_i + 2 \cdot t_w$, where D_i is the inner diameter of overpack, the minimum overpack wall thickness ($t_{w,min}$) of the overpack with the ideal conditions for a given repository lithostatic pressure is estimated from the calculated minimum thickness to diameter ratio as follows.

$$R_{min} = \frac{t_{w,min}}{D_i + 2 \cdot t_{w,min}} \quad (3)$$

$$t_{w,min} = \frac{R_{min} \cdot D_i}{1 - 2 \cdot R_{min}} \quad (4)$$

For the current initial bounding analysis, the above equations were used for the analysis of the WP overpack material and wall thickness for the ER salt waste in a salt repository, and two common engineering structural materials, carbon steel and stainless steel were examined for a comparative analysis. The mechanical properties of the materials used in the analysis are listed in Table 3. Figure 4 shows the minimum wall-thickness to outer-diameter ratio to prevent buckling failure of carbon steel and stainless steel overpack as a function of lithostatic pressure (or external pressure). The calculated minimum ratios for the stainless steel overpack are slightly greater than the carbon steel overpack for the lithostatic pressure range considered in the bounding analysis. The analysis shows that at a given lithostatic pressure, the stainless steel overpack requires a slightly thicker minimum wall thickness than the carbon steel for the same overpack outer diameter.

Table 3. Mechanical Properties of Carbon Steel and Stainless Steel Overpack Used in the Minimum Overpack Wall Thickness Analysis.

	Carbon Steel Overpack	Stainless Steel Overpack
Yield Stress (MPa)	250	205
Young's Modulus (GPa)	210	190
Poisson's Ratio	0.33	0.33

The calculated minimum wall thickness of the carbon steel and stainless steel overpack for the ER salt WP is shown in Figure 5. For the analysis the outer diameter of the disposal canister (27 cm as discussed above) was taken as the inner diameter of the overpack, ignoring a likely small gap between the disposal canister and overpack. Also included in the figure for a comparison purpose is the minimum overpack wall thickness for a larger-diameter WP that may be considered for commercial UNF and DHLW, for which the overpack inner diameter of 150 cm was assumed. For a range of lithostatic pressure of 15 MPa (at about 600 m depth) to 20 MPa (at about 800 m depth) that is likely for a salt repository, the minimum overpack wall thickness for the ER salt WP is about 1 cm for both carbon steel and stainless steel. For the larger WP, the minimum overpack wall thickness for the above lithostatic pressure range is 5.1 cm to 5.6 cm for carbon steel and 5.3 cm to 5.8 cm for stainless steel.

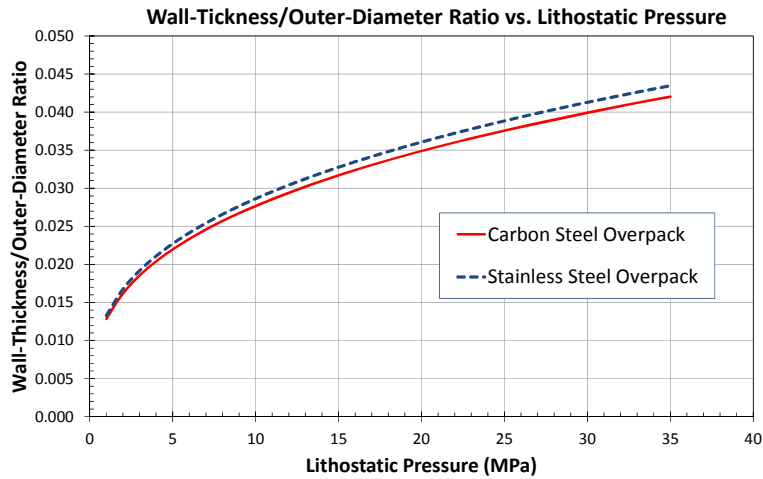
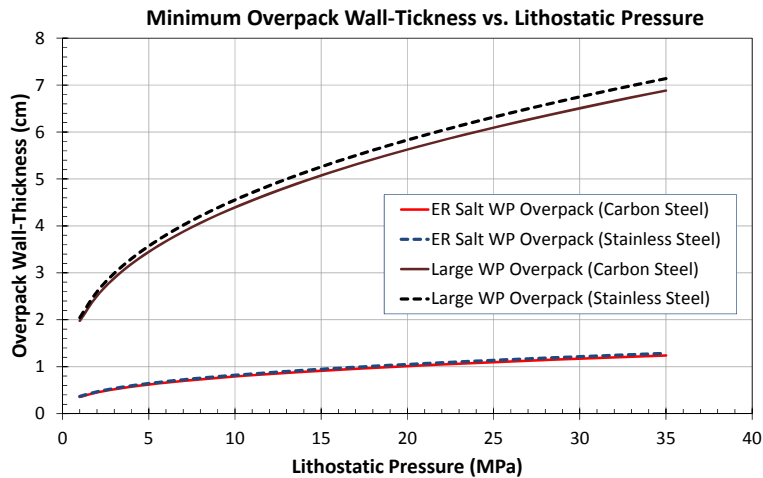


Figure 4. Minimum Wall-thickness to Outer-Diameter Ratio as a Function of Lithostatic Pressure to Prevent Buckling Failure of Carbon Steel and Stainless Steel Overpack.



(Inner diameter of overpack used in the analysis: 27 cm for ER salt WP and 150 cm for larger WP)

Figure 5. Minimum Wall Thickness of Carbon Steel and Stainless Steel Overpack as a Function of Lithostatic Pressure to Prevent Buckling Failure of ER Salt WP and Larger WP in Salt Repository.

The above estimated minimum wall thicknesses are likely conservative as the analysis does not take into account potential structural support by the overpack end caps and the disposal canister inside the overpack. While that is true, the actual required minimum wall thickness to prevent buckling failure could be greater than the estimates, because the bounding analysis does not take into consideration probably greater impacts of corrosion damage of the overpack. The irregularities in the geometry and wall thickness of the overpack from corrosion damage and resulting uneven external pressure distributions on the overpack could have a significant impact on the critical buckling pressure and required minimum wall thickness for a likely range of salt repository lithostatic pressures (Yeh and Kyriakides 1986; Sakakibara et al 2008; Netto et al 2007; Netto 2009; Kara et al 2010; Gong et al 2013).

As discussed above, the simple analytical equation used in the bounding analysis applies to a pipe with assumed ideal conditions of perfect geometry, uniform wall thickness, no imperfections and uniform external pressure on the pipe. In addition, the residual stress on the closure welds of overpack could lower the critical buckling pressure of overpack, therefore requiring a thicker minimum wall thickness.

Considering the factors and uncertainties discussed above, the PA analysis assumes a minimum wall thickness of 3 cm for the overpack for buckling failure of the WP under a likely range of salt repository lithostatic pressures, which has 2 cm thickness added, as a safety margin factor, to the minimum thickness estimate. The PA analysis assumes the ER salt WPs fail by mechanical collapse when the overpack is corroded to the remaining thickness of 3 cm.

The PA analysis also assumes carbon steel as the overpack material for the following reasons: 1) both carbon steel and stainless steel perform similarly in terms of providing structural stability for a likely range of repository lithostatic pressures, 2) carbon steel is much cheaper than stainless steel, and 3) carbon steel has a better predictable corrosion behavior than stainless steel for the salt repository exposure conditions (i.e., anoxic chemically reducing conditions, contact with concentrated brines at elevated temperatures, and stressed under repository lithostatic pressure; see Section 4.7). For such exposure conditions, stainless steel can be subject to different forms of localized corrosion attacks (i.e., pitting corrosion, crevice corrosion and stress corrosion cracking) that are highly uncertain in the prediction of their initiation and propagation.

The PA analysis has adopted the initial wall thickness of 7.5 cm for the carbon steel overpack that was recommended in a recent study (Sevougian et al 2012), and this gives a corrosion degradation layer of 4.5 cm for the overpack prior to the WP mechanical failure. Based on the published carbon steel general corrosion rates that are relevant to the salt repository exposure conditions (see Section 4.8), the 4.5 cm overpack corrosion degradation layer would give a long WP performance duration, although it is not the intended primary performance function for the WP configuration and design. With the carbon steel overpack, the dimension of the ER salt WP is 42 cm in the outer diameter and 170 cm in the length.

As noted above, the current bounding analysis for the critical buckling pressure and minimum wall thickness for the WP overpack is preliminary in nature and more detailed elaborate analysis is required to update the bounding analysis.

4.4 Waste Package Emplacement

The ER salt WP emplacement layout in a salt repository has been adopted from the latest UFD study on the repository thermal loading analysis (Hardin et al 2012). The current PA analysis assumes that the ER salt WPs are emplaced on the edge of the repository footprint, and the assumption was made in the current analysis to mitigate the issues related to potential impacts of other heat-generating HLW (commercial UNF and DHLW) near the ER salt WPs. The potential impact of the presence of other heat-generating HLW in the repository could include the ER salt WP temperature, overpack corrosion, near-field RN solubility, near-field brine movement, etc., and the effect will be evaluated in the next FY analysis.

Figure 6 shows a schematic that shows the layout of the ER salt WP emplacement on the edge of the footprint of a salt repository, as was implemented in the PA analysis. In the PA model nine Mark-IV ER salt WPs are placed along one side of the alcove access drift, and six Mark-V ER salt WPs along other side of the access drift.

As described in the latest UFD study (Hardin et al 2012), the PA model assumes a single ER salt WP is emplaced in an alcove and backfilled immediately with crushed salt (Figure 7). The PA model assumes

the WP to WP spacing (WP center to WP center) of 20 m and the alcove spacing of 20 m, as recommended by the UFD study (Hardin et al 2012).

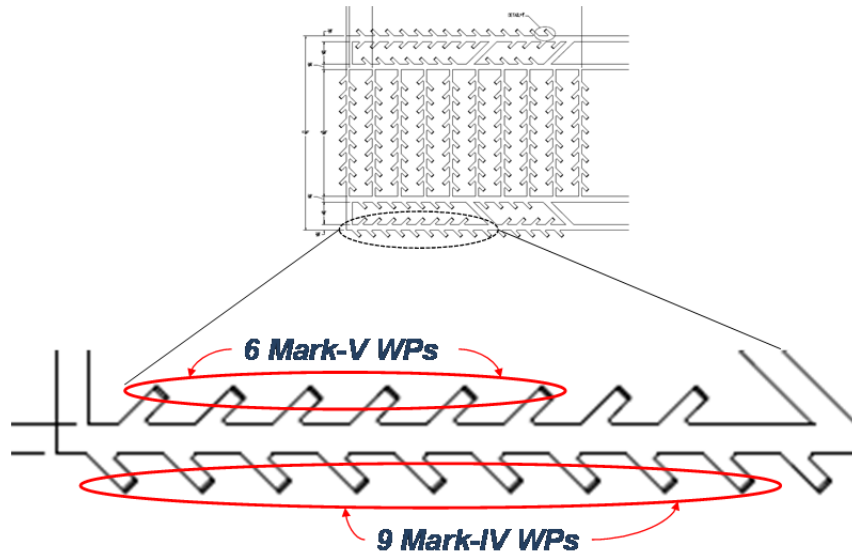
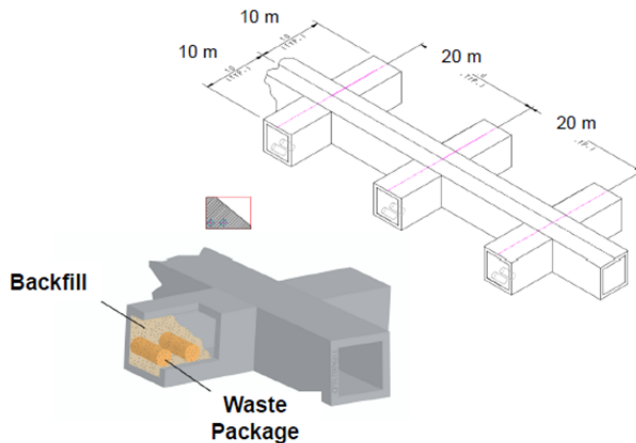


Figure 6. A Schematic Showing the ER Salt WP Emplacement Layout Implemented in the PA Analysis (adopted from Hardin et al 2012).



Note: The sketch depicting the alcove emplacement shows two WPs. It was created for a different alcove emplacement scheme and should be viewed as having one WP emplaced in the alcove as is the case implemented in the PA analysis.

Figure 7. A Schematic Showing Alcove Emplacement of ER Salt WP and Alcove and WP Spacing Implemented in the PA Analysis (adopted from Hardin et al 2012).

4.5 Salt Rock Creep and Waste Encapsulation

One of the major attributes of a salt repository is creep plastic deformation of salt rock driven by the lithostatic pressure at the repository depth, promoting “self-healing” of fractures and other damages to salt rock that could occur during the repository construction and operations and that could also incur from

thermal mechanical stresses during the early periods of post-closure repository. The inward creep deformation toward the waste emplacement area would apply the lithostatic pressure on the crushed salt backfill, resulting in reconsolidation and compaction of the salt backfill particles and gradual closure of the space in the disposal alcove. The process would result in close contact of the waste package surface with the consolidating salt backfill, resulting in the exertion of the lithostatic pressure on the WP surface. The creep process will consolidate the salt backfill to the condition of intact salt rock and ultimately result in encapsulation of the waste package by salt rock.

The most notable demonstration of the salt creep deformation and consolidation relevant to disposal of heat-generating waste was done by an in-situ simulated heater test performed in a domal salt site for the Thermal Simulation of Drift Emplacement (TSDE) at Asse Mine, Germany (Rothfuchs et al 2004). Figure 8 shows the reconsolidation of crushed salt backfill around a simulated waste canister after a 10-year testing period. The test was conducted at the 800-m level of the Asse Mine site from 1990 to 2000. The left picture shows the simulated canister being backfilled with crushed salt, and the right picture shows significant compaction of the backfill and enclosure of the simulated canister enclosed by consolidating salt after the 10 year testing period (Rothfuchs et al 2004). The canister surface temperature was peaked at about 210 °C following the test initiation, then slowly decreased to about 165 °C during the rest of the test period. The in-situ field test demonstrated significant consolidation and compaction of crushed salt around the simulated waste canister over a relatively short time period for the test conditions.

Figure 9 shows recent coupled thermal-mechanical process model results for consolidation and compaction of crushed salt backfill, using, as the heat source, a simulated decay heat output curve of heat-generating waste (Jove-Colon et al 2012; Hardin et al 2012). The simulation results on the left figure show that for the backfill water content of 0.01% to 1%, a significant backfill compaction (i.e., below 10% porosity) occurs in about 6 years, and the porosity reduction below 5% in about 10 years. Similar model results were also reported from a recent study by Hadgu et al (2013). As shown in the right figure, for completely dry condition (i.e., zero water content in the backfill) which could happen during an early thermal perturbation period of a high thermal loading case, the backfill compaction below 10% porosity takes longer and occurs in about 30 years. The model results are consistent with the German in-situ TSDE test results.

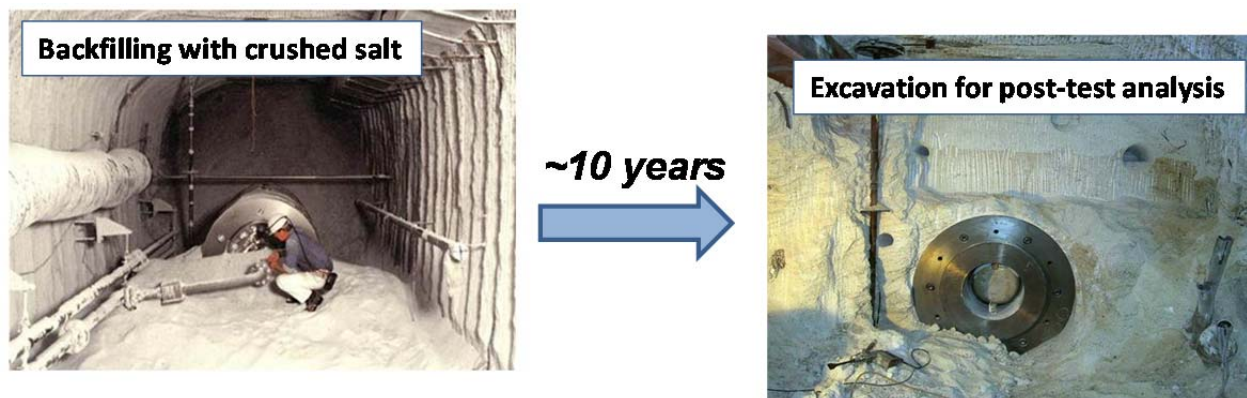
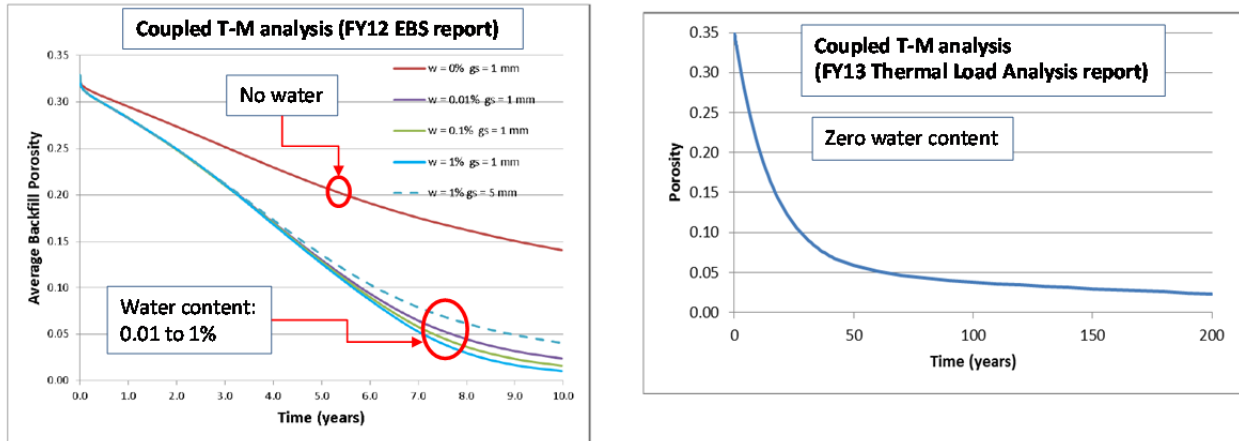


Figure 8. In-situ Simulated Heater Test for the Thermal Simulation of Drift Emplacement (TSDE) at Asse Mine: (left) simulated canister being backfilled with crushed salt, and (right) simulated canister surrounded by consolidating salt upon excavation for post-test.



(Source: Jove-Colon et al 2012; Hardin et al 2012)

Figure 9. Recent UFD Coupled Thermal-Mechanical Model Results for Salt Backfill Consolidation

4.6 Waste Package Thermal Conditions

Waste package thermal output from waste decay heat is one of the important parameters for repository design and thermal load management. It is also an important parameter to define and characterize evolution of the thermal conditions and other processes of the near-field subsystems (or domains) that could impact repository performance, and these include waste package degradation, near-field temperature and geochemical environment, brine and gas movement, salt backfill and salt rock creep deformation, waste form dissolution, radionuclide solubility, etc. Using the isotopic inventory of the Mark-IV and Mark-V ER salt waste, ORIGEN simulations were conducted to calculate the waste package decay heat outputs as function of time for the wastes.

Figure 10 shows the decay heat output histories per metric ton (MT) of the Mark-IV and Mark-V ER salt waste, and they are compared with those of commercial PWR UNF and DHLW. For the per-MT basis, the decay heat output of the Mark-IV ER salt waste is comparable to those of commercial PWR UNF and DHLW, and the Mark-V ER salt waste decay heat output is much less than the three other wastes in the first 100 years. The difference is due to the Mark-V ER salt waste having a smaller inventory of the activation product and fission product radionuclides. This is shown clearly in the decay heat output histories of the ER salt waste packages shown in Figure 11. In the legend of the plots, AP designates the activation product radionuclides, FP the fission product radionuclides, and ACT+D the actinide and decay daughter radionuclides. Note that the ER salt WP heat output is less than the per-MT heat output shown in Figure 10 as each WP contains 120 kg of salt waste.

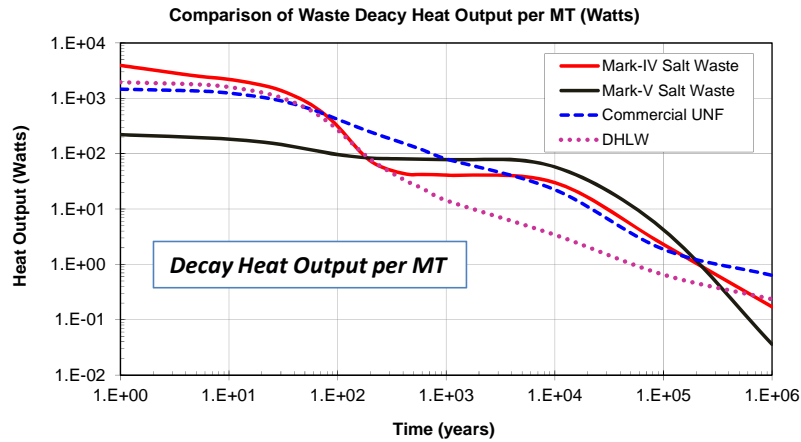
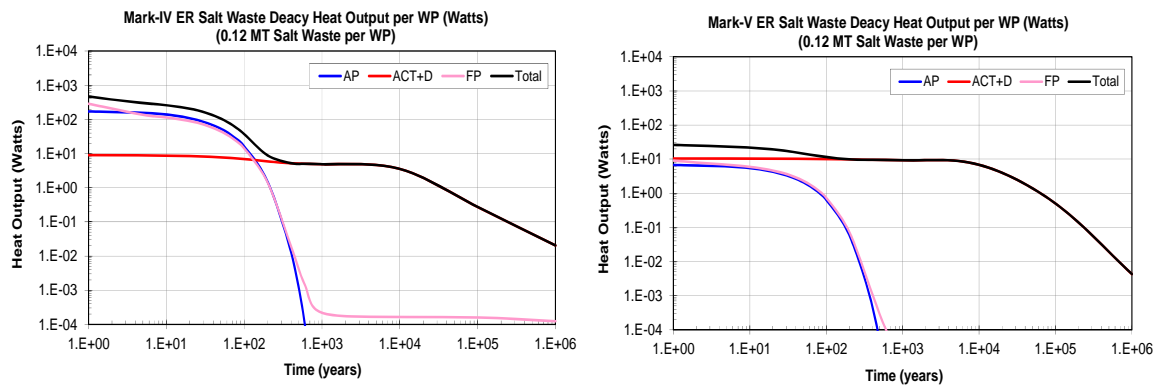


Figure 10. Decay Heat Output of Mark-IV and Mark-V ER Salt Waste per MT, Compared to That of Commercial UNF and DHLW.

The ER salt WP and emplacement alcove wall temperatures were calculated using the WP decay heat output data. The calculations were conducted using the analytical solution based model developed for the UFD repository thermal loading analysis (Hardin et al 2012). The calculation assumed a substantial salt backfill compaction at time zero and used the thermal conductivity value of the intact salt rock at 25 °C (4.2 W/m·K) for the salt backfill. It also assumed that the salt waste, after it was poured into and solidified in the disposal canister, was stored for 10 years prior to disposal in a salt repository and the waste decay heat during the storage time period was completely removed. This assumption on the storage duration has a minor impact on the ER salt WP temperature.

Figure 12 shows the calculated temperature histories of the Mark-IV and Mark-V ER salt WP and the emplacement alcove wall. Only moderate temperature increases are seen for the Mark-IV ER salt WP with the peak temperature at about 48°C right after the emplacement, and the WP temperature decreases to the ambient temperature in about 200 years. The moderate temperature increases are the result of low WP decay heat output from a low salt waste loading (120 kg/WP). Because of the low decay heat output of the Mark-V ER salt waste, the WP does not experience any appreciable temperature increases. The alcove wall temperature remains at the ambient temperature for the both type salt wastes.



AP = activation product radionuclides; FP = fission product radionuclides; ACT+D = actinide and decay daughter radionuclides

Figure 11. Decay Heat Output of (left) Mark-IV and (right) Mark-V ER Salt Waste Package (120 kg Salt Waste per WP).

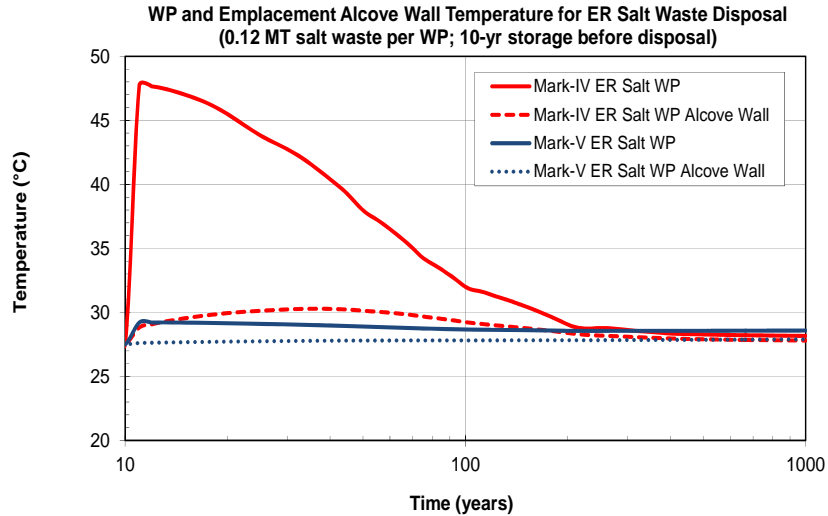


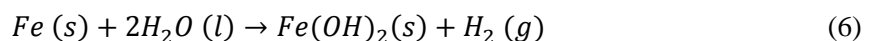
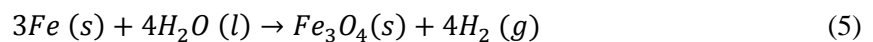
Figure 12. Temperature Histories of Mark-IV and Mark-V ER Salt Waste Package and Emplacement Alcove Wall.

4.7 Waste Package Corrosion Environment

In the post-closure repository, WPs would be encapsulated by crushed salt backfill undergoing consolidation and salt rock undergoing creep deformation. The EDZ in the emplacement alcove would also be healed with time, eventually to intact salt rock, by the salt creep. As the repository operations may take a few decades, WPs emplaced early may experience encapsulation by salt rock even prior to repository closure. The WPs would experience the lithostatic pressure exerted by salt rock creep deformation inward towards the WP. The process is illustrated with a conceptual schematic shown in Figure 13.

Anoxic, geochemically reducing conditions would prevail in the post-closure near-field, as residual oxygen in the repository would be consumed in a relatively short time period by WP overpack corrosion. Because the Mark-IV ER salt WP temperature is raised by only about 20°C (to the peak temperature of about 48 C, Figure 12) and the WP temperature perturbation above the ambient temperature lasts only for a short duration (about 200 years), the chemistry of brine around the WPs would not change significantly from the ambient geochemical conditions. The same assessment is applied to the Mark-V ER salt WPs as almost no temperature increases are estimated for the WPs. The WP overpack corrosion products would be compacted by the lithostatic pressure as illustrated in Figure 13.

Under anoxic geochemically reducing conditions, water reduction is the main cathodic reaction to support corrosion (anodic reaction) of the WP steel overpack, and the reactions generate hydrogen gas (H_2) (King 2007; Smart et al 2002a and 2002b; Telander and Westerman 1993; Westerman et al 1988; Rosselle 2013) according to the following reactions:



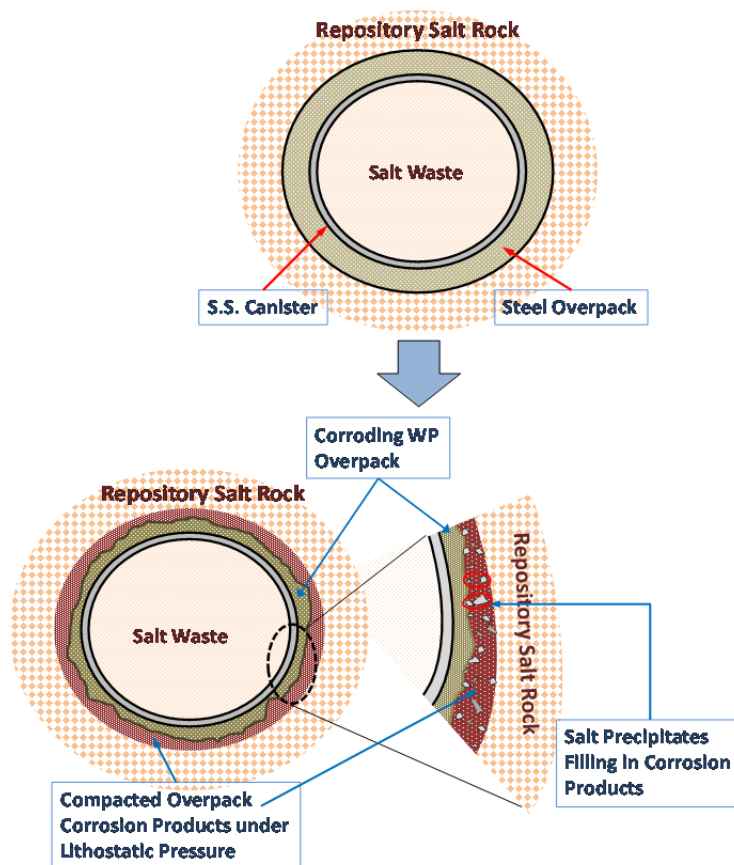


Figure 13. A Conceptual Schematic Illustrating WP Corrosion Environment in Post-Closure Repository.

The hydrogen gas generation would build up the gas overpressure in the “tight” confined space between the corroding overpack and contacting salt rock undergoing creep under the lithostatic pressure. Under anoxic conditions, magnetite (Fe_3O_4) is more stable with respect to ferrous hydroxide ($Fe(OH)_2$), especially under high hydrogen gas overpressure (King 2007; Smart et al 2002a; Telander and Westerman 1993; Westerman et al 1988), and Reaction (5) would be dominant over Reaction (6). The cathodic reduction of water in Reaction (5) consumes 4 moles (or 72 g) of water for one mole of magnetite formed (or 3 moles of iron corroded), and this results in precipitation of salt minerals from brine that crystallize within the pores of the corrosion products compacted under the lithostatic pressure. For an ERDA-6 type NaCl-saturated brine (112 g/L Na^+ , 4 g/L K^+ , 0.5 g/L Mg^{2+} and 171 g/L Cl^-) (Sevougian et al 2012), assuming all dissolved Na^+ and Cl^- precipitate as NaCl, about 20.5 g of NaCl precipitates out as 72 g of water is consumed by Reaction (5), and the NaCl precipitates occupy about 17% of the Fe_3O_4 -NaCl mixture volume, not taking into account the remaining pores. For a more concentrated Paradox Basin-type brine (168 g/L Na^+ , 63 g/L K^+ 9 g/L Mg^{2+} and 264 g/L Cl^-) (Sevougian et al 2012), applying the same approach, about 30.7 g of NaCl precipitates out, and the NaCl precipitates occupy about 24% of the Fe_3O_4 -NaCl mixture volume (not taking into account the remaining pores). The above preliminary bounding analysis shows that most of the pore space within corrosion products at the corroding surface would be filled by salt mineral precipitates, given the corrosion environment expected in a salt repository.

The porosity of steel corrosion products in the absence of significant external pressures is typically 0.3 to 0.35. The combined effects of the compaction of the overpack corrosion products under the lithostatic

pressure and precipitation of salt minerals in the pore space would significantly reduce the porosity of the mixture of overpack corrosion products and mineral precipitates surrounding the WP in a salt repository. The PA analysis models the overpack corrosion product porosity with a triangular distribution with the mode of 0.05 and the minimum of 0.01 and maximum of 0.1. In the PA analysis the overpack corrosion product pore volumes define the brine volume that is available to dissolve RNs released from the salt waste.

4.8 Waste Package Degradation

For the WP degradation model, the PA analysis takes a conservative approach by assuming the WP corrosion performance is by the carbon steel overpack only, that is, a potential waste containment performance by the stainless steel disposal canister or small ER salt waste containers (see Section 4.3) is not considered. The PA model assumes that the carbon steel overpack corrodes by general corrosion only in the salt repository exposure conditions, and is not subject to localized corrosion attacks (e.g., pitting, crevice corrosion and stress corrosion cracking). The approach is consistent with the experimental observations of carbon steel and similar materials tested for a range of salt repository exposure conditions (Roselle 2013; Telander and Westerman 1993; Westerman 1988).

As discussed above and also depicted in Figure 13, the WP is encapsulated by consolidating salt backfill in 10 to 30 years after emplacement, and the overpack corrosion products would be retained and accumulate on the overpack. The layer of the mixture of the overpack corrosion products and salt precipitates would be compacted under lithostatic pressure, and the porosity of the compacted mixture layer would remain very low. The mixture layer would continue to thicken as the overpack corrosion continues.

The processes would result in the overpack corrosion rates decreasing rapidly initially before reaching a steady-state rate. The overpack steady-state corrosion rate is controlled by the balance between the cathodic water reduction rates and the anodic iron oxidation rates. Assuming the water availability at the corroding surface is not a kinetic limiting factor, hydrogen gas pressure buildup at the corroding surface in the “tight” confined pores of the compacted mixture of overpack corrosion products and salt precipitates could influence and control the iron oxidation reaction rate (i.e. the overpack corrosion rate).

The corrosion model for the overpack was developed using the general corrosion data of carbon steel and similar materials from the literature for the test conditions that are relevant to the salt disposal conditions. Westerman et al (1988) reported corrosion data of steel coupons measured for up to 6 months for different combinations of exposure conditions: temperature, brine chemistry, brine contact mode (immersed or embedded in salt particles), metal condition (boldly exposed, creviced or welded) and gas overpressure (no gas, H₂ gas or N₂ gas overpressure). The 6-month data for the coupons of all three metal conditions that were tested in NaCl-saturated or MgCl₂-rich brines at all three temperatures (90, 150 and 200°C) were used for the model development. The tests showed no difference in the corrosion rates for all three metal conditions (boldly exposed, creviced and welded) for the test conditions. Only the data tested in contact with salt particles were used, which was to simulate the WP conditions in close contacts with salt rock. The PA corrosion model also included the 24-month test data (the longest duration) of steel corrosion at 30°C in MgCl₂-rich brine conducted for the WIPP (Telander and Westerman 1993). The corrosion data used in the corrosion model development are summarized in Table 4, along with the models implemented in the PA model.

The 6-month corrosion data at 90, 150 and 200°C clearly show the effect of brine chemistry on the steel corrosion rates, and the corrosion rates measured in the MgCl₂-rich brine are significantly higher than those in the NaCl-saturated brine (20 to 40 times higher in terms of the mean rate). Because the

chemistry of the brine contacting WP is not modeled or defined for the PA analysis, and because the brine chemistry evolution in the near field would be highly uncertain, the corrosion data for the two brines at the same temperature are combined, and new statistics of the combined data were calculated.

Table 4. WP Overpack General Corrosion Rate Model and Data Summary.

Temperature	Brine Type	Number of Test Coupons	Corrosion Rate Model (mm/yr)	WP Temperature (T_{WP}) for Corrosion Rate Model
200°C (6 month-test)	NaCl Saturated	27	Mean: 0.0221; s.d.: 0.0145 Min: 0.0081; Max.:0.0550	--
	MgCl ₂ Rich	20	Mean: 0.5835; s.d.: 0.4130 Min: 0.1000; Max.:1.5000	--
	Combined for Corrosion Rate Model	47	Truncated normal distribution: Mean: 0.2610; s.d.: 0.3864 Min: 0.0081; Max: 1.5000	160°C < T_{WP}
150°C (6-month test)	NaCl Saturated	39	Mean: 0.0108; s.d.: 0.0080 Min: 0.0010; Max.:0.0330	--
	MgCl ₂ Rich	78	Mean: 0.4765; s.d.: 0.2835 Min: 0.0780; Max.:1.2100	--
	Combined for Corrosion Rate Model	117	Truncated normal distribution: Mean: 0.3213; s.d.: 0.3193 Min: 0.0010; Max: 1.2100	160°C ≥ T_{WP} > 110°C
90°C (6-month test)	NaCl Saturated	18	Mean: 0.0028; s.d.: 0.0012 Min: 0.0009; Max.:0.0044	--
	MgCl ₂ Rich	39	Mean: 0.0402; s.d.: 0.0256 Min: 0.0120; Max: 0.1210	--
	Combined for Corrosion Rate Model	57	Truncated normal distribution: Mean: 0.0284; s.d.: 0.0274 Min: 0.0009; Max: 0.1210	110°C ≥ T_{WP} > 35°C
30°C (24-month test)	MgCl ₂ Rich	20	Normal distribution: Mean: 0.0010; s.d.: 0.0001	35°C ≥ T_{WP}
Corrosion rate reduction factor for H ₂ gas overpressure: 0.325				
Corrosion rate enhancement factor for surface roughness: triangular distribution (mode: 1.25; min: 1.0; max: 1.5)				

In the PA analysis, the corrosion rate for a given temperature is modeled with a normal distribution with the mean and standard deviation (s.d.) of the combined data, and the corrosion rate distributions of four different temperatures (i.e., 30, 90, 150 and 200°C) are correlated positively. This means that, for a given realization of the PA analysis, corrosion rates are sampled at the same percentile of the distributions for the four temperatures. In the PA analysis, a corrosion rate sampled at a percentile higher than the 50th

percentile (i.e., corrosion rates populated on the right side of the 50th percentile of the distribution) implies that the near-field brine of more corrosive chemistry (i.e., a higher concentration of MgCl₂). A corrosion rate sampled at a percentile lower than the 50th percentile (i.e., rates populated on the left side of the distribution) implies the near-field brine similar to NaCl-saturated brines with a lesser MgCl₂ concentration.

As seen from the statistics for the corrosion rate models based on the 6-month data (90, 150 and 200°C), the corrosion rate data have a significant scatter, and the standard deviation (s.d.) of the rate data for a given temperature is comparable to the mean rate. To avoid sampling corrosion rates from the tails beyond the measured data, the corrosion rate is modeled with a truncated normal distribution of the mean and s.d. of the data and truncated at the minimum and maximum of the data. For the 30°C model, the s.d. is about 10% of the mean rate, and the corrosion rate is modeled with a normal distribution of the mean and s.d of the data without truncation.

As shown in Table 4, the PA model applies the corrosion rate models of the four different temperatures to the WP overpack corrosion degradation in a step-wise manner, conditional to the WP temperature. However, because the WP temperatures are at the ambient temperature for the entire simulation period, except the first 200 years for the Mark-IV ER salt WPs, the corrosion rates sampled from the 30°C corrosion rate model are applied to the WP overpack corrosion for nearly the entire simulation period. Therefore, the current approach of a step-wise corrosion rate model application is appropriate for the ER salt WP corrosion degradation analysis. A mechanistic approach will be utilized to improve the model for the overpack corrosion analysis in the next model analysis iteration.

Effect of H₂ gas overpressure on the WP overpack corrosion is modeled with a corrosion rate reduction factor, calculated from the corrosion rate data from Westerman et al (1988). The factor was calculated as the ratio of the mean corrosion rate (CR_{mean}) of coupons tested with H₂ gas overpressure to the mean rate without H₂ overpressure, of the same test conditions (150°C, MgCl₂-rich brine, and 1 month test) as follows.

$$\frac{CR_{mean}(H_2\text{overpressure})}{CR_{mean}(no\ H_2\text{overpressure})} = 0.325$$

The above factor for the H₂ gas overpressure is multiplied to the corrosion rate of the model summarized in Table 4 to model the effect of the gas overpressure on the overpack corrosion.

The steel corrosion rate data (Westerman et al 1988; Telander and Westerman 1993) used for the overpack corrosion degradation model are calculated rates based on the measurements of weight loss of test coupons due to corrosion, and the data represent an average corrosion rate (or an average corrosion depth divided by the test duration time) of the coupon. However, the test coupons typically have irregular corrosion depths, and some parts of the coupon have deeper corrosion depths than the calculated average depth and other parts have shallower depths than the average depth. Therefore the calculated average corrosion rates are not a conservative estimate of the corrosion penetration time (or the deepest corrosion depth) of the overpack wall. A roughness factor is used to account for the surface roughness effect, and the factor is multiplied to the corrosion rate model based on the average corrosion rate data. The roughness factor implemented in the PA model is modeled as a triangular distribution with the mode of 1.25, the minimum of 1.0 and maximum of 1.5.

As discussed above, the PA model assumes that the WP fails mechanically under the lithostatic pressure when the overpack corrodes to a threshold remaining thickness of 3 cm.

4.9 ER Salt Waste Dissolution

The PA model assumes that the WP overpack corrosion products are fully saturated with brine, and upon WP failure, the ER salt waste of the failed WP dissolves in contact with the brine. The volume of the brine that is available to dissolve the salt waste is assumed to be equal to the pore volume of the overpack corrosion product surrounding the WP.

In the current PA analysis, the model conservatively assumes that the salt waste dissolution rate (therefore the RN release rate from the waste) is congruent to the dissolution of LiCl, the most abundant salt compound in the waste. That is, if 10% of LiCl in the salt waste is dissolved in contact with the brine for a given simulation time step, the model dissolves 10% of the waste for the time step, mobilizing 10% of the RN inventory in the salt waste. The LiCl solubility of 13.9 moles/L is used for all the temperatures for the PA model.

The current approach results in rapid dissolution of the salt waste and fast release of RNs from the waste. The approach is conservative because some RNs would be embedded in other salt phases (i.e., NaCl, KCl, etc.) and may not be readily available for dissolution and releases as the salt phases could be stable in contact with the brine that may have been saturated with these salts present in the salt rock formation.

Most of the RNs (except I, Cs, Sr, and Ra) released from the waste would be subject to their solubility constraints under geochemically reducing conditions and would precipitate in the near-field as a component of the solubility-controlling solid phase. Those RNs would be released slowly from the solid phase constrained by its solubility.

4.10 Brine Flows Analysis

This section summarizes the brine flow analysis to estimate brine flow rate out of the waste disposal area and in the underlying interbed (Clayton et al 2011) and the flow rates used in the current PA analysis. The BRAGFLO software (Nemer 2007) that is currently used to model the brine and gas flow in and around the WIPP was used to calculate the brine flow fields in the waste emplacement and surrounding areas. BRAGFLO models two phase flow through porous media and includes the effects of many other processes such as gas generation from iron corrosion and rock compressibility. The NUTS software (Gilkey 2006) is currently used to simulate the transport in and around the WIPP, and the software was used to determine, based on the flow fields from BRAGFLO, the flow rates of brine “contaminated” with dissolved radionuclides from the waste package to the surroundings. The NUTS analysis results of “contaminated” brine flow rates were used as input to the PA analysis. Details of the brine flow analysis are documented in (Clayton et al 2011).

The modeling grid used in the brine flow analysis is shown in Figure 14 and is a vertical two-dimensional (2D) grid, oriented along the length of the alcove. The grid is shown as a logical grid in the figure, with the length (Δx), width (Δz) and height (Δy) of each grid cell indicated (in meters). A technique of “radial flaring” was used to capture three-dimensional (3D) flow effects. The width of each grid cell increases with distance away from the center of the alcove, simulating the convergent or divergent flow centered on the alcove.

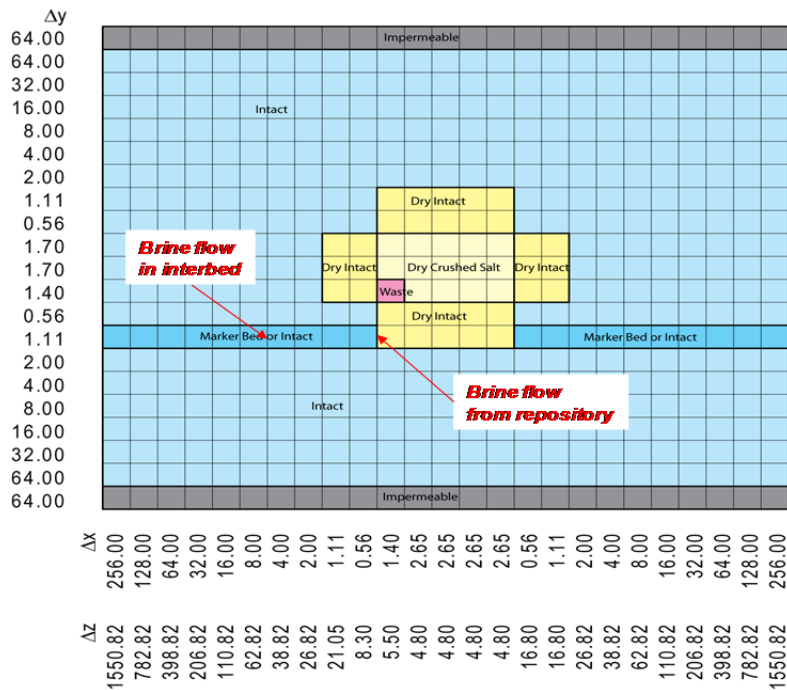


Figure 14. Long-term Brine Flow Grid Used in Analysis (Clayton et al 2011)

The grid contains six different materials: (1) impermeable (gray); (2) saturated intact salt (light blue); (3) dry intact salt (yellow); (4) dry reconsolidated crushed salt (light yellow); (5) waste material (pink); and (6) interbed (or marker bed) (blue). The properties of an anhydrite layer were used for the interbed material.

There is a significant amount of uncertainty associated with the properties of geologic materials such as permeability and porosity, and these properties can vary significantly depending on location. For this analysis, these uncertainties were dealt with by sampling the values of 19 important uncertain parameters from their respective range of values. A total of 100 distinct parameters sets were created for the analysis that span the full range of the parameter uncertainty (Clayton et al 2011).

Two locations were selected to develop the brine flow rate histories to be used in the PA analysis (Figure 14): (1) brine velocities from the repository chosen at the edge of the initial dry-out region right below the waste disposal area; and (2) brine velocities in the underlying interbed chosen at 8 m from the edge of initial dry-out region. For each location, a set of 100 flow rate histories (or 100 realizations) for each of the 100 distinct parameters sets were calculated to represent the uncertainty in the brine outflow rate, and the results are shown in Figure 15. The interbed brine velocities are also used for the brine flows in the far-field interbed and the repository access shaft. This is conservative because brine velocities are expected to decrease with the distance from the repository due to increased spread-out of brines with distance and associated pressure drop.

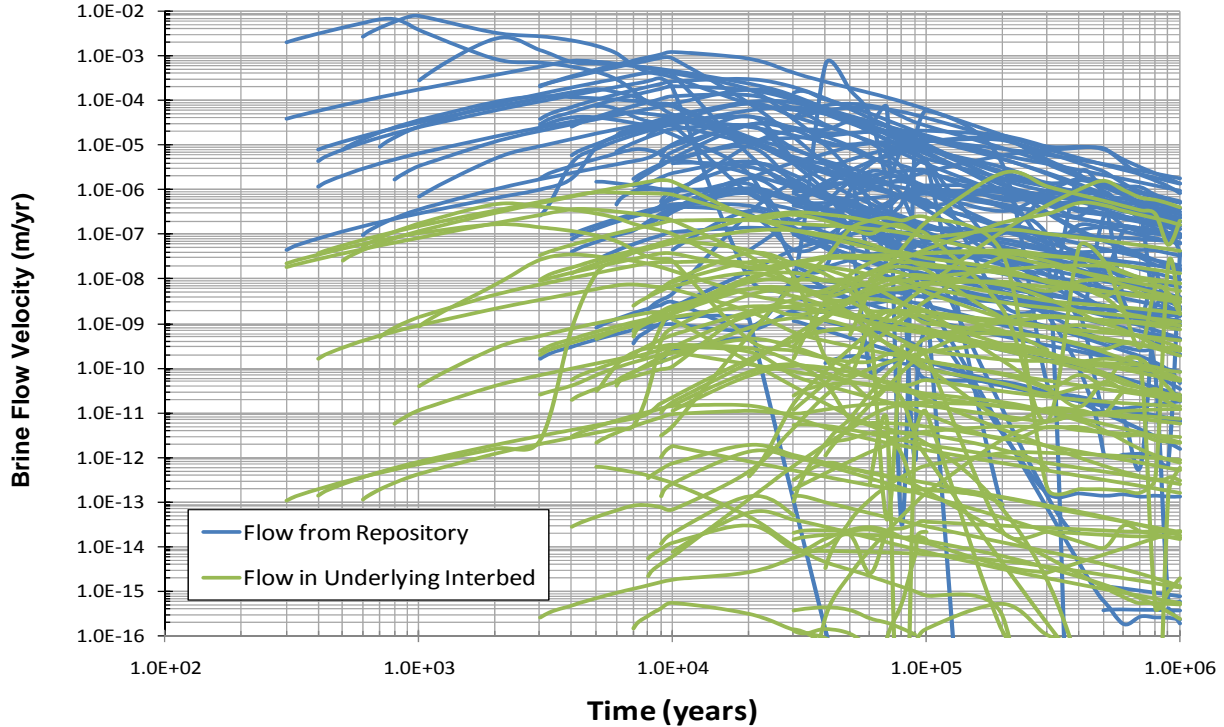


Figure 15. Brine Flow Rate Histories from the Repository and in Underlying Interbed Used in the PA Analysis (Clayton et al 2011).

As discussed above, the calculated brine flow velocities include the effect of hydrogen gas pressure build-up from the WP overpack corrosion. Although the brine flow analysis is for the ambient temperature condition and does not include near-field temperature perturbation effects, it is still applicable to the PA analysis. This is because the thermal perturbation period for the Mark-IV ER salt WP is short and no appreciable thermal perturbation occurs for the Mark-V ER salt WP. In addition, the WP and near-field temperatures are back to the ambient temperature in a few hundred years after closure, long before the WP fails. In the PA analysis, initiation of the brine velocity histories in Figure 15 is delayed until the WP fails (see Sections 4.8 and 5.1.1 for WP degradation model and failure analysis result).

The velocities are lower the further from the dry-out region due to the dilution with the surrounding uncontaminated brine. As the brine flow rates are very low for most of the realizations, especially in the interbed and access shaft, radionuclide transport in the interbed and access shaft would be dominated by diffusion. The flow rate histories are implemented in the PA model as a look-up table. The histories are sampled randomly in the PA analysis, and the histories at the two locations are perfectly correlated, which means the values of the uncertain property parameters used to calculate the brine velocities at the two locations are from the same set of sampled parameters of the 100 distinct sets.

4.11 Natural Barrier System Parameters

This section documents the key features of the natural barrier system (NBS) of a salt repository that were implemented in the PA analysis. The NBS features were adopted from the reference case parameters that were recommended in the recent generic salt repository total system performance assessment (TSPA)

report (Sevougian et al 2012). The recommended features and assumptions that are implemented in the PA analysis are summarized as follows.

- The repository horizon is located in a relatively pure halite stratum that is at least 12 meters thick.
- The salt and interbed are uniform over the lateral extent of the repository and the entire underground area, encompassed by the 5-km boundary from the waste disposal area boundary.
- A major interbed below the massive salt encompassing the repository horizon is considered to be 2 feet (0.61 m) thick with a range of 0.5 feet to 4 feet (0.15 m to 1.2 m).
- The closest edge of the assumed interbed below repository is taken to be in the range of 12 meters to 15 meters from the repository floor and ceiling.
- An aquifer is considered to be approximately 750 feet (229 m) above the repository with a range of 500 feet to 1,500 feet (152 m – 457 m).
- The effective thickness (water producing interval) of the overlying aquifer is taken as 50 feet (15 m) with a range of 10 feet to 75 feet (3 m – 23 m).
- The aquifer is assumed to be a saturated, single-porosity sedimentary formation in the regional groundwater basin containing the repository. It is assumed to have a uniform thickness, a constant porosity, and a constant regional Darcy velocity in the portion of the aquifer that might communicate with both the repository horizon and the biosphere location.

Table 5 lists the NBS parameters and their values that were implemented in the PA analysis. The repository access shaft diameter in the table is adopted from the recent repository thermal loading analysis (Hardin et al 2012).

Table 5. Natural Barrier System Parameters and Their Values Implemented in the PA Analysis.

Parameter Description	Distribution Type	Values
Thickness of overlying aquifer	Triangular	3 m (min); 15 m (mode); 23 m (max)
Formation thickness between repository and aquifer	Triangular	152 m (min); 229 m (mode); 457 m (max)
Formation thickness between repository floor and interbed	Uniform	12 m (min); 15 m (max)
Interbed thickness	Triangular	0.15 m (min); 0.61 m (mode); 1.2 m (max)
Diameter of repository access shaft	Constant	5 m
Length of repository access shaft	Triangular	152 m (min); 229 m (mode); 457 m (max)
Distance between repository edge and site boundary	Constant	5 km

4.12 Radionuclide Solubility

This section documents the RN elemental solubilities that were implemented in the near-field and far-field transport models of the PA analysis. The solubility values are from the previous UFD analysis (Wang and Lee 2010, Clayton et al 2011) and are reproduced in this section to have this report serve as a standalone documentation and data source for the current PA analysis.

Dissolved radionuclide concentrations in the near field are determined by the mass of radionuclides released from the waste form (constrained by the waste form degradation rate), the volume of brine available in the near field, and the radionuclide solubility if it is subject to its solubility constraint. Radionuclide solubility is affected at varying degrees by various geochemical conditions, including redox condition of contacting water, temperature, pH, and presence and concentration of other dissolved species.

The PA analysis considers two redox conditions for salt brine: (1) chemically reducing condition brine, and (2) less reducing or slightly oxidizing brine. Solubility calculations for these two redox conditions were based on the chemical compositions of two well-studied brines from the WIPP site: (1) a concentrated brine derived either from the repository horizon or the pressurized brine reservoir beneath the repository, representative of a chemically reducing condition; and (2) a dilute brine from the interface between the near field and the far field, representative of a much less reducing condition. The chemical compositions of the two brines are given in Wang and Lee (2010).

Solubility calculations for U, Pu, Am, Np, Th, and Sn at different temperatures were performed with computer code EQ3/6 and an enhanced Pitzer thermodynamic database (Wolery and Jarek 2003). Details of the solubility analysis for the representative groundwater are documented in Wang and Lee (2010). In the PA analysis, the reducing condition is representative of the brine in the near field, and the less reducing or slightly oxidizing condition is representative of the brine away from the near field (i.e., repository interbed, far-field interbed, repository access shaft, and overlying aquifer).

Table 6 shows the elemental solubilities of the five actinides (U, Pu, Am, Np and Th) in near-field chemically reducing concentrated brines as a function of temperature. The plots to better present the temperature dependency of the solubilities are shown in Figure 16. In addition to the calculated solubilities for the elements described above, elemental solubilities for other radionuclides (Ac, C, Cl, Cm, Cs, I, Li, Nb, Pa, Pd, Ra, Sb, Se, Sr, and Zr) are shown. Elements C, Ra and Sr are implemented as unconstrained (or unlimited) solubility because their solubility calculations have not been completed. The elemental solubilities have been implemented in the source-term model of the PA analysis. Note that, although it is not radioactive and not considered in the repository PA analysis, the Li elemental solubility is included in the source-term model because the dissolution of LiCl in the ER salt waste is used as the marker for the salt waste dissolution (see Section 4.9 for additional discussions).

The elemental solubilities in dilute far-field brines (representing less chemically reducing or slightly oxidizing conditions) are shown in Table 7, and the solubilities are implemented in the far-field transport model (i.e., repository interbed, far-field interbed, repository access shaft, and overlying aquifer) of the PA analysis. Ambient temperature is assumed for the far-field transport analysis.

Table 6. Elemental Solubility of Radionuclides in Near-Field Brine as a Function of Temperature Implemented in the PA analysis.

Element	Temperature (°C)	Distribution Type	Solubility (molal)	Source
U	25	Triangular	4.89E-08 (min); 1.12E-07 (mode); 2.57E-07 (max)	Wang and Lee (2010)
	50	Triangular	3.63E-10 (min); 8.27E-10 (mode); 1.91E-09 (max)	
	100	Triangular	4.17E-13 (min); 9.46E-13 (mode); 2.19E-12 (max)	
	150	Triangular	6.40E-14 (min); 1.46E-13 (mode); 3.36E-13 (max)	
	200	Triangular	2.88E-14 (min); 6.54E-14 (mode); 1.51E-13 (max)	
Pu	25	Triangular	1.40E-06 (min); 4.62E-06 (mode); 1.53E-05 (max)	Wang and Lee (2010)
	50	Triangular	4.62E-13 (min); 1.53E-12 (mode); 5.07E-12 (max)	
	100	Triangular	3.40E-14 (min); 3.56E-14 (mode); 3.73E-13 (max)	
	150	Triangular	1.08E-16 (min); 3.56E-16 (mode); 1.18E-15 (max)	
	200	Triangular	4.44E-15 (min); 1.47E-14 (mode); 4.87E-14 (max)	
Am	25	Triangular	1.85E-07 (min); 5.85E-07 (mode); 1.85E-06 (max)	Wang and Lee (2010)
	50	Triangular	6.80E-08 (min); 3.12E-07 (mode); 8.81E-07 (max)	
	100	Triangular	7.80E-10 (min); 6.50E-09 (mode); 4.37E-08 (max)	
	150	Triangular	5.39E-09 (min); 4.50E-08 (mode); 3.05E-07 (max)	
	200	Triangular	5.82E-08 (min); 4.86E-07 (mode); 3.29E-06 (max)	
Np	25	Triangular	4.79E-10 (min); 1.51E-09 (mode); 4.79E-09 (max)	Wang and Lee (2010)
	50	Triangular	7.91E-09 (min); 2.50E-08 (mode); 7.91E-08 (max)	
	100	Triangular	6.00E-07 (min); 1.90E-06 (mode); 6.00E-06 (max)	
	150	Triangular	2.55E-05 (min); 8.08E-05 (mode); 2.55E-04 (max)	
	200	Triangular	1.38E-03 (min); 4.37E-03 (mode); 1.38E-02 (max)	
Th	25	Triangular	2.00E-03 (min); 4.00E-03 (mode); 7.97E-03 (max)	Wang and Lee (2010)
	50	Triangular	1.48E-05 (min); 2.95E-05 (mode); 5.92E-05 (max)	
	100	Triangular	1.71E-08 (min); 3.37E-08 (mode); 6.79E-08 (max)	
	150	Triangular	2.62E-09 (min); 5.20E-09 (mode); 1.04E-08 (max)	
	200	Triangular	1.18E-09 (min); 2.33E-09 (mode); 4.68E-09 (max)	
Tc	All temp.	Log-Triangular	4.56E-10 (min); 1.33E-08 (mode); 3.91E-07 (max)	Wang and Lee (2010)
Sn	All temp.	Triangular	9.87E-09 (min); 2.66E-08 (mode); 7.15E-08 (max)	
Ac, Cm	All temp.	Constant	5.85E-07	Clayton et al (2011)
Cl	All temp.	Constant	4.20	
Nb	All temp.	Constant	1.60E-05	
Pa	All temp.	Constant	1.51E-09	
Pd	All temp.	Constant	4.00E-04	

Element	Temperature (°C)	Distribution Type	Solubility (molal)	Source
Sb	All temp.	Constant	6.30E-05	
Se	All temp.	Constant	2.00E-05	
Zr	All temp.	Constant	1.00E-10	
C, Cs, I, Ra, Sr	All temp.	n/a	Unconstrained solubility	
Li	All temp.	Constant	12.9 (Note : LiCl dissolution is used as the marker for the ER salt waste dissolution in the source-term model)	

Table 7. Elemental Solubility of Radionuclides in Far-Field Dilute Brine Implemented in the PA analysis.

Element	Distribution Type	Solubility (molal)	Source
U	Triangular	9.16E-05 (min); 2.64E-04 (mode); 7.62E-04 (max)	Wang and Lee (2010)
Pu	Triangular	7.80E-07 (min); 2.58E-06 (mode); 8.55E-06 (max)	
Am	Triangular	3.34E-07 (min); 1.06E-06 (mode); 3.34E-06 (max)	
Np	Log-triangular	1.11E-06 (min); 1.11E-05 (mode); 1.11E-04 (max)	
Th	Triangular	8.84E-06 (min); 1.76E-05 (mode); 3.52E-05 (max)	
Sn	Triangular	1.78E-08 (min); 4.80E-08 (mode); 1.29E-07 (max)	
Ac, Cm	Constant	5.85E-07	Claton et al (2011)
Cl	Constant	4.20	
Nb	Constant	1.60E-05	
Pa	Constant	1.51E-09	
Pd	Constant	4.00E-04	
Sb	Constant	6.30E-05	
Se	Constant	2.00E-05	
Zr	Constant	1.00E-10	
C, Cs, I, Ra, Sr, Tc	N/A	Unconstrained solubility	

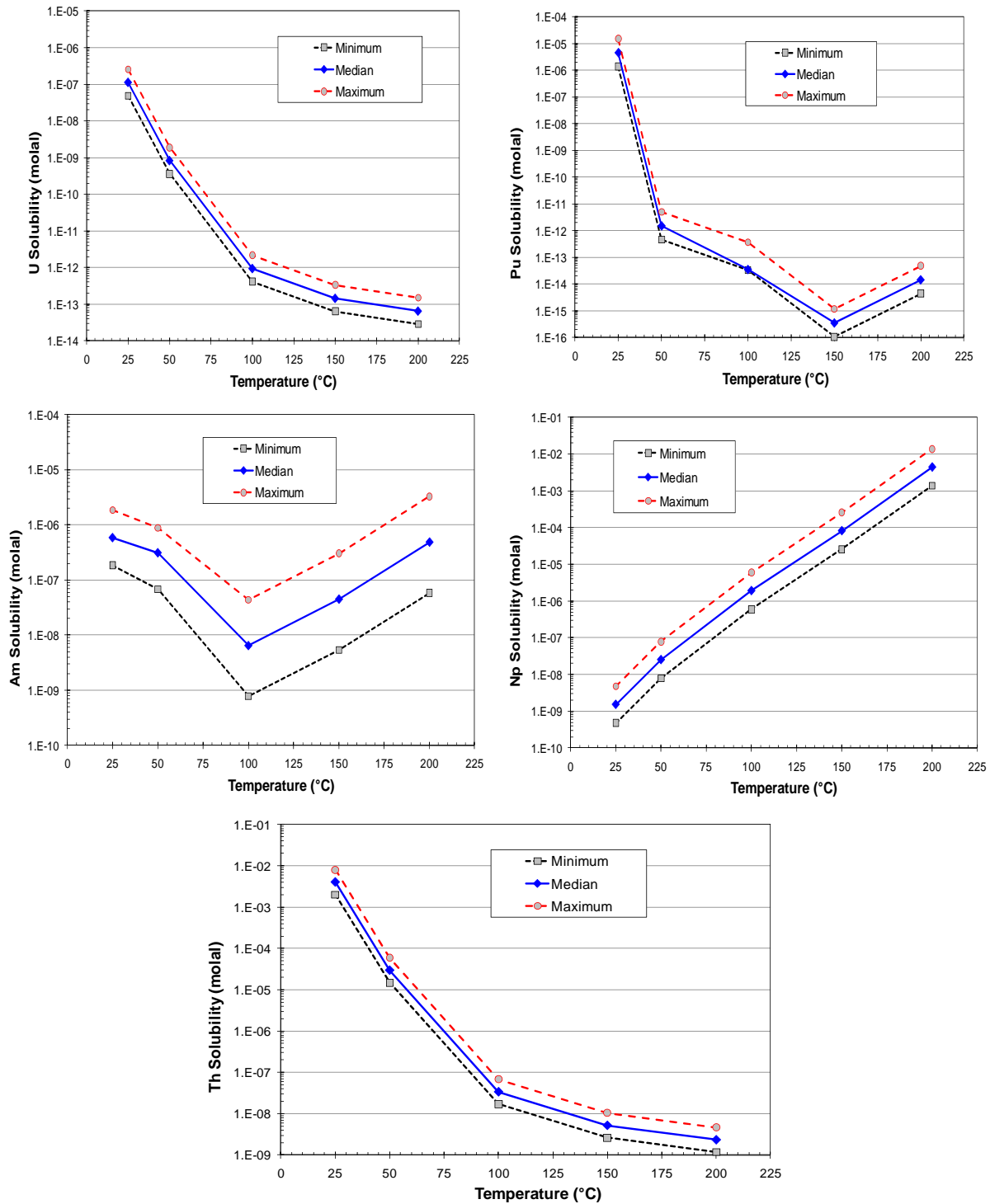


Figure 16. Solubility of Uranium, Plutonium, Americium, Neptunium and Thorium As a Function of Temperature in Near-Field Concentrated Brine Implemented in the PA Analysis (Wang and Lee 2010).

4.13 Biosphere Model

As discussed in Section 3, the subsystem performance is measured in terms of RN fluxes across the subsystem boundary, and radiation exposure (or dose) to a receptor in the biosphere is also used as a performance metric for the PA analysis to evaluate the ER salt waste direct disposal feasibility. The PA model includes a “hypothetical” biosphere that is assumed to be located at the site boundary, 5-km down-gradient from the repository footprint boundary.

Development of a generic biosphere model is very challenging. In general the biosphere is highly site specific, and a generic biosphere model is therefore inherently highly uncertain. However, such a biosphere model can drive the performance measure of a generic repository, if the dose to a receptor is the repository performance measure.

A simple generic biosphere model based on the drinking water consumption such as the International Atomic Energy Agency’s (IAEA) BIOMASS Example Reference Biosphere 1 (ERB 1) dose model (IAEA 2003) is available. The ERB 1 dose model is deliberately designed to be very simple, being focused on a simple biosphere system and single exposure pathway. It is characterized by a drinking water well, bored through the overburden into an aquifer that has been contaminated by radionuclide releases from the repository. Previous experience from more comprehensive biosphere modeling studies has shown that a drinking water well may sometimes represent a significant or even, depending on other aspects of the assessment context, a dominant pathway for release and exposure (IAEA 2003).

For the ERB 1B dose mode, a variant of the ERB 1 dose model, the drinking well discharge rate is the dominant parameter and highly uncertain because it is dependent largely on, among others, the size of the community (number of pumping wells and their discharge rates), types and life-style of the community (rural, agricultural, urban, industrial, pasturing, ranch, etc.), and climate conditions (desert, semi-desert, wet, etc.). In previous generic repository performance analysis (Wang and Lee 2010; Clayton et al 2011; Vaughn et al 2012), the BIOMASS ERB 1B model (IAEA 2003) was used with an arbitrary “constant” dilution rate (10^4 m³/yr) by well pumping. The constant dilution rate was chosen purposely to avoid unwarranted uncertainties in the repository performance, driven by the highly uncertain biosphere model (i.e., from highly uncertain well discharge rates for a poorly defined “hypothetical” generic biosphere community).

For the now-cancelled Yucca Mountain repository, the regulation provided a guideline such that a representative groundwater volume of 3,000 acre-ft is withdrawn annually for the target biosphere community in the Armargosa Valley (10 CFR Part 63). As one acre-ft of water is 1,233.5 m³, the representative groundwater volume withdrawn per year is equivalent to a well pumping rate of 3.7×10^6 m³/yr. As a rule of thumb, one acre-ft/yr water is the planned water consumption rate for a household of rural community (Montana 2004). The recommended annual groundwater withdraw rate for the target biosphere of the Yucca Mountain repository may be considered the groundwater consumption rate for a rural community of about 3,000 households.

In the total system performance assessment (TSPA) of the Yucca Mountain repository, all the RN masses crossing into the biosphere boundary were mixed with the representative groundwater volume to calculate the RN concentrations of well water used by the target community. The same approach was used in the previous generic salt repository analyses (Wang and Lee 2010; clayton et al 2011; Vaughn et al 2012), except the effective annual dilution rate (10^4 m³/yr) for the RNs from well pumping was about two orders of magnitude less than the rate (3.7×10^6 m³/yr) used in the Yucca Mountain TSPA. The effective annual dilution rate of 10^4 m³/yr used for the previous analyses corresponds to the groundwater consumption rate for a rural community of about 8 households (a very small community).

Table 8. IAEA ERB 1A Parameters Implemented in the Biosphere Model

Well-water consumption rate: 1.2 m ³ /yr			
ERB 1 Dose Coefficient			
Isotope	Sv/Bq	Isotope	Sv/Bq
²²⁷ Ac	0.00E+00	²⁴² Pu	2.40E-07
²⁴¹ Am	2.00E-07	²²⁶ Ra	2.17E-06
²⁴³ Am	2.01E-07	²²⁸ Ra	0.00E+00
¹⁴ C	5.80E-10	¹²⁶ Sb	0.00E+00
³⁶ Cl	9.30E-10	⁷⁹ Se	2.90E-09
²⁴⁵ Cm	2.15E-07	¹²⁶ Sn	4.70E-09
¹³⁵ Cs	2.00E-09	⁹⁰ Sr	3.07E-08
¹³⁷ Cs	1.30E-08	⁹⁹ Tc	6.40E-10
¹²⁹ I	1.10E-07	²²⁹ Th	6.13E-07
⁹³ Nb	0.00E+00	²³⁰ Th	2.10E-07
²³⁷ Np	1.11E-07	²³² Th	1.06E-06
²³¹ Pa	1.92E-06	²³² U	0.00E+00
²¹⁰ Pb	0.00E+00	²³³ U	5.10E-08
¹⁰⁷ Pd	3.70E-11	²³⁴ U	4.90E-08
²³⁸ Pu	2.30E-07	²³⁵ U	4.73E-08
²³⁹ Pu	2.50E-07	²³⁶ U	4.70E-08
²⁴⁰ Pu	2.50E-07	²³⁸ U	4.84E-08
²⁴¹ Pu	0.00E+00	⁹³ Zr	1.22E-09

Source: IAEA 2003, Table C.5.

In the current PA analysis, in order to avoid the issues associated with highly uncertain groundwater well discharge rates that are required as input to the BIOMASS ERB 1B dose model (IAEA 2003), the BIOMASS ERB 1A dose model (IAEA 2003) is used instead to convert the dissolved radionuclide concentrations in groundwater at a hypothetical drinking well location to an estimate of annual dose to a receptor based on drinking well water consumption. The ERB 1A dose model requires as input the RN concentrations in the aquifer, from which an individual takes drinking water. The RN concentrations in the aquifer are typically calculated by a geosphere model. The biosphere model assumes an individual water consumption rate of 1.2 m³/yr (IAEA 2003), and uses the PA model-calculated RN concentrations in the far-field aquifer at the site boundary. The ERB 1A parameters used to represent the biosphere are provided in Table 8.

4.14 Performance Assessment Model Implementation

This section discusses implementation of the conceptual model (Section 4.1) and component submodels in the PA model framework for evaluation of the feasibility of the ER salt waste direct disposal. The section also documents the RN transport parameters that are implemented in the near-field and far-field transport models for the PA analysis. Most of the parameters have already been documented with detailed discussions in previous UFD reports (Wang and Lee 2010, Clayton et al 2011). The parameter values are reproduced in this section to maintain this report as the standalone documentation and data source for the current PA analysis.

The PA model was implemented in the Goldsim framework (Goldsim 2010), utilizing its probabilistic analysis feature. The routine PA analysis runs were conducted with 100 realizations for a simulation time period of 1 million years. Figure 17 shows a schematic to illustrate the model implementation configuration of the PA model. As shown in the figure, because the estimated total inventory can be disposed of in 15 WPs (9 Mark-IV ER salt WPs and 6 Mark-V ER salt WPs), the PA analysis simulates individual WPs. The distance between WPs across the repository salt block corresponds to the alcove spacing of 20 m, and the distance between neighboring WPs is 18.3 m [WP-to-WP spacing (10 m) – WP length (1.7 m)]. The cell elements representing WPs have the surface area of the intact WP (2.52 m²).

Each rectangular prism in the figure represents a Cell Pathway element of the Goldsim framework, in which various transport processes (diffusion and advection) and reactions (dissolution, precipitation, sorption and radioactive decay and in-growth) are modeled along the transport pathway. The PA model utilizes many series of the Cell Pathway elements having appropriate transport and reaction properties to simulate transport of RNs along the transport pathways. A Pipe Pathway element of the Goldsim framework having appropriate transport properties is used to simulate RN transport in the overlying aquifer.

When a WP fails, the ER salt waste dissolves in contact with brine, releasing RNs to the brine, and the released RNs, if constrained by its solubility limit, precipitate out of the brine. The dissolved RNs are transported out of the failed WP by both advection and diffusion through the corrosion product layer surrounding the WP. The blue arrows in Figure 17 indicate the direction of brine flows (or brine “migration” as the flow rates are so small (Section 4.10), which is the direction of RN advective transport. The PA model assumes that half of the advective flux from the failed WP is transported to a nearby repository access shaft, and then transported upward through the shaft seals by diffusion and advection and released into the overlying aquifer. The other half of advective flux from the failed WP is transported downward toward the underlying interbed. The PA model does not consider the RN diffusion from the repository upward to the overlying aquifer because the diffusive mass flux through intact salt rock and other overburden formations would be negligible.

Each rectangular prism in the figure, representing a transport cell pathway, is linked to all neighboring prisms (up to six prisms or six cells) for diffusive transport to all six directions. Therefore diffusive transport towards the underlying interbed is simulated with a pseudo-3D finite difference scheme, and advective transport towards the interbed is modeled using the pre-determined brine flow directions as shown by the blue arrows in the figure. Upon being transported to the horizontally oriented interbed, RNs are transported laterally in the interbed by both advection and diffusion. As discussed above, the width of the underlying interbed is limited to 40 m (twice the alcove spacing) to limit the spread of RN plumes in the interbed. The RN transport in the repository shaft upward towards the overlying aquifer is by both advection and diffusion and is modeled with 1-D finite difference scheme.

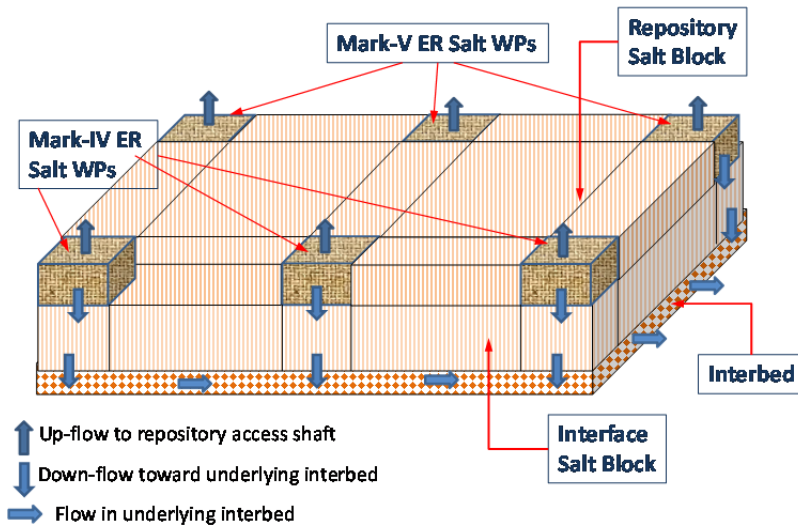


Figure 17. A Schematic Illustrating the Model Implementation Configuration of the PA Model for ER Salt Waste Direct Disposal.

4.14.1 Near-Field Model Implementation

The PA analysis models conservatively no radionuclide sorption for the near-field transport. This is a highly conservative approach as many radionuclides are known to sorb on geologic materials and, in particular, strongly on metal corrosion products in a chemically reducing condition. The impact of this conservative assumption will be evaluated in the next iteration of the PA analysis.

As shown in Figure 17, the PA model includes a region of salt rock formation (or interface rock block) between the repository and underlying interbed (also see Figure 1). The interface region thickness is given in Table 5 (Section 4.11). The PA model simulates release of dissolved radionuclides from the waste emplacement area to the interface region and subsequent transport through the interface region, both by diffusion and advection. As for the near field transport, the model conservatively assumes no sorption of radionuclides in the interface region, and the far-field elemental solubility (Table 7) is applied to radionuclides in the interface region.

The brine flow rates in the emplacement area and interface region are sampled from 100 time-dependent brine flow rate histories, which are abstracted from detailed brine migration process simulations as discussed in Section 4.10. The PA model parameters for the near-field and interface region are summarized in Table 9.

Table 9. Model Parameters for the Near-Field and Interface Block Region Implemented in the PA Analysis

Parameter	Distribution Type	Parameter Value and Description	Source
<i>Near Field</i>			
Porosity (salt bedrock)	Log-uniform	0.001 (min); 0.0519 (max)	Clayton et al. (2011)
Density (salt bedrock)	Constant	2500 kg/m ³	
Porosity (WP overpack corrosion products)	Triangular	0.01 (min); mode (0.05); 0.1 (max)	Section 4.7 of this report
Density (WP overpack corrosion products)	Constant	5170 kg/m ³	
Brine Flow Rate to Interface Rock Block (m/yr)	N/A	Sampled from 100 brine flow rate histories	Section 4.10 of this report
Radionuclide Sorption	N/A	Assume no sorption	
Radionuclide Solubility	N/A	Near-field brine solubility	Table 6 of this report
<i>Interface Rock Block</i>			
Porosity (salt bedrock)	Log-uniform	0.001 (min); 0.0519 (max)	Clayton et al. (2011)
Density (salt bedrock)	Constant	2500 kg/m ³	
Brine Flow Rate to Underlying Interbed (m/yr)	N/A	Sampled from 100 brine flow rate histories	Section 4.10 of this report
Radionuclide Sorption	N/A	Assume no sorption	
Radionuclide Solubility	N/A	Far-field brine solubility	Table 7 of this report

4.14.2 Far-Field Model Implementation

As discussed in Section 4.1, the PA analysis assumes that an interbed below the repository and a repository access shaft are the major pathways for radionuclide release and transport from the repository, and this assumption is supported by the model results from WIPP (Helton et al. 1998) and German salt repository program (Buhmann et al 2009, Rubel et al 2009). The interbed is assumed to be composed of a mixture of evaporite minerals (such as anhydrite) and clay, and is assumed to run horizontally in parallel with the repository (Figure 1). The same materials are assumed for the access shaft seals for the current PA analysis, and a better representation of the seal materials and associated transport parameters will be implemented in the next iteration of the PA analysis.

As discussed in Section 4.11, the interbed is considered to be 0.61 m thick with a range of 0.15 m to 1.2 m, and the access shaft is 5m in the diameter. For the PA analysis, the width of underlying interbed is limited to 40 m (twice the alcove spacing, and this conservative approach is to limit the spread of RN plume in the interbed. The interbed cross sectional area to advective (by brine flow) and diffusive transport is the bed thickness times the width. The interbed features were adopted from the dominant underlying marker bed of the WIPP (Helton et al. 1998). As illustrated in Figure 17, dissolved radionuclides are transported into the interbed over its length below the emplacement alcoves. As discussed in Section 4.1, the RNs released into the interbed remain in the interbed because there are no hydrogeological features for brine flow from the interbed to biosphere. Diffusive transport of RNs from

the interbed upward to the overlying aquifer can occur, but the upward flux through intact salt rock and other overburden formations would be negligible even considering diffusive flux to all other directions.

Table 10. Far-Field Model Parameters for Radionuclide Transport in the Interbed and Repository Access Shaft Implemented in the PA Analysis

Parameter	Distribution Type	Parameter Value and Description	Source
Porosity	Uniform	0.006 (min); 0.017 (max)	Clayton et al. (2011)
Density	Constant	2500 kg/m ³	
Brine Flow Rate in Interbed and Shaft (m/yr)	N/A	Sample from 100 time-dependent flow rate histories	Section 4.10 of this report
<i>Kd for radioelements (mL/g):</i>			
U	Uniform	0.2 (min); 1 (max)	Lappin et al. (1989); McKinley and Scholtis (1992); Muller et al. (1981); Tien et al. (1983)
Pu	Uniform	70 (min); 100 (max)	
Np	Uniform	1 (min); 10 (max)	
Am	Uniform	25 (min); 100 (max)	
Th	Uniform	100 (min); 1000 (max)	
Tc	Uniform	0 (min); 2 (max)	
Cs	Uniform	1 (min); 20 (max)	
Sr	Uniform	1 (min); 80 (max)	
Ac, Cm	Log-uniform	5 (min); 500 (max)	McKinley and Scholtis (1992) (Kd values were reduced by a factor of 10 to account for the high salinity of brine.)
C	Uniform	0 (min); 0.6 (max)	
Nb, Pd	Constant	0.1	
Pa	Log-uniform	1 (min); 500 (max)	
Sb	Constant	10	
Se	Uniform	0.2 (min); 0.5 (max)	
Sn	Uniform	2 (min); 10 (max)	
Zr	Log-uniform	3 (min); 500 (max)	Miller and Wang (2012)
I	Uniform	0 (min); 1 (max)	
Cl, Pb	Constant	0 (no sorption)	

As for the interbed, advective and diffusive processes are modeled for the RN transport in the access shaft seals, and the RNs are released to the overlying aquifer. Lateral diffusion from the outer surface of the shaft seals into the surroundings is not modeled conservatively in the PA analysis; the lateral diffusion of RNs would further reduce the RN releases into the overlying aquifer.

The far-field elemental solubilities in dilute brines at 25°C (Table 7) are applied for the interbed and access shaft transport. As described in Section 4.12, these elemental solubilities are based on the data and calculation from Wang and Lee (2010) and Clayton et al (2011). Elements C, Ra, Sr and Tc are implemented as unconstrained solubility in the far-field transport model because their solubility calculations have not been completed. Sorption of radionuclides on the filling materials of the interbed and access shaft is modeled with an equilibrium Kd approach. The model parameters for radionuclide transport in the interbed and access shaft are listed in Table 10. Element Pb is implemented as non-sorbing in the interbed and access shaft because analysis for its sorption behavior on the filling materials has not been completed.

The overlying aquifer is assumed to be comprised primarily of a dolomite matrix with clays dispersed in the matrix. The PA model assumes the repository access shaft considered in the PA analysis is located on the edge (or boundary) of the repository footprint in the direction of the overlying aquifer down-gradient towards the hypothetical biosphere located at the site boundary.

The mass of radionuclides released to the overlying aquifer are evaluated against the elemental solubility for the far-field dilute brine (Table 7). If the concentrations of radionuclides exceed their elemental solubility limits, the excess mass of the radionuclides precipitates out of the water and remains as a solid until it dissolves back into the water. The dissolved radionuclides are transported within the aquifer to a drinking well location of the hypothetical biosphere, 5 km down-gradient from the repository boundary. Sorption of radionuclides on the aquifer filling medium is modeled with an equilibrium Kd approach. Table 11 lists key transport parameters and their values for the overlying aquifer. Element Pb is implemented as non-sorbing in the assumed carbonate aquifer because analysis for its sorption behavior on the aquifer filling materials has not been completed. The dose rate at the biosphere is calculated with the reference biosphere model discussed in Section 4.13, using the dose conversation factor of the IAEA ERB 1B model (IAEA 2003).

5. MODEL RESULTS

This section discusses the initial PA analysis results to evaluate the technical feasibility of direct disposal of the ER salt waste in a salt repository. As described in Section 3, the model results are presented in terms of the mean radionuclide mass release rate from the repository subsystems (such as salt waste form, repository interbed, repository access shaft, far-field to the biosphere, etc.) as the intermediate metrics of performance, and the mean annual dose (mrem/yr) by individual radionuclide at the hypothetical biosphere. The model analysis was performed probabilistically, with 100 realizations over a time period of 1,000,000 yr.

Table 11. Far-Field Model Parameters for Radionuclide Transport in Overlying Carbonate Aquifer

Parameter	Distribution Type	Parameter Value and Description	Source
Matrix Porosity	Uniform	0.07 (min); 0.3 (max)	Lappin et al. (1989), Table E-6; Brush and Storz (1996)
Bulk Density	Constant	2800 kg/m ³	
Matrix Tortuosity	Uniform	0.03 (min); 0.5 (max)	
Brine Flow Rate Upward through Repository Access Shaft (m/yr)	N/A	Sample from 100 time-dependent flow rate histories	Section 4.10 of this report
Aquifer Groundwater Flow Rate (m/yr)	Log-uniform	3.15E-03 (min); 3.15E+01 (max)	Helton et al. (1998), Figure 12.1.1
Longitudinal Dispersivity	Constant	10% of flow conduit length	
<i>Kd for radioelements (mL/g):</i>			
U	Uniform	0.03 (min); 20 (max)	Brush and Storz (1996); Muller et al. (1981); Pepping et al. (1983); Tien et al. (1983)
Pu	Log-uniform	20 (min); 1.0E+04 (max)	
Np	Log-uniform	1 (min); 200 (max)	
Am	Uniform	20 (min); 400 (max)	
Th	Log-uniform	7.0E+02 (min); 1.0E+04 (max)	
Tc	Triangular	0 (min); 50 (mode); 100 (max)	
Cs	Triangular	40 (min); 500 (mode); 3000 (max)	
Sr	Triangular	5 (min); 13 (mode); 4.0E+04 (max)	
Ac, Cm	Log-uniform	100 (min); 1.0E+05 (max)	McKinley and Scholtis (1992)
C	Log-uniform	1.0E-04 (min); 2000 (max)	
Nb	Constant	10	
Pa	Log-uniform	10 (min); 1000 (max)	
Pd	Uniform	4 (min); 100 (max)	
Sb	Constant	100	
Se	Uniform	1 (min); 8 (max)	
Sn	Log-uniform	50 (min); 700 (max)	
Zr	Log-uniform	10 (min); 8300 (max)	Miller and Wang (2012)
I	Uniform	0 (min); 1 (max)	
Cl, Pb	Constant	0 (no sorption)	

5.1 Reference Case Analysis

This section discusses the reference case analysis performed to evaluate the feasibility of direct disposal of ER salt waste in salt repository. The reference case is the baseline salt repository performance scenario to evaluate the impact of the ER salt waste disposal in a salt repository. The case evaluates RN releases and transport from the repository by a sequence of processes that are expected to occur in a generic salt repository. The case considers that the repository drift and shaft seals and the underlying interbed are the primary pathways for radionuclide release and transport from the repository to the biosphere.

5.1.1 Waste Package Failure

As discussed above, the salt disposal concept does not rely heavily on robust WP performance, but a reasonable wall thickness and mechanical strength is required to meet the WP design functions to prevent premature failure of WP during pre-closure operations: 1) handling and shielding, and 2) mechanical strength to withstand lithostatic pressure. The PA analysis has adopted the initial wall thickness of 7.5 cm for the carbon steel overpack as recommended in a recent study (Sevougian et al 2012), and assumes WP fails mechanically under lithostatic pressure when the remaining wall thickness of the overpack is reduced to 3 cm (Section 4.3). This gives a corrosion degradation layer of 4.5 cm for the overpack prior to the WP mechanical failure and renders a long WP performance time period, although it is not the intended primary performance function of the WP.

Figure 18 shows the model results of the mean overpack corrosion rate and mean overpack corrosion degradation depth as a function of time for the Mark-IV and Mark-V ER salt WPs. Figure 19 shows the model result for Realization 82, which has the highest overpack corrosion rates sampled for the Mark-IV ER salt WP. Results for other realizations show similar results and are not shown. As shown in the figures, there is no significant difference in the corrosion depth profile with time between the WPs, and this is because, except the first few hundred years, temperatures of both Mark-IV and Mark-V ER salt WPs are at the ambient temperature and because the overpack of the WPs corrodes at the low corrosion rates sampled from the 30°C corrosion rate model for most of the simulation period as shown in the left figures of Figure 18 and Figure 19 (also see Table 4).

The failure time distributions for Mark-IV and Mark-V ER salt WPs are similar, and they range from ~70,000 years to 150,000 years, with higher probabilities between ~90,000 and ~120,000 years. The analysis indicates that a thinner wall overpack may be sufficient for the ER salt WPs, and sensitivity analyses were conducted to investigate this WP design aspect (Section 5.2.1).

The pore volumes of the overpack corrosion products per WP (see Section 4.7), which is the volume of brine for each WP that is available to dissolve salt waste and RNs, range from 4.3 L to 29 L with the most frequency at ~16.5 L.

5.1.2 Salt Waste Form Releases

The salt waste dissolution and RN release rate is assumed conservatively to be congruent to the dissolution of LiCl, which is highly soluble in water. The PA model uses the LiCl solubility of 12.9 M, or the Li elemental solubility of 90 g/L. In the Goldsim framework, the congruent dissolution of waste form is modeled following the dissolution process of its matrix material, or the material with the greatest mass, which is LiCl for the ER salt waste. The dissolution process is modeled as follows. Once the WP fails, the entire inventory of waste form in the failed WP is exposed, and initially, all of the exposed inventory is treated as 'precipitated mass'. As the simulation progresses, an increasing fraction of the matrix material (i.e., LiCl for the ER salt waste) dissolves subject to its solubility constraint, and simultaneously the same fraction of the other species in the inventory is separated from the matrix and

made available for transport. These other species then either dissolve or precipitate out, depending on their solubility limits (Goldsim 2010).

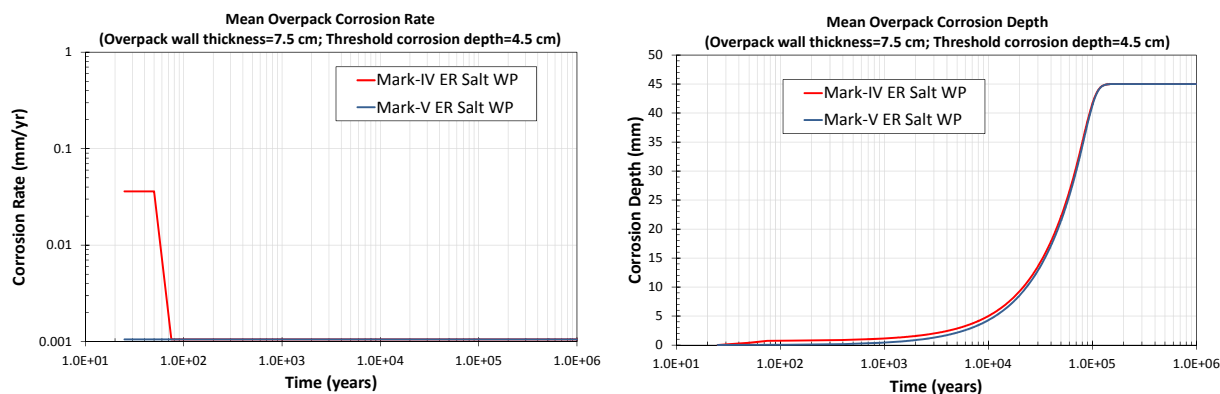


Figure 18. Model Result of Mean Overpack Corrosion Rate (left) and Mean Overpack Corrosion Depth (right) as a Function of Time for Mark-IV and Mark-V ER Salt Waste Packages.

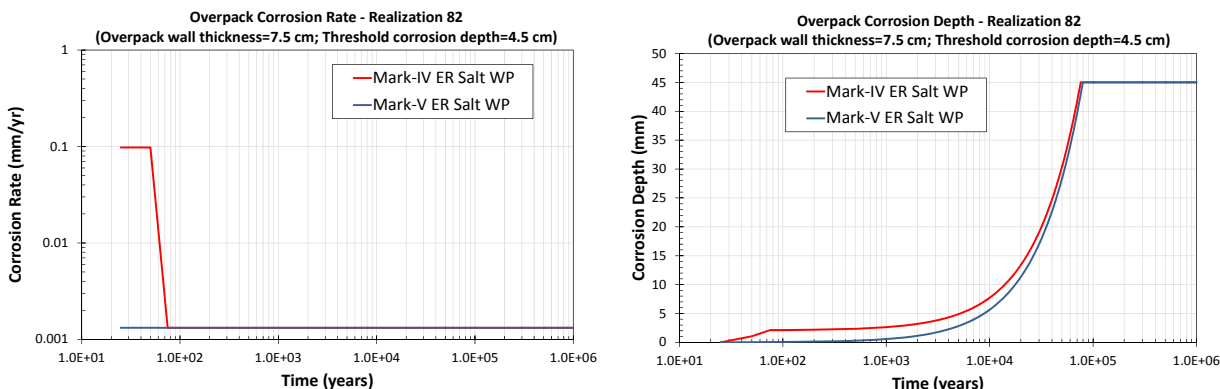


Figure 19. Model Result of Overpack Corrosion Rate (left) and Overpack Corrosion Depth (right) as a Function of Time for Mark-IV and Mark-V ER Salt Waste Package for Realization 82.

Figure 20 shows the model results of the mean masses of major RNs in the Mark-IV ER salt waste up to WP failure. The left figure shows the mean masses, and the RN masses are the mean of 100 values at each simulation time step. Decrease in Pu-239 mass and increase in U-235 mass prior to the WP failure are due to the decay of Pu-239 (half-life of 2.41×10^4 years) to U-235. The modeled RN masses after WP failure are shown better in individual realizations. As shown in the right figure for Realization 88 and as discussed above for the congruent salt waste form dissolution, upon WP failure, the entire inventory is treated as exposed and precipitated mass.

Although it is not radioactive and does not pose radiological hazards, Li is included in all the result plots because dissolution of LiCl in the ER salt waste is used as the marker for the salt waste dissolution (i.e., salt waste dissolution congruent to LiCl dissolution, see Section 4.9) and also because its transport behavior is useful to understand transport of other RNs as it is highly soluble, non-sorbing, non-decaying and the most abundant element in terms of moles in the salt waste (see Section 4.2).

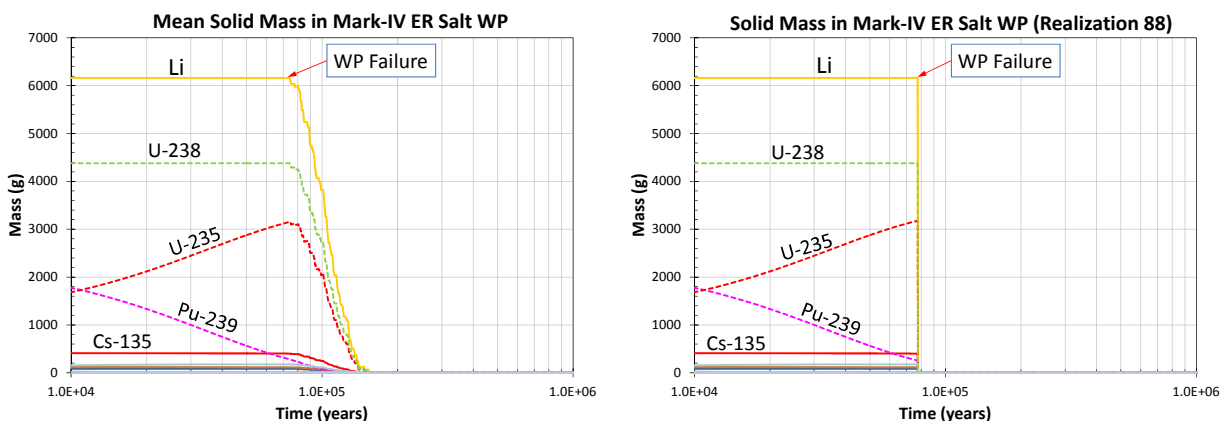


Figure 20. Model Result of Major RNs in Salt Waste of Mark-IV ER Salt WP: Mean RN Masses (left), and RN Masses for Realization 88 (right).

Figure 21 shows the modeled result for the mean dissolution of salt waste in the Mark-IV ER salt WP, shown as the mean remaining masses of ER salt waste components. Only Li, Cs-135 and I-129 are shown in the figure, and their mean remaining masses follow the pattern of Li as the salt waste dissolution is congruent to LiCl dissolution. Dissolution of other components with a smaller mass (not shown in the figure) also follows the pattern of LiCl dissolution. The figure also shows the model result of the mean masses of precipitates of actinides with a low solubility constraint. Again, decrease in Pu-239 mass in the precipitate is due to the decay of Pu-239 to U-235.

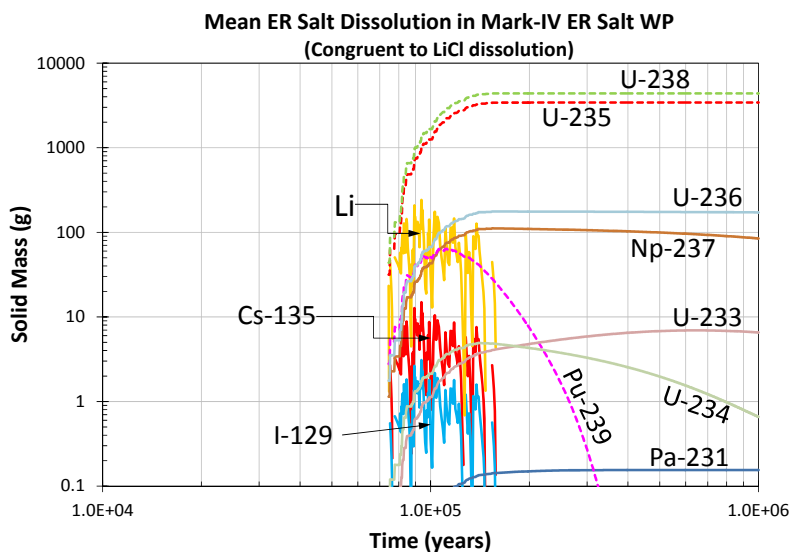


Figure 21. Model Result of Mean ER Salt Dissolution and Mean RN Precipitate Masses in Mark-IV ER Salt WP.

The modeled ER salt waste dissolution is better shown in individual realizations, and Figure 22 shows the modeled results for Realization 88 (left figure for the longest duration of LiCl dissolution-controlled salt waste dissolution) and Realization 82 (right figure for no LiCl dissolution-controlled, i.e., instantaneous salt waste dissolution). Only six of 100 realizations of the modeled result show some noticeable duration

of LiCl dissolution-controlled salt waste dissolution, which ranges from 5,000 years to 15,000 years, and three of them have longer than 10,000 years.

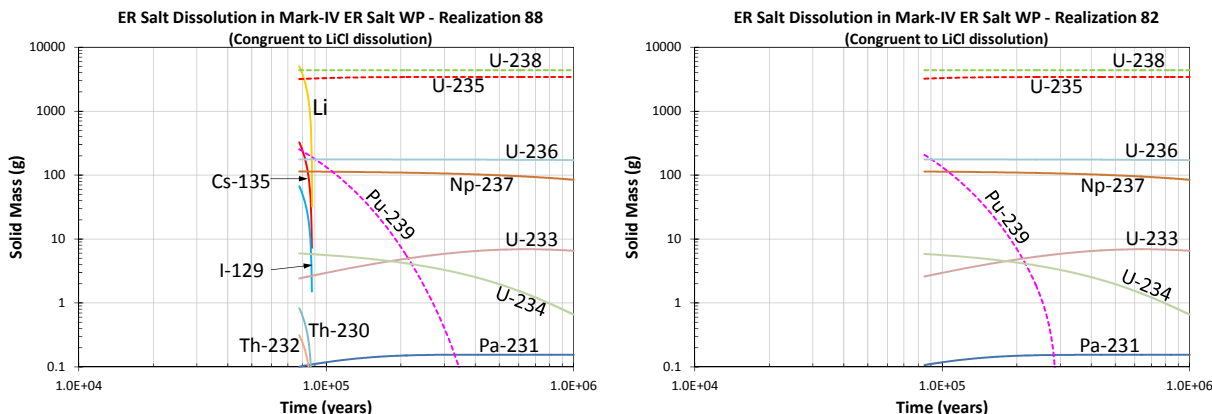


Figure 22. Model Result of ER Salt Waste Dissolution and RN Precipitate Masses in Mark-IV ER Salt WP: Realization 88 for LiCl dissolution control (left) and Realization 82 for no LiCl dissolution control (right).

As shown in the figures, the salt waste dissolution is fast, almost instantaneous relative to the simulation time steps, for most of the realizations. However, the geochemically reducing condition results in precipitation of most RNs as they are released from the salt waste due to low solubility of the solubility-controlling phases of the RNs in geochemically reducing conditions. This allows the released RNs to remain in the near-field as incorporated in the solubility-controlling solid phases and to be released slowly from the solid phases constrained by their low solubility. Only the RNs with the controlling solid phase with a high solubility (e.g., Cl-36) or with unconstrained solubility (e.g., I-129 and Cs-135) remain dissolved in the brine and continue to transport away from the repository and in the transport pathways towards the far-field and eventually the biosphere.

5.1.3 Repository Releases

The model results of the mean mass flux of RNs from the repository are shown in Figure 23. The flux curves of only a few RNs that are of interest to the analysis are labeled in the figures. The release rates in the figure represent the total releases from all the ER salt WPs (i.e., 9 Mark-IV and 6 Mark-V ER salt WPs). Note that the current PA analysis is conservative in that no RN sorption is modeled for the WP corrosion products and geologic materials in the repository near-field (see Section 4.14.1).

Comparisons of the mass fluxes of the RNs with high releases (i.e., Li (non-radioactive), Cs-135, I-129, Th-229, etc.) show that the mean total mass flux (top figure) from the repository is dominantly by diffusive flux (bottom left figure). Brine flows in the near-field are much greater than those away from it (see Section 4.10), but the near-field brine movements are not high enough that the advective mass fluxes (bottom right figure) of RNs are two to three orders of magnitude less than the diffusive mass flux. Difference in the RN mass transport rates between the two transport mechanisms becomes larger in the far-field mass releases, as discussed in the far-field RN release result sections.

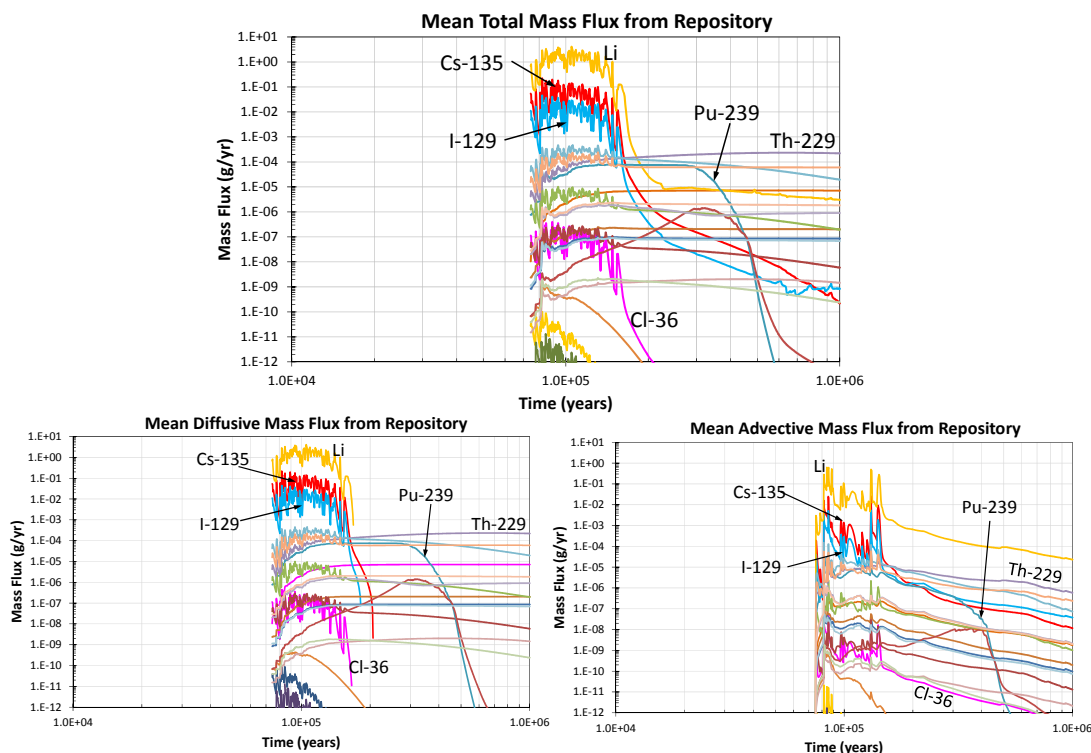


Figure 23. Model Result of Mean Mass Flux of RNs from Repository.

5.1.4 Interbed Releases

The RNs released from the repository are transported downward toward the underlying interbed by advection and diffusion and also transported to a nearby repository access shaft by advection (see Section 4.14). The RNs released into the interbed are transported laterally in the interbed by diffusion and advection in the direction of down-gradient toward the site boundary. The RNs in the interbed remain in the interbed as there are no hydrogeological features for brine flows from the interbed to biosphere. The PA model does not consider the RN diffusion from the interbed upward to the overlying aquifer because diffusive mass flux through intact salt rock and other overburden formations would be negligible. The PA model conservatively restricts the spreading of RN plumes in the interbed by limiting the width of interbed to 40 m (see Section 4.14).

Figure 24 shows the model result of the mean mass fluxes of RNs from the interbed at the repository footprint, which is below the ER salt waste emplacement area; the current PA assumes that the ER salt waste is emplaced on the edge of the repository footprint (see Section 4.4). The mean total mass fluxes of RNs are lowered significantly as the transport is retarded in the interbed by sorption on the interbed filling materials. Only non-sorbing Li (non-radioactive) still has a fairly high mass flux. As shown in Figure 24, diffusion is the dominant transport process, and the diffusive mass fluxes of RNs are four to five orders of magnitude greater than the advective mass fluxes. The brine movement in the interbed is negligibly slow (see Figure 15).

Figure 25 shows the model result of the mean total mass fluxes of RNs from the interbed at 1,000 m from the repository footprint. Except Li, only Cl-36 and I-129 have calculated mass flux at the location, and

their mass fluxes are negligibly small. No calculated releases of the RNs are reported beyond the location.

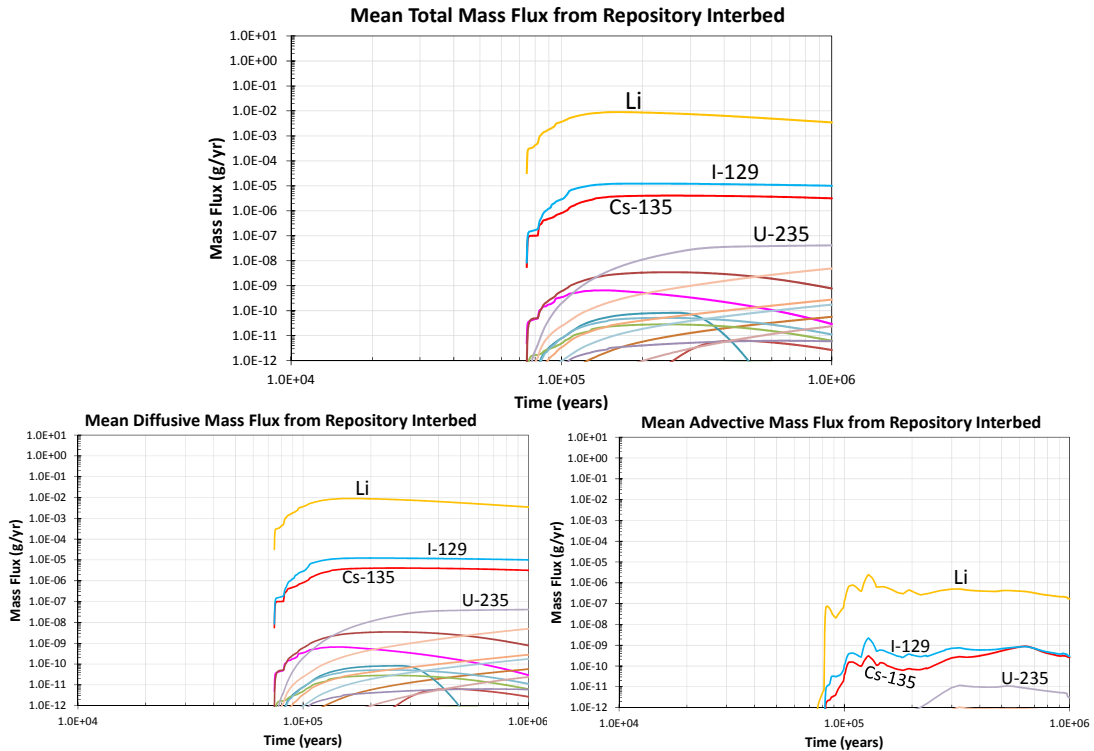


Figure 24. Model Result of Mean Mass Flux of RNs from Interbed at the Repository Footprint.

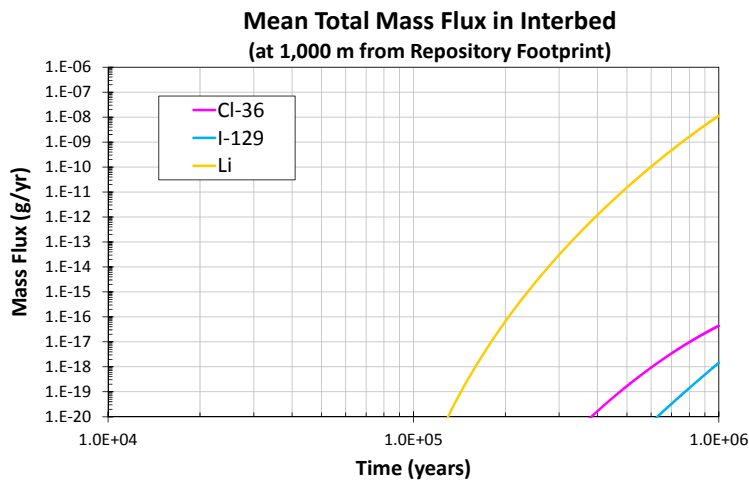


Figure 25. Model Result of Mean Mass Flux of RNs from Interbed at 1,000 m from the Repository Footprint.

5.1.5 Repository Shaft Releases

The RNs transported to a nearby repository access shaft from the ER salt WPs are transported upward in the shaft seal materials upward toward the overlying aquifer, and the length of the shaft ranges from 152 m to 457 m with the mode of 229 m (Table 5). The PA model assumes the shaft seal materials and their sorption properties for RNs are same as the interbed filling medium in the absence of the shaft seal material information. Because the shaft seal materials can be engineered to enhance long-term performance, the current PA approach is considered conservative.

Figure 26 shows the model result of the mean mass flux of RNs from the bottom a third section of the repository shaft. The mean total flux is dictated by the diffusive flux, and is dominated by the mean mass flux of I-129 (weakly sorbing) and Cl-36 (non-sorbing). Other RNs including Cs-135 have calculated mass fluxes by diffusion, but at much lower values. Advective flux of the RNs are four to five orders of magnitude lower than the diffusive flux because of very low brine movement in the shaft seals.

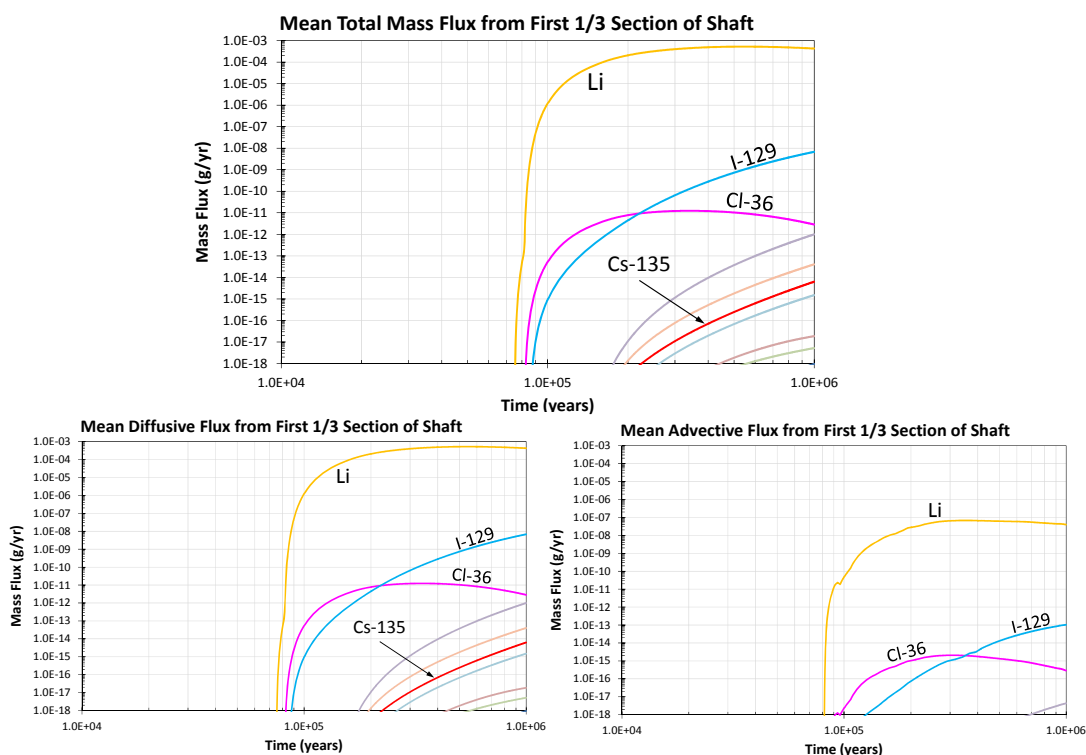


Figure 26. Model Result of Mean Mass Flux of RNs from Bottom Third Section of Repository Access Shaft.

The calculated mean mass flux from the top of the shaft is shown in Figure 27. Only the non-sorbing (Cl-36) or weakly sorbing (I-129) RNs are released from the shaft to the overlying aquifer, mostly by the diffusive transport; advective mass flux of the RNs at the shaft top is almost nil. A weak sorption of I-129 (K_d from zero to 1.0 mL/g, see Table 10) reduces the mass flux at the top by about eight orders of magnitude, compared to the mass flux at the bottom third of shaft (Figure 26). All other RNs do not have calculated mass flux from the shaft top as their transport is further retarded in the shaft by sorption.

The positive impact of the limited, very slow brine movement is obvious as the transport of any mobilized RNs (e.g., Cl-36 and I-129) in and away from the repository would be dominantly by very slow diffusional processes, and advective transport processes would be secondary in terms of the transport rates of the RNs. This results in very slow releases of RNs from the repository and very slow transport in the repository shaft.

In addition, transport of RNs entering the repository shaft is significantly retarded by sorption of the RNs on the shaft seals. The RNs would remain attached to the sorbent materials permanently or, at some degrees, to the materials sorption capacity, depending on the responsible sorption mechanisms. This would block the RNs from transporting further beyond or slow down significantly their transport, which will contribute to the effective isolation of the RNs from the biosphere.

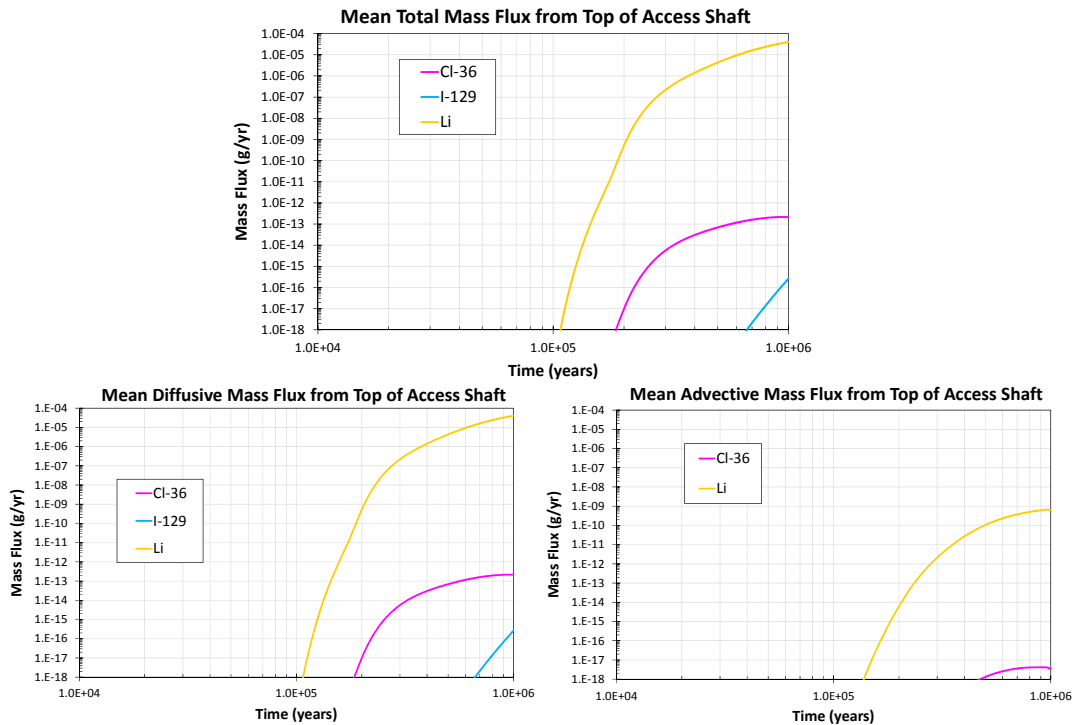


Figure 27. Model Result of Mean Mass Flux of RNs from Top of Repository Access Shaft.

5.1.6 Biosphere Releases and Dose

Figure 28 shows the model result of the mean mass flux of RNs from the overlying aquifer to a hypothetical biosphere located at the repository site boundary, which is 5 km down-gradient from the repository footprint. Only non-sorbing or weakly sorbing RNs (i.e., I-129 and Cl-36) with a significant inventory have calculated mass flux to the biosphere, but the mass release rates are insignificantly small. The contribution of the ER salt waste to the RN releases to the hypothetical biosphere considered in the PA analysis will be negligibly small. Although Li has the greatest flux, it is non-radioactive and not of interest. These RNs are those released from the access shaft to the overlying aquifer (see Figure 27). As discussed above, the RNs released to the underlying interbed remain in the interbed, and do not contribute to the releases to the overlying aquifer or biosphere.

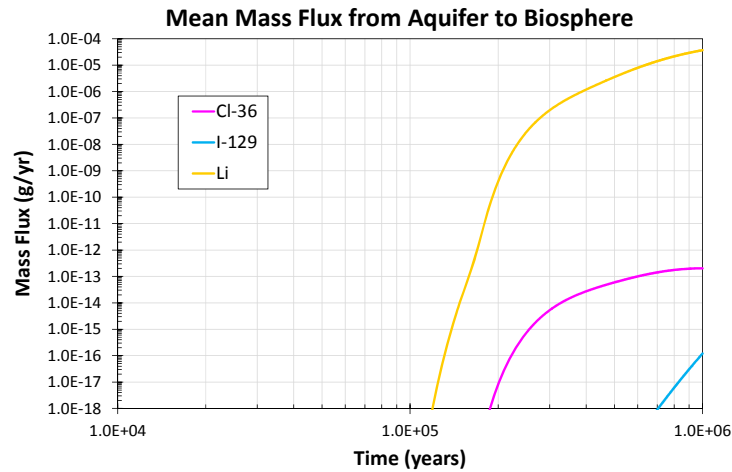


Figure 28. Model result of Mean Mass Flux of RNs from the Overlying Aquifer to the Hypothetical Biosphere Located at the Repository Site Boundary.

The model result of the mean annual dose at a hypothetical biosphere is shown in Figure 29. The dose rates by the RNs (I-129 and Cl-36) are negligibly small and will not have any impact on the repository performance. The PA analysis demonstrates the ER salt waste can be disposed of safely without extensive treatments in a bedded salt repository (a type of salt formation for the generic repository of this study). The analysis also demonstrates how a PA tools can be utilized to develop guidance for HLW waste management strategy.

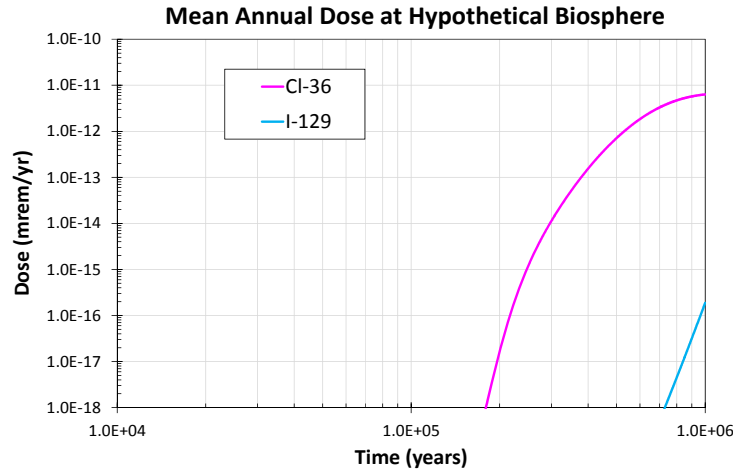


Figure 29. Model Result of Mean Annual Dose at the Hypothetical Biosphere Located at the Repository Site Boundary.

5.2 Sensitivity Analysis

Sensitivity analyses were conducted to evaluate salt repository performance responses to key system parameters that are relevant to the ER salt waste disposal. This FY analysis focused on two key parameters: WP overpack wall thickness, and salt waste dissolution rate. Additional and more detailed analyses for other parameters are planned in the future study.

5.2.1 Waste Package Overpack Wall Thickness

The reference case assumed the initial wall thickness of 7.5 cm for the carbon steel overpack, and WP fails mechanically under lithostatic pressure when the remaining wall thickness of the overpack is reduced to 3 cm (Section 4.3). This gives a corrosion degradation layer of 4.5 cm for the overpack prior to the WP mechanical failure and renders a long WP performance life (on the order of 100,000 years), although it is not the intended primary performance function of the WP in a salt repository disposal. A thinner carbon steel overpack would be sufficient for the salt disposal of ER salt waste, and a sensitivity analysis was conducted to evaluate the impact of a thinner overpack wall thickness on the repository performance response. The analysis was conducted for an overpack wall thickness of 5 cm, which provides a corrosion degradation layer of 2 cm prior to assumed mechanical failure of WP under lithostatic pressure. All other model parameters were kept the same as the reference case.

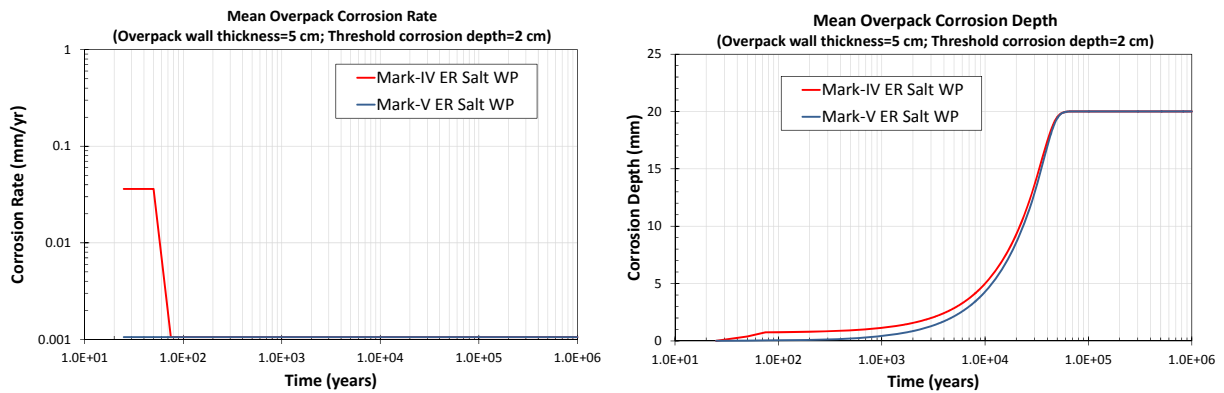


Figure 30. Sensitivity Analysis for Thinner WP Overpack: Model Result of Mean Overpack Corrosion Rate (left) and Mean Overpack Corrosion Depth (right) as a Function of Time for Mark-IV and Mark-V ER Salt Waste Packages.

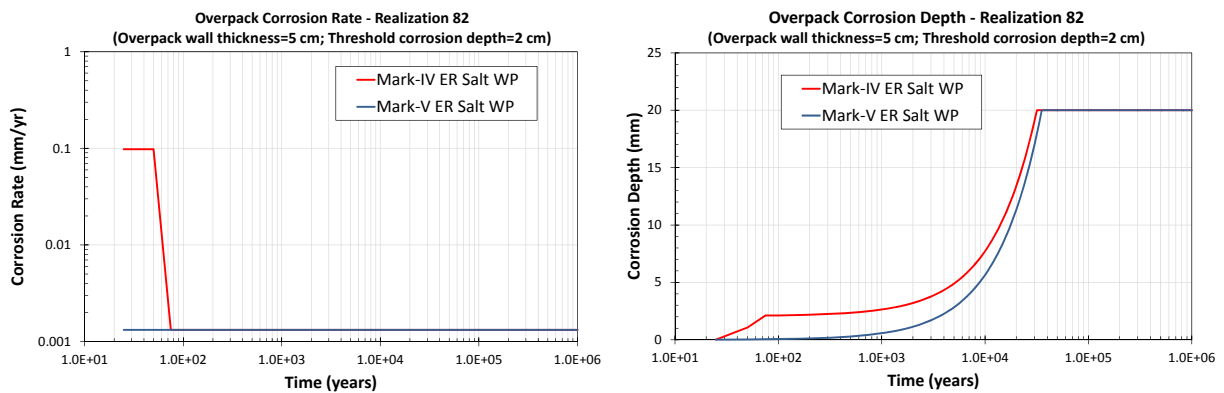


Figure 31. Sensitivity Analysis for Thinner WP Overpack: Model Result of Overpack Corrosion Rate (left) and Overpack Corrosion Depth (right) as a Function of Time for Mark-IV and Mark-V ER Salt Waste Packages for Realization 82.

The model results of the mean overpack corrosion rate and mean overpack corrosion degradation depth as a function of time for the Mark-IV and Mark-V ER salt WPs are shown in Figure 30. Figure 31 shows the model result for Realization 82 with the highest overpack corrosion rates sampled for the Mark-IV ER salt WP. As shown in the figures, there is no significant difference in the corrosion depth profile with

time between the WPs. This is because, for most of the simulation period, temperatures of both Mark-IV and Mark-V ER salt WPs are at the ambient temperature (Figure 12) and the WP overpack corrodes at low corrosion rates sampled from the 30°C corrosion rate model as shown in the left figures of Figure 30 and Figure 31 (also see Table 4).

The failure time distributions for Mark-IV and Mark-V ER salt WPs are similar, and they range from ~30,000 years to 66,000 years with the mean at ~46,000 years for Mark-IV ER salt WPs and from ~33,000 years to ~67,000 years with the mean at ~48,000 years for Mark-V ER salt WPs. The 2 cm corrosion degradation layer for the carbon steel overpack is enough to render long WP containment performance times for ER salt waste disposal.

The current PA model assumes that the pore volume of the overpack corrosion products surrounding the WP are the volume of brine for each WP that is available to dissolve salt waste and RNs (see Section 4.7). The corrosion product pore volumes per WP range from 2.6 L to 18 L with the mean at ~10 L; the resulting smaller volumes of brine, compared to the reference case, would render longer salt waste dissolution times for some realizations.

The modeled result for the mean dissolution of salt waste in the Mark-IV ER salt WP is shown in Figure 32 as the mean remaining masses of ER salt waste components. As shown in the figure, the mean remaining masses of Cs-135 and I-129 follow the pattern of Li as the salt waste dissolution is congruent to LiCl dissolution. Dissolution of other components with a smaller mass (not shown in the figure) also follows the pattern of LiCl dissolution. The figure also shows the model result of the mean masses of precipitates of actinides with low solubility constraints. Decrease in Pu-239 mass in the precipitate is due to the decay of Pu-239 to U-235.

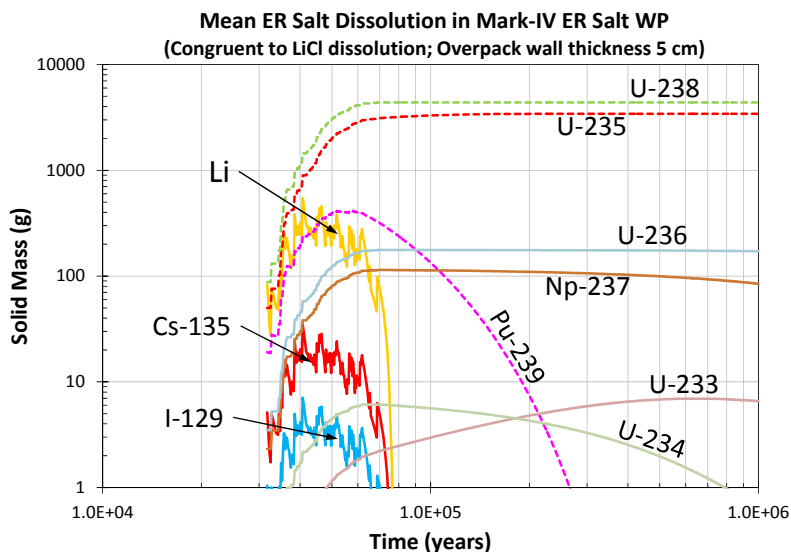


Figure 32. Sensitivity Analysis for Thinner WP Overpack: Model Result of Mean ER Salt Dissolution and Mean RN Precipitate Masses in Mark-IV ER Salt WP.

The modeled ER salt waste dissolution is better shown in individual realizations, and Figure 33 shows the modeled results for Realization 88 (left figure for the longest duration of LiCl dissolution-controlled salt waste dissolution) and Realization 82 (right figure for no LiCl dissolution-controlled, i.e., instantaneous salt waste dissolution). Nineteen (19) of 100 realizations of the modeled result show some noticeable

duration of LiCl dissolution-controlled salt waste dissolution, which ranges from 5,000 years to 20,000 years, and 10 of them have between 10,000 and 20,000 years.

As shown in the figures, the salt waste dissolution for the smaller brine volumes of the thinner overpack wall thickness case is rapid relative to the simulation time steps for most of the realizations (i.e., 90 % of the realizations). Most of the RNs precipitate out as they are released from the salt waste due to low solubility of the solubility-controlling phases of the RNs in geochemically reducing conditions. This results in the released RNs to remain in the near-field as incorporated in the solubility-controlling solid phases and to be released slowly from the solid phases constrained by their low solubility. Only the RNs with the controlling solid phase with a high solubility (e.g., Cl-36) or with unconstrained solubility (e.g., I-129 and Cs-135) remain dissolved in the brine and continue to transport away from the repository.

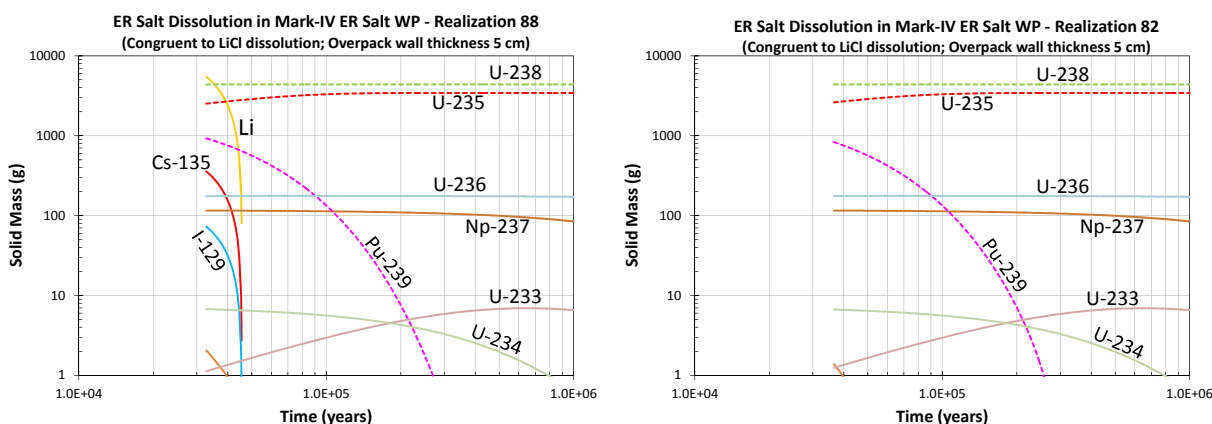


Figure 33. Sensitivity Analysis for Thinner WP Overpack: Model Result of ER Salt Waste Dissolution and RN Precipitate Masses in Mark-IV ER Salt WP: Realization 88 for LiCl-dissolution control (left) and Realization 82 for no LiCl-dissolution Control (right).

Figure 34 shows the model results of the mean mass flux of RNs from the repository. The flux curves of only a few RNs that are of interest to the analysis are labeled in the figures. The release rates in the figure represent the total releases from all the ER salt WPs (i.e., 9 Mark-IV and 6 Mark-V ER salt WPs). The PA analysis treats conservatively no sorption of RNs on the WP corrosion products and geologic materials in the repository near-field (Section 4.14.1).

As for the reference case analysis (Figure 23), the mean total mass flux (top figure) from the repository is dominantly by diffusive flux (bottom left figure). The near-field brine movements are not high enough that the advective mass fluxes (bottom right figure) of RNs are two to three orders of magnitude less than the diffusive mass flux. Difference in the RN mass transport rates between the two transport mechanisms becomes larger in the far-field mass releases. As shown in the figures, the repository RN release behaviors such as the mean peak release rate and mean release curve shapes are similar to the reference case releases (Figure 23) except the earlier release times from earlier WP failure times. The result shows that the WP failure time does not affect the mean repository RN mass release rates, except the release time profiles, for the ER salt waste disposal in a salt repository.

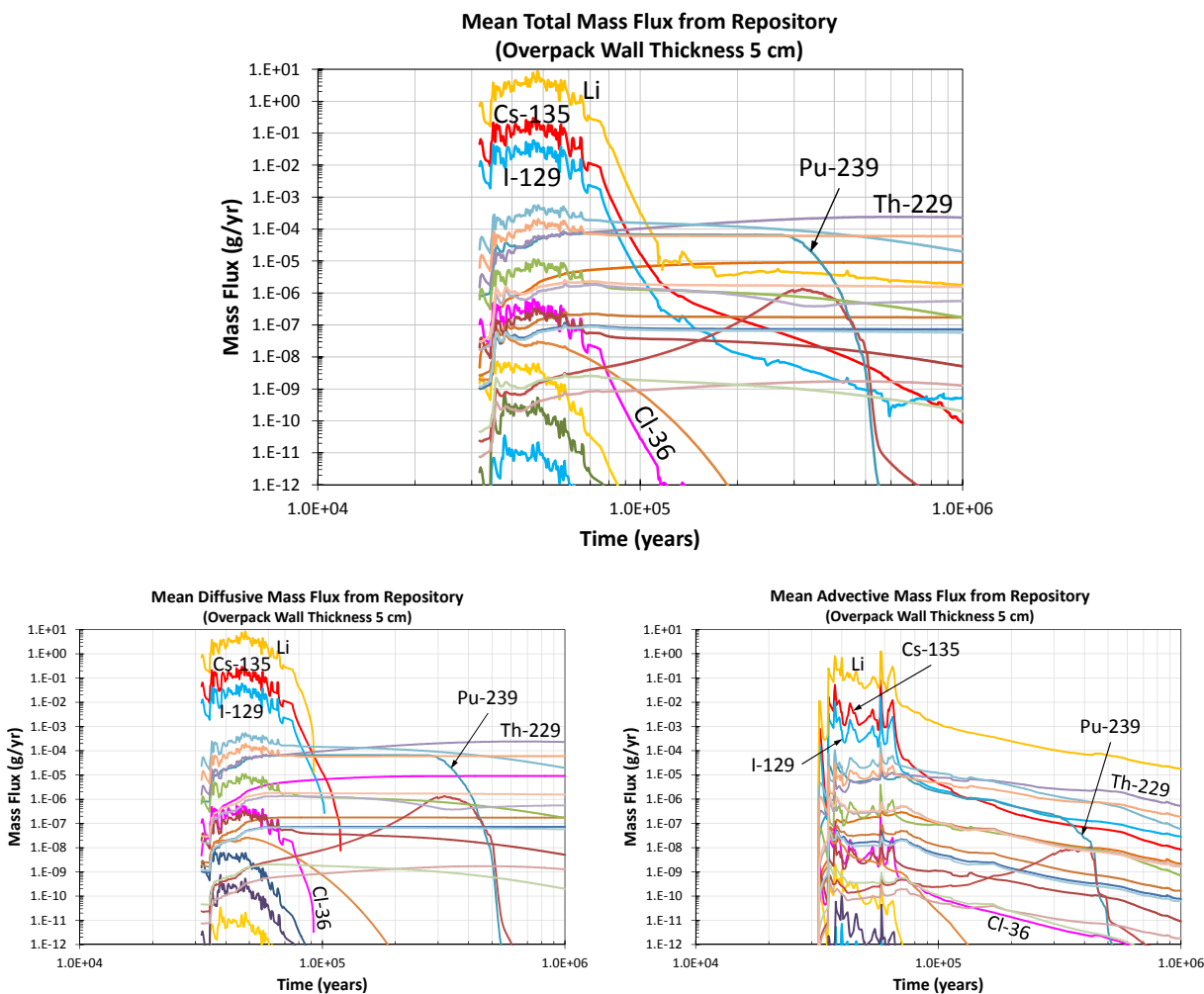


Figure 34. Sensitivity Analysis for Thinner WP Overpack: Model Result of Mean Mass Flux of RNs from Repository: Mean total mass flux (top), Mean diffusive mass flux (bottom left), and Mean advective mass flux (bottom right).

Figure 35 shows the model result of the mean total RN mass fluxes from the interbed at the repository footprint (left figure) and the mean total RN mass fluxes from the interbed at 1,000 m from the repository footprint (right figure). The mean interbed total releases are similar to the reference case releases, except earlier releases (Figure 24 and Figure 25). Note that the PA model assumes that the ER salt waste is emplaced on the edge of the repository footprint (Section 4.4). The mean RN total mass fluxes decrease significantly as the transport is retarded in the interbed by sorption on the interbed filling materials. Only non-sorbing Li (non-radioactive) still has a fairly high mass flux in the interbed at the repository boundary. At 1,000 m from the repository footprint, only Cl-36 and I-129, except Li, have calculated mass flux, and their mass fluxes are negligibly small. No calculated releases of the RNs are reported beyond the location.

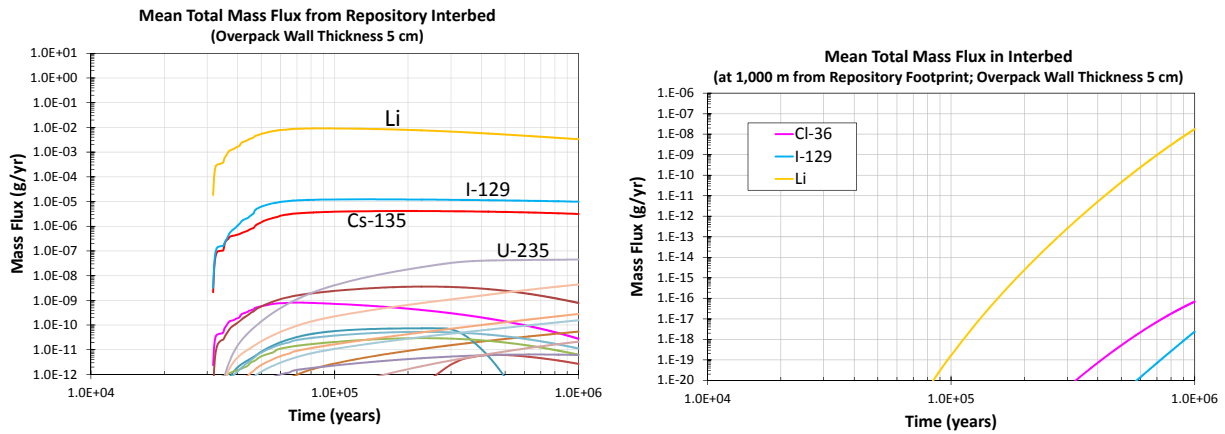


Figure 35. Sensitivity Analysis for Thinner WP Overpack: Model Result of RN Mass Flux in Interbed: Mean total mass flux at the repository boundary (left), and at 1,000 m from repository boundary (right).

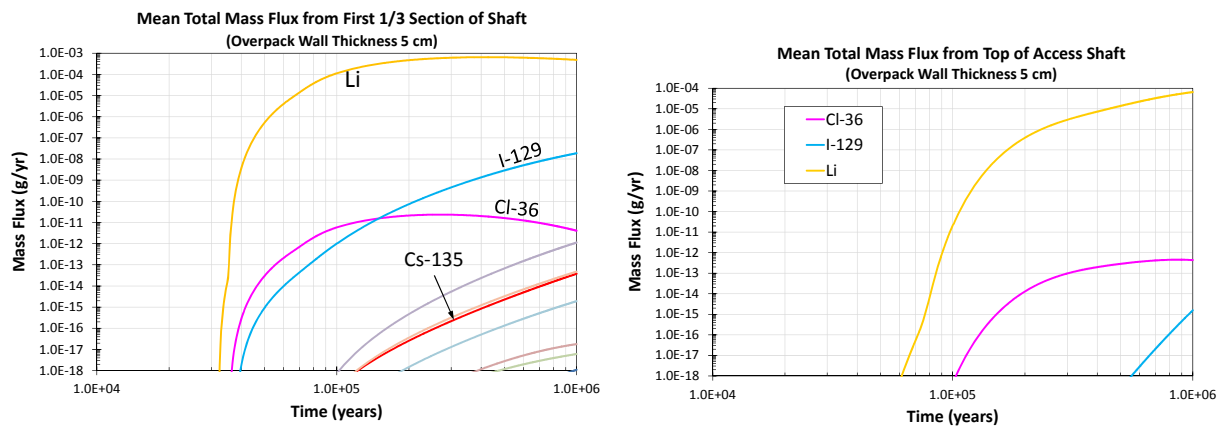


Figure 36. Sensitivity Analysis for Thinner WP Overpack: Model Result of RN Mass Flux in Repository Access Shaft: Mean total mass flux from the bottom a third section (left), and at the shaft top (right).

Figure 36 shows the model result of the mean RN total mass flux from the bottom a third section (left figure) and top (right figure) of the repository shaft. Again the RN mass releases from the repository shaft are similar to the reference case releases in terms of the release rate and release curve shapes (Figure 26 and Figure 27). The mean total flux is dominated by the diffusive mass flux of I-129 (weakly sorbing) and Cl-36 (non-sorbing). Other RNs including Cs-135 have calculated mass fluxes by diffusion at the bottom a third section, but at much lower values; the advective flux is four to five orders of magnitude lower than the diffusive flux.

Only the non-sorbing (Cl-36) or weakly sorbing (I-129) RNs are released from the shaft to the overlying aquifer, mostly by the diffusive transport; advective mass flux of the RNs at the shaft top is almost nil. All other RNs do not have calculated mass flux from the shaft top as their transport is further retarded in the shaft by sorption.

Figure 37 shows the model result of the mean mass flux of RNs from the overlying aquifer to a hypothetical biosphere (left figure) located at the repository site boundary (5 km down-gradient from the repository footprint) and the mean annual dose at the biosphere (right figure). As for the reference case, only non-sorbing (i.e., Cl-36) or weakly sorbing RNs (i.e., I-129) have calculated mass flux to the biosphere, and the Cl-36 and I-129 peak mean mass release rates are slightly higher than the corresponding reference case peak mean release rates (Figure 28). However, the biosphere RN mass release rates are insignificantly small, and the contribution of the ER salt waste to the RN releases to the hypothetical biosphere for the thinner overpack wall thickness case is negligibly small. The mean annual dose rates by the RNs (I-129 and Cl-36) are negligibly small and do not have any impact on the repository performance.

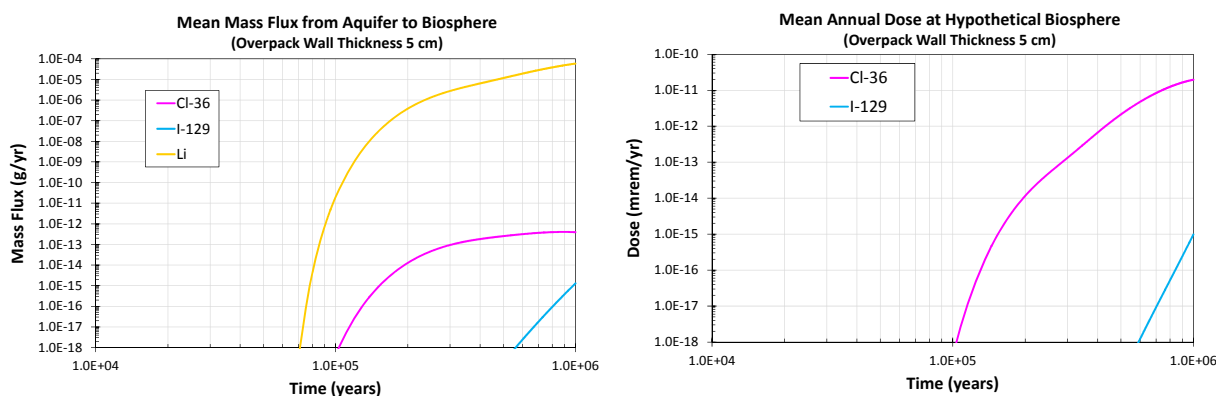


Figure 37. Sensitivity Analysis for Thinner WP Overpack: Mean total RN mass flux from overlying aquifer to hypothetical biosphere (left), and Mean annual dose by RNs (right).

5.2.2 ER Salt Waste Form Degradation

The reference case has adopted a conservative approach for dissolution of the ER salt waste by modeling its dissolution congruent to dissolution of LiCl, which is the most abundant salt compounds in the salt waste and highly soluble in water (12.9 M solubility). The approach resulted in rapid dissolution of the salt waste and fast release of RNs from the waste. However, as discussed in Section 5.1.2, most of the RNs released from the waste are subject to their solubility constraints in geochemically reducing conditions and precipitate out in the near-field. This allows the released RNs to remain in the near-field as incorporated in the solubility-controlling solid phases and to be released slowly from the solid phases constrained by their low solubility. Only the RNs with the controlling solid phase with a high solubility (e.g., Cl-36) or with unconstrained solubility (e.g., I-129 and Cs-135) remain dissolved in the brine and continue to transport away from the repository as they are released from the salt waste.

The geochemically reducing condition that is prevalent in the near field is one of the major attributes of a salt repository. The condition makes the salt repository disposal performance nearly insensitive to the waste form durability. A sensitivity analysis was conducted to evaluate the impact of a durable waste form for the ER salt waste on the salt repository performance response. The analysis assumes that the ER salt waste is incorporated into a borosilicate-like glass matrix, and the assumed waste form is referred to as "salt waste glass" in the report. Although it is not realistic, simplifying assumptions were made for the sensitivity analysis: 1) 100% loading of the salt waste in the glass matrix, and 2) the same salt waste mass

loading per WP as the reference case. The analysis assumes that the salt waste glass degrades in contact with brine at an annual fractional rate of $3.4 \times 10^{-6} \text{ yr}^{-1}$ to $3.4 \times 10^{-3} \text{ yr}^{-1}$ (log-uniform distribution), which are typical degradation rates for borosilicate glass waste form (Clayton et al 2011, Lee et al 2012). The analysis assumes 5 cm thick carbon steel overpack for the WP and uses the WP failure time distributions of the previous sensitivity analysis (Section 5.2.1).

The modeled result for the mean degradation of the Mark-IV ER salt waste glass in WP is shown in Figure 38 as the mean remaining masses of salt waste glass components. As shown in the figure, the mean degradation of the waste glass lasts very long for several 10^5 years after an initial high degradation rate period. Decrease in Pu-239 mass and increase in U-235 mass in the salt waste glass prior to WP failure is due to the decay of Pu-239 to U-235.

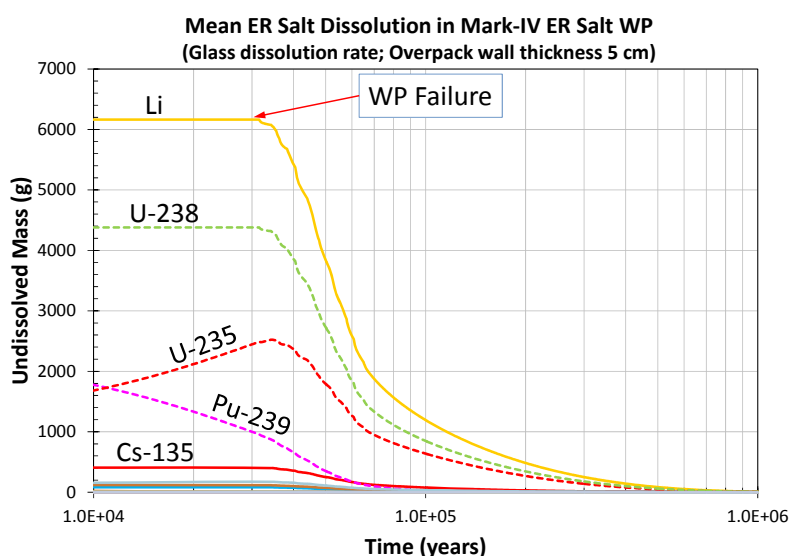


Figure 38. Sensitivity Analysis for Assumed ER Salt Waste Glass: Model Result of Mean ER Salt Waste Glass Degradation in Mark-IV ER Salt WP.

Figure 39 shows the modeled results for salt waste glass degradation for Realization 74 (left figure for the lowest degradation rate of $3.54 \times 10^{-6} \text{ yr}^{-1}$) and Realization 82 (right figure for the highest degradation rate of $3.24 \times 10^{-3} \text{ yr}^{-1}$) of the sampled rates for 100 realizations. At the lowest rate sampled for Realization 74, the assumed salt waste glass degrades extremely slowly over the entire simulation time period, while the waste glass dissolves rapidly, almost instantaneously relative to the simulation time step, at the highest rate sampled for Realization 82.

In the both end-member cases of the glass degradation rates, most of the RNs precipitate out as they are released from the salt waste glass because of the low solubility of the solubility-controlling phases of the RNs in geochemically reducing conditions, and their dissolved concentrations in the brine are same for the end-member cases, controlled by the solubility of their solubility-controlling solid phases. Only the RNs with the controlling solid phase with a high solubility (e.g., Cl-36) or with unconstrained solubility (e.g., I-129 and Cs-135) remain dissolved in the brine at high concentrations and continue to transport away from the repository. Typically Cl-36 and I-129 are the RNs that contribute dominantly to the RN mass releases from the repository and downstream repository subsystems (i.e., near-field, far-field, aquifer, etc.) and to the dose in the biosphere. Note that because of its strong sorption on geological

materials, Cs-135 transport in the near-field and far-field geologic systems is greatly retarded, and its releases from the geosphere are typically negligibly insignificant.

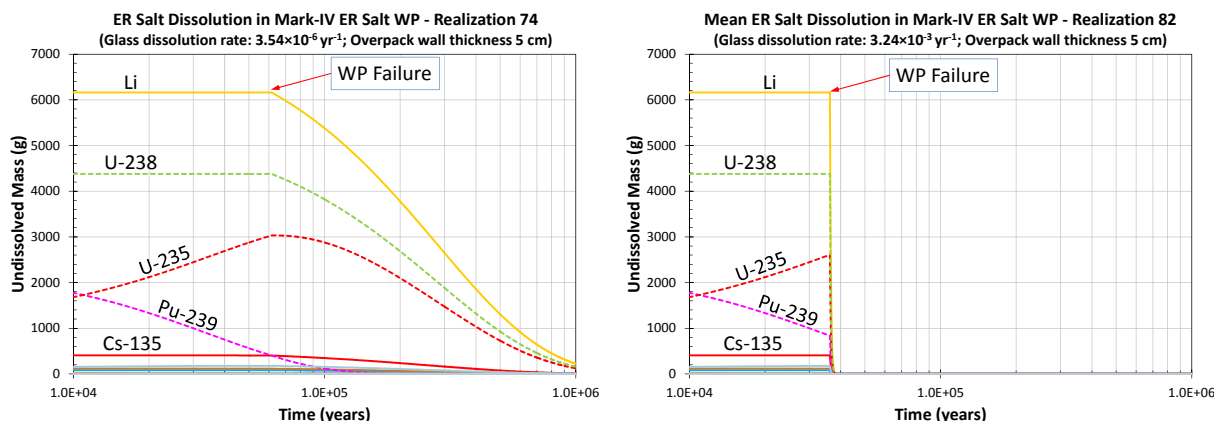


Figure 39. Sensitivity Analysis for Assumed ER Salt Waste Glass: Model Result of ER Salt Waste Glass Degradation in Mark-IV ER Salt WP: Realization 74 for the lowest degradation rate (left) and Realization 82 for the highest degradation rate (right).

As discussed later in this section, the above-mentioned geochemical condition feature, in combination with very limited brine movements, provides a basis that the waste form durability is not important to the safe permanent disposal of high-level nuclear waste in a salt repository.

The model results of the mean mass flux of RNs from the repository are shown in Figure 40. As for the previous analyses, the flux curves of only a few RNs that are of interest to the analysis are labeled in the figures. The release rates in the figure represent the total releases from all the ER salt WPs (i.e., 9 Mark-IV and 6 Mark-V ER salt WPs). The PA analysis assumes conservatively no sorption of RNs on the WP corrosion products and geologic materials in the repository near-field (Section 4.14.1).

As for the reference case analysis (Figure 23), the mean total mass flux (top figure) from the repository is dominantly by diffusive flux (bottom left figure), and the advective mass fluxes (bottom right figure) are two to three orders of magnitude less than the diffusive mass flux. Comparison of the results in the figures with the repository releases of the sensitivity analysis for thinner (5 cm thick) overpack with the reference-case salt waste dissolution (congruent dissolution to LiCl dissolution) (Figure 34) shows the mean peak release rates are similar to those of the sensitivity analysis, reinforcing the basis that the mean peak release rates are not affected by the waste form durability.

The release rate behaviors (i.e., release rate curve shapes) are impacted by the waste form durability, and the mean release rates following the peak rate decrease much more slowly than those of the reference case (Figure 23) or the sensitivity analysis for thinner overpack (Figure 34). This is due to much slower degradation rates of the salt waste glass assumed in the current sensitivity analysis than the ER salt waste dissolution (congruent to LiCl dissolution) modeled in the reference case (Figure 21 and Figure 22) or in the other sensitivity analysis (Figure 32 and Figure 33). Impact of lower salt waste glass dissolution rates is however not shown in the RN releases further away from the source-term as discussed below for the interbed and repository shaft releases.

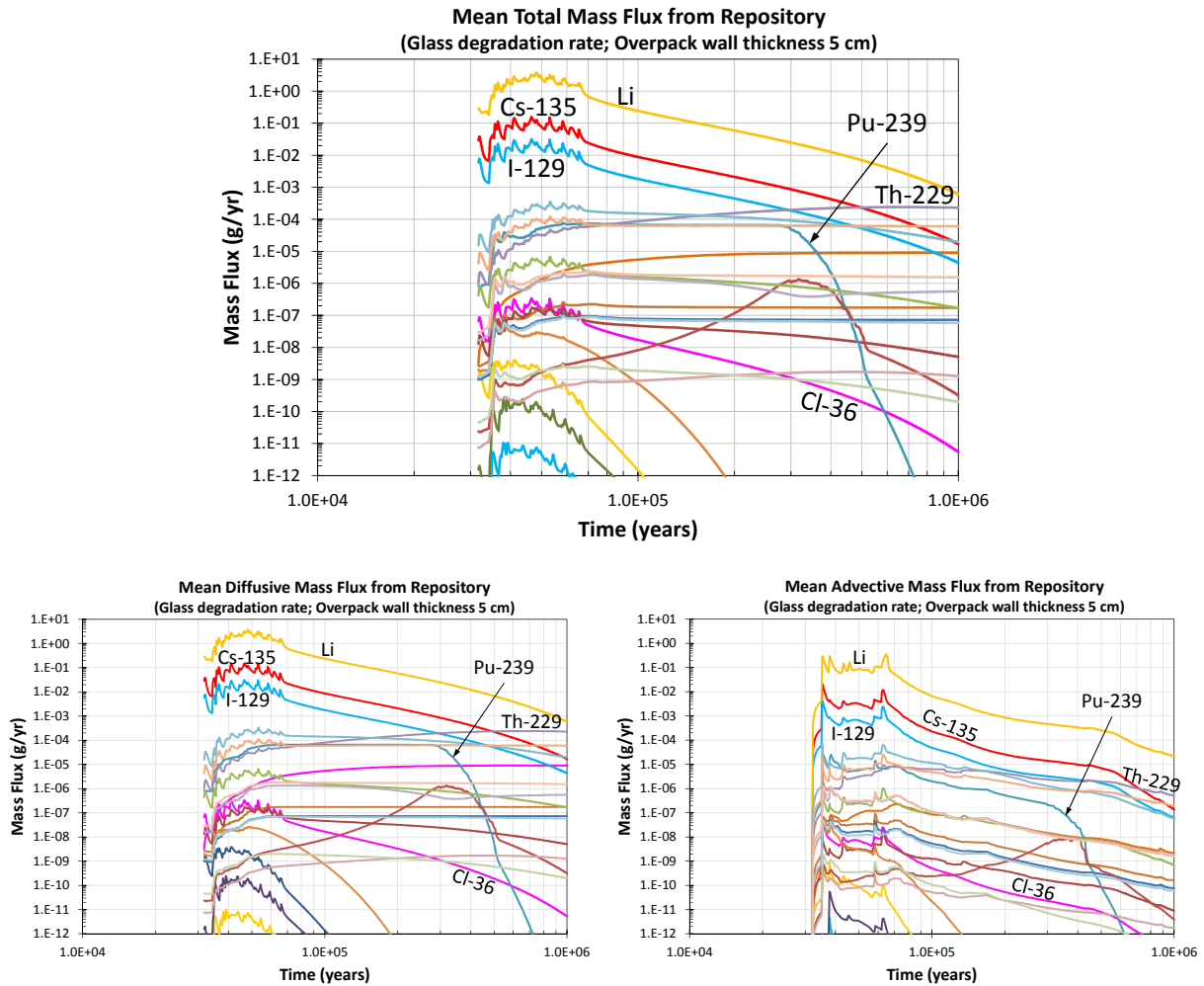


Figure 40. Sensitivity Analysis for Assumed ER Salt Waste Glass: Model Result of Mean Mass Flux of RNs from Repository: Mean total mass flux (top), Mean diffusive mass flux (bottom left), and Mean advective mass flux (bottom right).

Figure 41 shows the model result of the mean total RN mass fluxes from the interbed at the repository footprint (left figure) and the mean total RN mass fluxes from the interbed at 1,000 m from the repository footprint (right figure). The mean interbed total release rates are close to those of the sensitivity analysis for the 5 cm-thick overpack case (Figure 35). The mean RN total mass fluxes decrease significantly as the RN transport is retarded in the interbed by sorption on the interbed filling materials. As for the previous analyses, only non-sorbing Li (non-radioactive) has a fairly high mass flux in the interbed at the repository boundary. For RN releases at 1,000 m from the repository footprint, only Cl-36 and I-129 have calculated mass flux, but their mass fluxes are negligibly small. No calculated releases of the RNs are reported beyond the location.

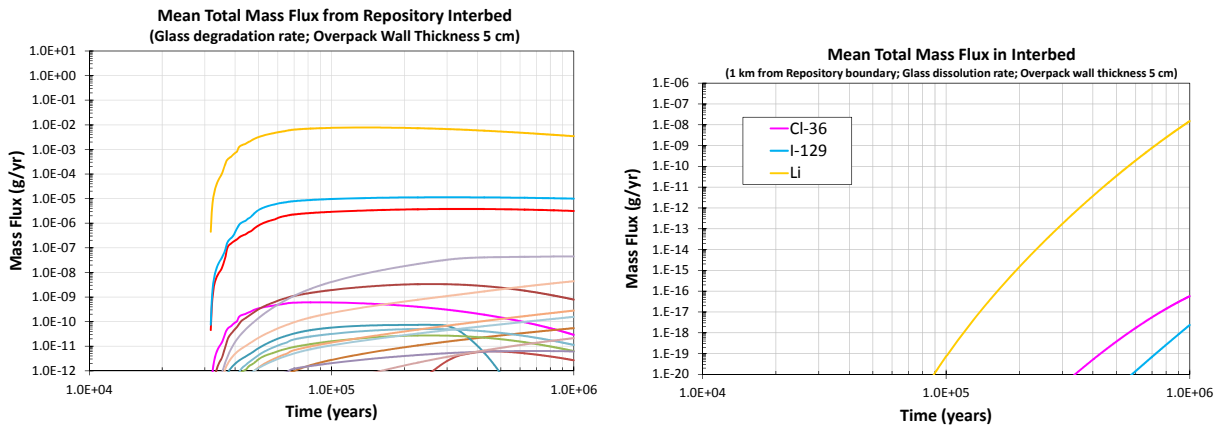


Figure 41. Sensitivity Analysis for Assumed ER Salt Waste Glass: Model Result of RN Mass Flux in Interbed: Mean total mass flux at the repository boundary (left), and at 1,000 m from repository boundary (right).

Figure 42 shows the model result of the mean RN total mass flux from the bottom a third section (left figure) and top (right figure) of the repository shaft. Again the RN mass releases from the repository shaft are similar to those of the sensitivity analysis for the thinner WP overpack case (Figure 36). Similar analyses are drawn such that the mean total flux is dominated by the diffusive mass flux of I-129 (weakly sorbing) and Cl-36 (non-sorbing). Other RNs including Cs-135 have calculated mass fluxes by diffusion at the bottom a third section at much lower values, and the advective flux is four to five orders of magnitude lower than the diffusive flux. Only Cl-36 and I-129, except non-radioactive Li, are released from the shaft to the overlying aquifer, dominantly by the diffusive transport. All other RNs do not have calculated mass flux from the shaft top as their transport is further retarded in the shaft by sorption.

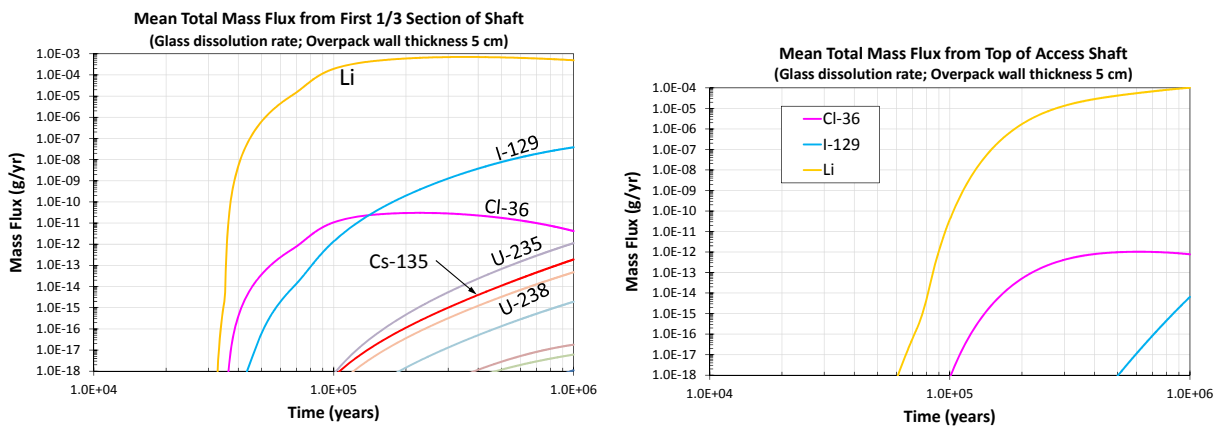


Figure 42. Sensitivity Analysis for Assumed ER Salt Waste Glass: Model Result of RN Mass Flux in Repository Access Shaft: Mean total mass flux from the bottom a third section (left), and at the shaft top (right).

Figure 43 shows the model result of the mean mass flux of RNs from the overlying aquifer to a hypothetical biosphere (left figure) located at the repository site boundary (5 km down-gradient from the repository footprint) and the mean annual dose at the biosphere (right figure). As for the reference case

(Figure 28 and Figure 29) and the sensitivity analysis case for thinner WP overpack (Figure 37), only Cl-36 (non-sorbing) and I-129 (weakly sorbing) have calculated mass flux to the biosphere, and the Cl-36 and I-129 peak mean mass release rates are slightly higher than the corresponding peak mean release rates of the sensitivity analysis case for thinner overpack (Figure 37). The biosphere RN mass release rates are insignificantly small, and the contribution of the ER salt waste to the RN releases to the hypothetical biosphere is negligibly small. The mean annual dose rates by the RNs (I-129 and Cl-36) are negligibly small and do not have any impact on the repository performance.

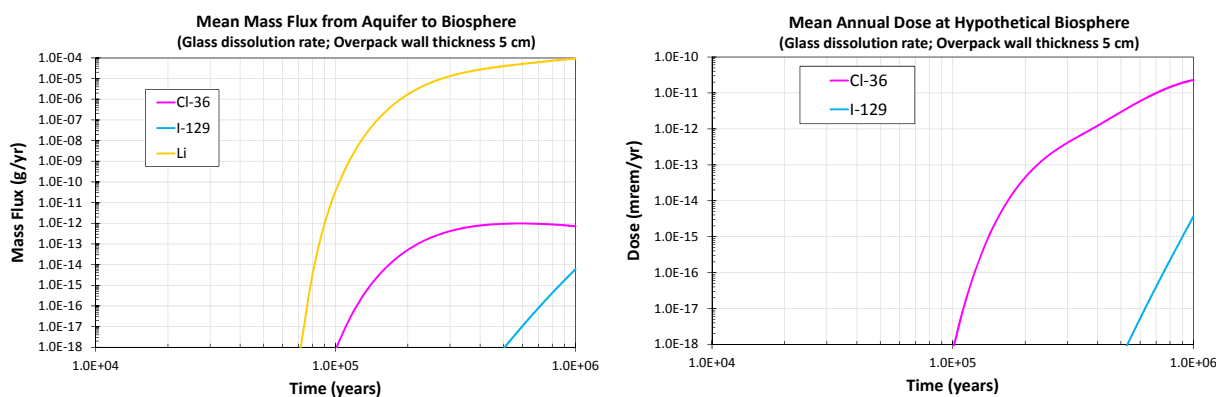


Figure 43. Sensitivity Analysis for Assumed ER Salt Waste Glass: Mean total RN mass flux from overlying aquifer to hypothetical biosphere (left), and Mean annual dose by RNs (right).

5.3 Disturbed Case Analysis

This section discusses the analysis performed to evaluate the impact of a disturbed case on the feasibility of direct disposal of ER salt waste in salt repository. As discussed in Section 5.1, the reference case PA analysis has shown that the contribution of the ER salt waste to the RN releases to the biosphere and to the dose rate of an individual will be negligibly small, and the ER salt waste can be directly disposed of safely in a bedded salt repository. The disturbed case is designed to provide a fast pathway for radionuclide release to the far field, bypassing a sequence of RN transport processes that would occur in a salt repository, and to evaluate the effect of the far-field performance on the salt waste disposal concept in response to the fast-pathway releases. The disturbed case analysis was conducted to provide additional information on the impact of the ER salt waste disposal in salt repository, and the analysis result is not considered as part of the baseline analysis for the disposal concept feasibility evaluation.

The very stable geology of salt formation allows elimination with a high confidence of potentially damaging disruptive events such as earth quakes and volcanic eruptions; these events are not applicable to the disturbed case analysis. One most probable case would be intrusion by future human drilling activity exploring natural resources, which is referred collectively to as the human intrusion for the disturbed case analysis.

The disturbed case is analyzed with a “stylized” human intrusion scenario, which assumes that a single borehole penetrates one Mark-IV ER salt WP at 1,000 years after repository closure, and other WPs are not affected by the event as WPs are encapsulated by salt backfill reconsolidation and salt rock creep deformation (see Sections 4.5 and 4.7). The case also assumes that a large pressurized brine reservoir exists below the repository and is also penetrated by the borehole. The brine in the reservoir could be at the pressure of the lithostatic pressure at the reservoir depth.

The human intrusion case assumes that the WP that is to be affected remains intact until a borehole penetration occurs. When borehole penetration has occurred (i.e., 1,000 year after repository closure), the affected WP and the disposal canister and salt containers inside the WP provide no barrier performance. The salt waste inside the affected WP starts to dissolve in contact with the brine.

As the penetrating borehole drill may not have a tight contact with the host rock, pressurized brines will also flow through the gaps between the drill and salt rock, flooding the area around the borehole including the damaged WP. In addition, upon contact with concentrated brines, the borehole drill (assumed to be metallic) would corrode and lose the structural feature in a relatively short time period. These would result in the brines from the penetrated reservoir flowing into the damaged WP and mixing of the brines the waste in the damaged WP. This will allow full contamination of the brine with dissolved RNs.

The pressurized brine would continue to allow the flow of contaminated brines upward inside the borehole as well as through the gaps between the drill and salt rock above the repository, resulting in the direct release of radionuclides into the overlying aquifer. Pressurized brine would move dissolved radionuclides from the affected WP up through the borehole, resulting in the direct release of radionuclides into the overlying aquifer. Pressurized brine reservoirs are found in a salt formation, and the feature is consistent with a human intrusion scenario developed for the performance assessment of the WIPP (Helton et al 1988). The current human intrusion scenario does not consider the potential dose impacts of the waste that could be brought up directly to the surface as a result of the drilling activities, as the analysis is designed to evaluate the effect of the far-field (or aquifer for this case) performance on the salt waste disposal concept, in response to the fast-pathway releases. The PA model assumes that the affected WP is located on the edge of repository footprint.

The steady-state brine flow rate through the borehole is sampled between 0.1 and 5.0 m³/yr (uniform distribution), which is the range used in the WIPP PA (Helton et al 1988). The reservoir capacity is modeled with a triangular distribution with the mode of 75,000 m³, lower bound of 30,000 m³ and upper bound of 150,000 m³ (Sevougian et al 2012). When brine in the reservoir is depleted, brine flow rate in borehole is changed to 0.0 to 0.1 m³/yr (uniform distribution), which is the range corresponding to the borehole brine flow rate with no brine reservoir penetration used in the WIPP PA (Helton et al 1988).

As for the reference case analysis, RNs released to overlying aquifer are transported advectively to a “hypothetical” biosphere located at the site boundary (5 km down-gradient from the repository footprint). The overlying aquifer is assumed to comprise primarily dolomite matrix with clays dispersed in the matrix, and the same geologic features and transport properties as the reference case are used in the analysis (see Table 11 for the transport parameters of the aquifer). The mass of radionuclides released to the overlying aquifer are evaluated against the solubility for the far-field dilute brine (Table 7). If the concentrations of radionuclides exceed their solubility limits, the excess mass of the radionuclides precipitates out of the water and remains as a solid until it dissolves back to the water. Sorption of radionuclides on the aquifer filling medium is modeled with an equilibrium K_d approach (Table 11). Element Pb is implemented as non-sorbing in the assumed carbonate aquifer because analysis for its sorption behavior on the aquifer filling materials has not been completed. The same reference biosphere model (IAEA ERB 1A model) (IAEA 2003) as for the reference case analysis is applied to calculate the dose.

Figure 44 shows the human intrusion case model result of the mean mass flux of RNs from the overlying aquifer to the hypothetical biosphere located at the repository site boundary, and Figure 45 shows the model result of the mean annual dose by RNs at the biosphere. As shown in the figures, the mean mass release rate and mean annual dose histories of the human intrusion case are very different from those of the reference case.

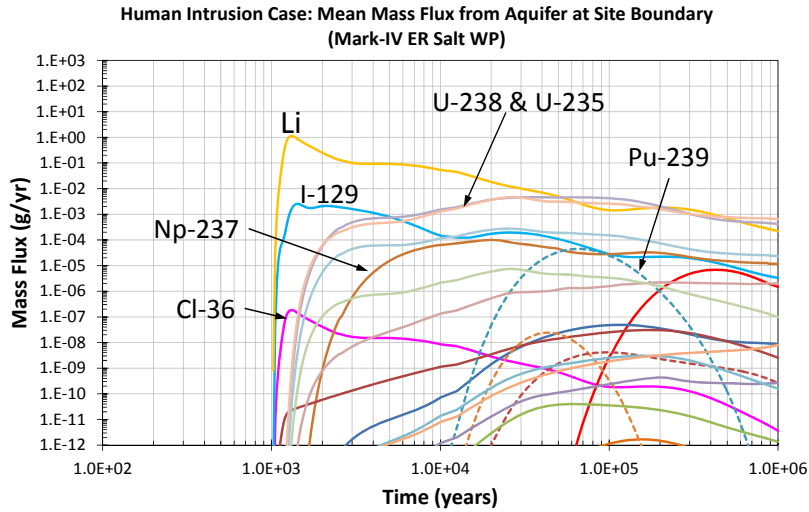


Figure 44. Human Intrusion Case Model Result of Mean Mass Flux of RNs from the Overlying Aquifer to the Hypothetical Biosphere Located at the Repository Site Boundary.

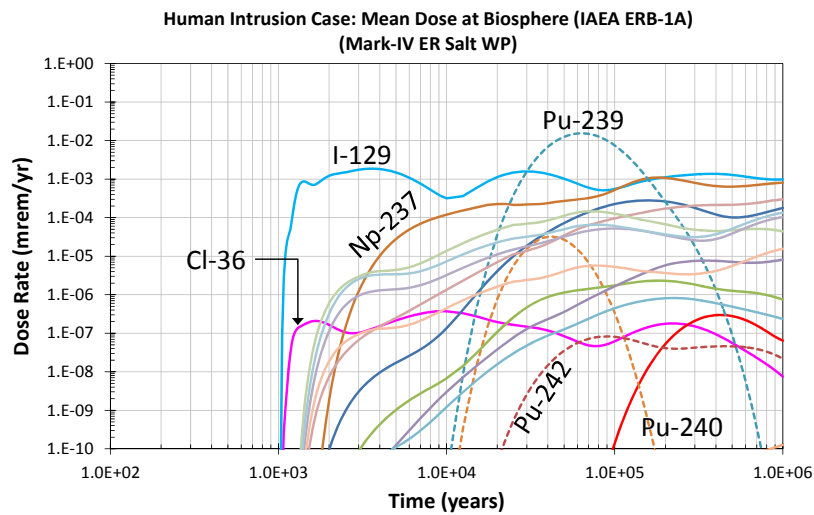


Figure 45. Human Intrusion Case Model Result of Mean Annual Dose at the Hypothetical Biosphere Located at the Repository Site Boundary.

Although the available inventory for the human intrusion case is much smaller than the reference case, that is, only one Mark-IV ER salt WP is affected by the event, the RN release rates to the biosphere and dose rates are much higher than the reference case. A few factors have contributed:

- RNs are released directly to the overlying aquifer at much higher rates than from the repository access shaft in the reference case,
- RNs released from the salt waste are subject to the solubility constraints first in the aquifer, for which condition RNs have higher solubility constraints (i.e., less reducing or slightly oxidizing conditions, see Table 7)

- RNs released to the aquifer are transported advectively in the aquifer at high groundwater flow rates

For the human intrusion case, Pu-239 is the dominant dose contributor, with I-129 and Np-237 being the early dominant dose contributors. The peak mean dose of about 0.01 mrem/yr by Pu-239 is still very low. For example, for the Yucca Mountain repository regulation, the individual radiation protection standard after permanent closure is 100 mrem/yr after 10,000 years, but within the period of geologic stability (10 CFR Part 63).

The long-term dose rate by Np-237 is about the same as I-129. Cl-36 is no longer a dominant dose contributor because of its limited inventory compared to the dominant actinide dose contributors. Compared to the reference case, the relative annual dose contributions by soluble, non-sorbing or weakly sorbing RNs, particularly Cl-36 and I-129, are much lower than those by actinides including ²³⁹Pu and ²³⁷Np. Especially the higher mean annual doses by the actinides are the outcome of the direct release of the radionuclides in the aquifer with high groundwater flow rates, thereby resulting in an early arrival of higher concentrations of the radionuclides at the biosphere drinking water well prior to their significant decay.

6. SUMMARY AND CONCLUSION

As part of the study to evaluate technical feasibility of direct disposal of ER salt waste in a salt repository, an existing PA model for a generic salt repository was improved substantially with the implementation of the source-term and WP configuration that are specific to the ER salt waste, and the incorporation of the latest understanding and representative geologic settings and features of generic salt disposal system processes. The models and processes of the repository subsystems that were newly implemented and/or updated for the current PA analysis include:

- ER salt waste inventory (Section 4.2)
- ER salt WP design and configuration (Section 4.3)
- WP thermal condition analysis (Section 4.6)
- WP corrosion environment (Section 4.7)
- WP overpack corrosion degradation (Section 4.8)
- ER salt waste dissolution (Section 4.9)
- Repository RN release and transport pathway conceptual model (Section 4.1)

Other processes and parameters were adopted for the PA analysis from the latest understanding and analysis related to the generic repository processes, and these include:

- WP emplacement in salt repository (Section 4.4)
- Salt consolidation and creep deformation (Section 4.5)
- Repository brine flow analysis (Section 4.10)
- Radionuclide solubility (Section 4.12)
- Salt repository natural barrier system parameters (Section 4.11)
- Generic biosphere model (Section 4.13)

The PA model was developed by implementing the above models and parameters in the Goldsim model framework (Goldsim 2010), utilizing the probabilistic analysis capability.

For the WP configuration and salt waste loading (~120 kg salt waste per WP) considered in the PA analysis, the per-WP decay heat output is low that no noticeable thermal perturbations were calculated for the Mark-V ER salt WPs, and moderate temperature increases (up to ~48 °C) only during first 200 years for the Mark-IV ER salt WPs. This low thermal perturbation renders no significant changes to the near-field thermal and geochemical conditions and allows use of the ambient geochemical conditions for the PA analysis. This provides the WP exposure conditions of low overpack corrosion rates, which results in a long WP lifetime, although it was not the intended design function of the WPs in salt repository. The salt waste dissolution in contact with brine, upon WP failure, is rapid, but as discussed below, most of the released RNs precipitate out as incorporated in the solubility controlling solid phase under geochemically reducing conditions and are released slowly from the solid phase in the near-field for very long time.

The initial PA analysis shows the ER salt waste can be disposed of safely without “extensive” treatments in a bedded salt repository (a type of salt formation in this study). The contribution of the ER salt waste to the RN releases to the biosphere and to the dose rate of an individual will be negligibly small. The conclusion is contributed by the major attributes of salt repository: 1) very stable geology, 2) anoxic geochemically reducing condition, 3) very limited brine movement, and 4) “self-healing” of salt rock by creep deformation.

The very stable geology attributes allows elimination with a high confidence of potentially damaging disruptive events such as earth quakes and volcanic eruptions that could present a high uncertainty in the future repository performance.

The geochemically reducing condition attribute results in precipitation of most RNs as they are released from the waste form, because of low solubility of the solubility-controlling phases of the RNs in geochemically reducing conditions. This attribute allows the released RNs to remain in the near-field as incorporated in the solubility-controlling solid phases and to be released slowly from the solid phases constrained by their low solubility. Only the RNs with the controlling solid phase with a high solubility (e.g, Cl-36) or with unconstrained solubility (e.g., I-129) would remain dissolved in the brine and continue to transport away from the repository and in the transport pathways towards the far-field and eventually the biosphere.

The positive impact of the limited brine movement attribute is obvious as the transport of any mobilized RNs (e.g., Cl-36 and I-129) in and away from the repository would be dominantly by very slow diffusional processes, and advective transport processes would be secondary in terms of the transport rates of the RNs. The attribute allows very slow releases of RNs from the repository and very slow transport in the repository far-field transport pathways.

The self-healing attribute, although not explicitly modeled in the PA analysis, refers to the healing by salt creep deformation of fractures and damages in the salt rock that could result from repository construction and pre-closure operations (especially in the excavation damage zones (EDZ)) and also from active thermal mechanical perturbations during the early post-closure time periods. The attribute allows restoration and healing of fractured and damaged salt rocks to the condition of or at least close to the intact salt rock within a time period that is “short” relative to the repository time frame and therefore allows such assumptions and treatments in the PA analysis.

In addition, other important attributes of a salt repository, which would be the same for other deep mined geological repository, would include sorption of mobilized RNs on geologic materials in the transport pathways such as the interbed, access shaft seals, and overlying aquifer. The RNs would remain attached to the sorbent materials permanently or, at some degrees, to the materials sorption capacity, depending on the responsible sorption mechanisms. This would block the RNs from transporting further beyond or

slow down significantly their transport, which will contribute to the effective isolation of the RNs from the biosphere.

The PA analysis also demonstrated salt repository performance is not sensitivity to the waste form durability. Figure 46 shows the effect of the durability of two ER salt waste types on the long-term repository performance in terms of the mean annual dose by radionuclides at a hypothetical biosphere as defined in the IAEA BIOMASS ERB 1A model (IAEA 2003): 1) raw ER salt waste with no treatments (salt waste dissolving congruent to LiCl dissolution, Section 5.2.1 for details of the sensitivity analysis) and 2) ER salt incorporated into a borosilicate-like glass (Section 5.2.2 for details of the sensitivity analysis). In the PA model the raw ER salt dissolves rapidly in contact with salt brine, almost instantaneously relative to the repository time frame, and the ER salt waste glass dissolves slowly with an annual fractional degradation rate ranging from $3.4 \times 10^{-6} \text{ yr}^{-1}$ to $3.4 \times 10^{-3} \text{ yr}^{-1}$ (log-uniform distribution), which are typical dissolution rates for borosilicate glass waste form. For the both cases the WP has the carbon steel overpack of 5 cm thick. As shown in the figure, the dose contributions by both the ER salt waste forms are negligibly small, and there are *practically no differences* in the peak mean annual dose and mean annual dose histories between the raw ER salt waste and assumed glass-incorporated ER salt waste. The PA analysis demonstrated that the waste form durability *is not important* to the disposal performance of a salt repository, as its performance is driven by its key performance attributes, not by waste form durability (i.e., very stable geology, geochemically reducing conditions, very limited brine movement, fracture healing and damage repair mechanism by creep deformation, radionuclide sorption on geologic materials, etc.). The analysis also demonstrates that high-level nuclear waste can be disposed of safely in a salt repository, with no or minimal treatments of the waste.

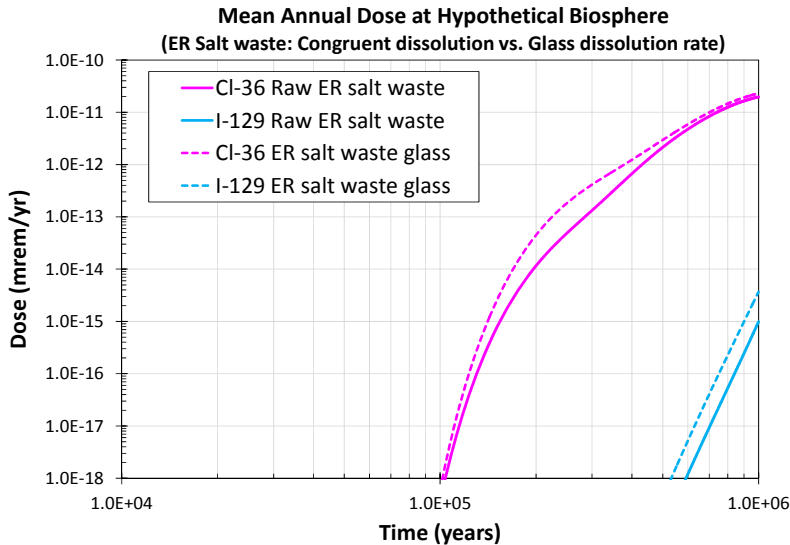


Figure 46. Comparison of the Effect of Durability of Two ER Salt Waste Types (Raw Salt without Treatment vs. Borosilicate-Like Salt Waste Glass) on Disposal Performance of a Generic Salt Repository in Terms of Mean Annual Dose by Radionuclides at Hypothetical Biosphere.

The feasibility of the direct disposal concept feasibility in a salt repository, as demonstrated by the PA analysis, is highly attractive relative to the current baseline ceramic waste form process because of the 13-fold increase in the salt waste mass loading per a unit mass of waste form. Two major problems related to

of the current baseline ceramic waste form are waste loading and process throughput. The salt waste loading of the ceramic waste form is only about 7.5 wt%. In addition, the consolidation process can take over two weeks to process a single full-scale ceramic waste form (Simpson et al 2013). The direct disposal concept is expected to dramatically reduce the cost of completing the EBR-II spent fuel treatment project as part of the Spent Fuel Treatment Program at INL. It also improves the attractiveness of the electrochemical treatment of used nuclear fuel for potential commercial implementation with respect to waste disposal requirements.

To add a defense-in-depth approach to the direct disposal concept, the options to consider may include selective separation and recycle of useful salts (LiCl-KCl) back to the electrorefiner as well as stabilization of the salt waste in zeolite without subsequent conversion to a ceramic waste form. These are the two base salts for the electrolyte that need not be disposed if they can be separated from the fission product chlorides and returned to the electrorefiners.

One process of current interest for the separation is salt deposition on a cold finger. Although it should be further investigated, the cold finger process could recycle a significant fraction of the LiCl-KCl back to the electrorefiner, which would reduce the salt waste volume and potentially increase salt waste dissolution performance in the repository as the LiCl content in the salt waste decreases.

The current study has demonstrated a great potential of utilizing a PA tools to develop guidance for HLW waste management strategy. A great amount of resources and time has been invested to develop highly durable waste forms for the HLW in the DOE complex, and this study and its outcome, although it is still an initial phase of the evaluation, provides an opportunity to re-consider the current baseline disposal approach, which is based on high performing and highly durable waste forms. This approach can also be applied to develop the management and disposal strategy for other HLW in the DOE complex that needs treatments for final disposal.

7. FUTURE WORK

This section discusses the future work to be done to improve the PA model capability to further represent the processes in the repository, and to enhance the confidence of the feasibility analysis results and conclusions. Although it is believed that the improvements from the proposed future work would not change the conclusions of the current analysis, the improvements are needed to improve the confidence and maturity of the PA model and analysis, and to gather and develop analysis and information that may be required to address associated technical issues and to meet regulatory requirements for transportation and disposal of the ER salt waste.

The proposed future work is grouped in two categories: the near-term work for next FY, and the intermediate (or longer)-term work for next two to four years. The proposed near-term work also includes the key task activities that were identified by the project participants and management, and is summarized in an extended bullet format as follows.

- Detailed scoping analysis for the package design for transportation and disposal in salt repository. The WP configuration used in the PA analysis is highly simplified and preliminary in nature, and was developed for use in this year's feasibility analysis. The scoping design analysis may result in WP design changes, and the PA model will be updated to incorporate the design update.
- Scoping analysis for criticality potential during transportation, interim storage and permanent disposal in salt repository. Because of relatively large contents of fissile materials (especially Pu-239), detailed scoping analysis is needed to address the criticality potential of the salt waste. The criticality potential may impose constraints on the package design for transportation, interim storage and

permanent disposal. The criticality issue may also require some waste stabilization measures such as loading of the waste into the zeolite. The PA model will be updated for these changes.

- Update and improvement of the PA model incorporating new analysis and development. The above activities may result in a different disposal WP design and configuration, which will require the PA model update and additional PA analysis to be consistent with the design update. This year's PA analysis considered the untreated raw salt waste as the waste form. Additional PA analyses will be performed to evaluate effect of alternative waste forms, which may include the baseline ceramic waste form and other candidate waste forms. The PA analysis will also evaluate the concept of microencapsulation of LiCl and RNs in the salt waste, which can be achieved by recycling LiCl and KCl and/or addition of NaCl to the ER salt waste.

The PA model will incorporate the latest improvements of the processes related to salt disposal as they become available. These improvements could include near-field thermal conditions, brine movement, waste package degradation and corrosion product evolution, near-field geochemistry, salt creep, etc.

- ER salt PA incorporating impact of the presence of other primary heat-generating HLW wastes (commercial UNF and DOE HLW glass). This year's PA analysis treated the ER salt WPs independent of the primary heat-generating HLW. Because the ER salt waste will be disposed with the primary HLW, the impact of the HLW needs to be analyzed. The downstream processes that may be impacted include 1) repository layout and footprint, 2) WP and near-field thermal conditions and potentially near-field brine movement, and 3) radionuclide solubilities due potentially to elevated temperatures. The PA model will be updated for the impacted processes and parameters, and additional PA analyses will be conducted with the updates.
- Uncertainty and sensitivity analysis. Uncertainty analysis will be conducted to evaluate effect of important repository parameters on ER salt direct disposal such as brine flows, overpack corrosion products pore volume, salt dissolution rate, etc. Also a series of sensitivity analyses will be performed to analyze effect of important disposal and repository process parameters such as higher salt waste loadings per WP within the criticality constraints. This will impact many downstream processes and parameters, including the WP heat output, WP temperature, overpack corrosion rate, WP failure, etc.

For the intermediate- or longer-term work, the current PA analysis has also identified the following recommendations and/or knowledge gaps to improve the confidence of salt repository performance analysis. Most of the recommended future work require a capability of detailed coupled process model analysis and will be generated from the on-going and/or planned work by other UFD work packages.

- Incorporation of improved process-level analysis for brine flows in generic salt repository (other UFD work packages). The work requires a capability of coupled T-M-H-C processes to model brine flows in 1) disposal rooms, alcoves and access drift seals, 2) interbeds above and below repository, and 3) repository access shaft seals. The work will improve the modeling capability for brine migration and radionuclide transport under the influence of thermal perturbation in generic salt repository environment, and the effect on the engineered barrier and near-field performance and far-field performance.
- RN sorption on steel corrosion products mixed with degrading salt waste. The current PA treats conservatively no sorption of RNs on the materials, however this could be important processes to retard RN transport from the failed WP.

- Incorporation of improved near-field geochemistry for generic salt repository environment (other UFD work packages). The near-field geochemistry of salt repository would be characterized as concentrated brines of high ionic strength in geochemically reducing conditions at elevated temperatures. These conditions could affect potentially significantly the solubility and sorption of RNs in the repository near-field. The current PA conservatively treats no sorption of RNs in the near-field.
- Incorporation of improved analysis for flow and transport in generic regional aquifer (other UFD work packages). The regional hydrology for a generic salt repository may remain highly uncertain as it would be site specific. The current PA uses the hydrologic features of the main regional aquifer of the WIPP.
- Disposal in an alternative salt formation (e.g., domal salt repository like in Germany). Extensive domal salt formations also exist in the U.S., and a feasibility study of the domal salt disposal needs to be performed. The current PA is focused on disposal in a repository in a bedded salt formation. The PA analysis for domal salt disposal may require modifications of some of the repository processes and parameters.

8. REFERENCES

10 CFR Part 63 – Disposal of high-level radioactive wastes in a geologic repository at Yucca Mountain, Nev.

Bornemann, O, et al (2008). *Description of the Gorleben Site Part 3: Results of Geological surface and Underground Exploration of the Gorleben Salt Dome*. Bundesanstalt für Geowissenschaften und Rohstoffe (BGR), Hannover, Germany.

Bradshaw, R. L. and McClain, W. C. (eds.) (1971) *Project Salt Vault: A demonstration of the disposal of high-activity solidified wastes in underground salt mines*. Oak Ridge, TN: Oak Ridge National Laboratory. ORNL 4555.

Bräuer, V, et al (2011). *Description of the Gorleben Site Part 4: Geotechnical Exploration of the Gorleben Salt Dome*. Bundesanstalt für Geowissenschaften und Rohstoffe (BGR), Hannover, Germany.

Brush, L.H., and L.J. Storz 1996. *Revised Ranges and Probability Distributions of Kds for Dissolved Pu, Am, U, Th, and Np in the Culebra for the PA Calculations to Support the WIPP CCA, in US DOE. 1996. Title 40 CFR Part 191 Compliance Certification Application, Appendix MASS, Attachment 15-1. DOE/CAO-1996-2184. Carlsbad, NM: U.S. Department of Energy, Carlsbad Area Office.*

Buhmann, D., et al (2009). *PAMINA Performance Assessment Methodologies in Application to Guide the Development of the Safety Case — Report on the Benchmarks on Rock Salt*. Deliverable (D-N: D4.1.1), PAMINA Sixth Framework Programme, European Commission.

Carter, J.T., F. Hansen, R. Kehrman, and T. Hayes 2011. *A Generic Salt Repository for Disposal of Waste from a Spent Nuclear Fuel Recycle Facility*. SRNL-RP-2011-00149 Rev. 0. Aiken, SC: Savannah River National Laboratory.

D. Clayton, G. Freeze, T. Hadgu, E. Hardin, J. Lee, J. Prouty, R. Rogers, W. M. Nutt, J. Birkholzer, H.H. Liu, L. Zheng, and S. Chu (2011). *Generic Disposal System Modeling—Fiscal Year 2011 Progress Report*, FCRD-USED-2011-000184, Fuel Cycle Research and Development; SAND2011-5828P, Sandia National Laboratories, Albuquerque, NM (August, 2011).

DOE (Department of Energy) 1988. *Site Characterization Plan Deaf Smith county Site, Texas*. DOE/RW-0162. Salt Repository Project Office, Office of Civilian Radioactive Waste Management, January 1988.

Fraldi, M. and Guarracino, F. (2011). “An improved formulation for the assessment of the capacity load of circular rings and cylindrical shells under external pressure. Part 1. Analytical derivation,” *Thin-Walled Structures*, Vol. 49, pp. 1054–1061.

Gilkey, A.P. 2006. *Software Installation and Checkout and Regression Testing Report of NUTS Version 2.05c on the Compaq ES40, ES45 and ES47 Platforms*. ERMS 543789. Carlsbad, NM: Sandia National Laboratories.

GoldSim (GoldSim Technology Group) 2010. *GoldSim User’s Guide* (Version 10.50), and *GoldSim Contaminant Transport Module* (Version 6.0), December 2010.

Gong, S.-F., Ni, X.-Y., Bao, S., and Bai, Y. (2013). “Asymmetric collapse of offshore pipelines under external pressure,” *Ships and Offshore Structures*, Vol. 8, pp. 176-188.

Hadgu, T., Martinez, M., Bean, J., Arguello, J. G., Jové-Colón, C. F. and Hansen, F. (2013). "Thermal-Hydrologic-Mechanical Modeling of a Generic Salt High-Level Radioactive Waste Repository," Proceedings of the 14th International High-Level Radioactive Waste Management Conference, April 28-May 2, 2013, Albuquerque, NM.

Hansen, F.D., and C.D. Leigh 2011. *Salt Disposal of Heat-Generating Nuclear Waste*. SAND2011-0161. Albuquerque, NM: Sandia National Laboratories.

Hardin, E., T. Hadgu, D. Clayton, R. Howard, H. Greenberg, J. Blink, M. Sharma, M. Sutton, J. Carter, M. Dupont, and P. Rodwell (2012). *Repository Reference Disposal Concepts and Thermal Load Management Analysis*. FCRD-USED-2012-000219 Rev. 2, U.S. Department of Energy Office of Used Fuel Disposition, November 2012.

Helton, J.C., J.E. Bean, J.W. Berglund, F.J. Davis, K. Economy, J.W. Garner, J.D. Johnson, R.J. MacKinnon, J. Miller, D.G. O'Brien, J.L. Ramsey, J.D. Schreiber, A. Shinta, L.N. Smith, D.M. Stoelzel, C. Stockman, and P. Vaughn 1998. *Uncertainty and Sensitivity Analysis Results Obtained in the 1996 Performance Assessment for the Waste Isolation Pilot Plant*. SAND98-0365. Albuquerque, NM: Sandia National Laboratories.

IAEA (International Atomic Energy Agency) 2003. *Reference Biospheres for Solid Radioactive Waste Disposal*. IAEA-BIOMASS-6. Vienna, Austria: International Atomic Energy Agency.

Inoue, T. and Koch L. (2008) Development of pyroprocessing and its future direction, *Nuclear Engineering and Technology*, 40(3), 183-190.

Jove-Colon, C. F. et al (2012). *Evaluation of Generic EBS Design Concepts and Process Models: Implications to EBS Design Optimization*, FCRD-USED-2012-000140, SAND2012-5083P, U.S. Department of Energy Office of Used Fuel Disposition, June 2012.

Kara, F., Navarro, J., and Allwood, R. L. (2010). "Effect of thickness variation on collapse pressure of seamless pipes," *Ocean Engineering*, Vol. 37, pp. 998-1006.

King, F. (2007). *Overview of a Carbon Steel Container Corrosion Model for a Deep Geological Repository in Sedimentary Rock*, Report NWMO TR-2007-01, Nuclear Waste Management Organization, Toronto, Ontario, Canada (March 2007).

Klinge, H., et al (2007). *Description of the Gorleben Site Part 1: Hydrology of the Overburden of the Gorleben Salt Dome*. Bundesanstalt für Geowissenschaften und Rohstoffe (BGR), Hannover, Germany.

Köthe, A., et al (2007). *Description of the Gorleben Site Part 2: Geology of the Overburden and Adjoining Rock of the Gorleben Salt Dome*. Bundesanstalt für Geowissenschaften und Rohstoffe (BGR), Hannover, Germany.

Lappin, A.R., R.L. Hunter, D.P. Garber, and P.B. Davies (eds.) 1989. *Systems Analysis, Long-Term Radionuclide Transport, and Dose Assessments, Waste Isolation Pilot Plant (WIPP), Southeastern New Mexico; March 1989*. SAND89-0462. Albuquerque, NM: Sandia National Laboratories.

Lee, J.H. M. Siegel, C. Jove-Colon, and Y. Wang (2011). *A Performance Assessment Model for Generic Repository in Salt Formation*. Proceedings of the 13th International High-Level Radioactive Waste Management Conference (IHLRWMC), April 10-14, 2011, Albuquerque, NM.

Lee, J.H., D. Clayton, C. Jove-Colon, and Y. Wang (2012). *A Preliminary Performance Assessment for Salt Disposal of High-Level Nuclear*. Proceedings of 2012 Waste Management Symposia, Paper # 12173, February 26 – March 1, 2012, Phoenix, AZ.

Lee, J. H., Michael Simpson and Yifeng Wang (2013). “Preliminary Feasibility Analyses for Electrorefining Waste Disposal in Salt Repository,” Presented at the 14th International High-Level Radioactive Waste Management Conference, April 28-May 2, 2013, Albuquerque, NM.

McKinley, I.G., and A. Scholtis 1992. Compilation and comparison of radionuclide sorption databases used in recent performance assessments. Radionuclide Sorption Safety Evaluation Perspectives. *NEA Workshop*, OECD, Paris, France, 21-55.

Miller, A. W. and Wang, Y. (2012). “Radionuclide Interaction with Clays in Dilute and Heavily Compacted Systems: A Critical Review,” *Environmental Science and Technology*, Vol. 46, pp. 1981-1994.

Montana (State of Montana) (2004). *Notice of Water Right*, Form No. 627 R8/03, Montana Department of Natural Resources and Conservation, Water Rights Bureau, Helena, MT 59620-1601.

Muller, A.B., N.C. Finley, and J. Pearson, Jr. 1981. *Geochemical Parameters used in the Bedded Salt Reference Repository Risk Assessment Methodology*. NUREG/CR-1996; SAND0557. Albuquerque, NM: Sandia National Laboratories.

Nemer, M.B. 2007. *Software Installation and Checkout for BRAGFLO, Version 6.0*. ERMS 545019. Carlsbad, NM: Sandia National Laboratories.

Netto, T. A. (2009). “On the effect of narrow and long corrosion defects on the collapse pressure of pipelines,” *Applied Ocean Research*, Vol. 31, pp. 75-81.

Netto, T. A., Ferraz, U.S., and Botto, A. (2007). “On the effect of corrosion defects on the collapse pressure of pipelines,” *International J. of Solids and Structures*, Vol. 44, pp. 7597-7614.

Pepping, R.E., M.S. Chu, and M.D. Siegel 1983. *Technical Assistance for Regulatory 26 Development: Review and Evaluation of the Draft EPA Standard 40CFR191 for Disposal of High-Level Waste, Volume 4: A Simplified Analysis of a Hypothetical Repository in a Bedded Salt Formation*. NUREG/CR-3235. Albuquerque, NM: Sandia National Laboratories.

Roselle, G. (2013). “Anoxic Corrosion of Steel and Lead in Na-Cl±Mg Dominated Brines,” Proceedings of the 14th International High-Level Radioactive Waste Management Conference, April 28-May 2, 2013, Albuquerque, NM.

Rothfuchs, T., Bollingerfehr, W., and Bechthold, W. (2004). *Lessons Learned from Large-Scale Experiments at the Asse Mine Germany*, Proceedings of the EURADWASTE '04: Sixth European Commission Conference on Management and Disposal of Radioactive Waste, March 29 – April 1, 2004, Luxembourg.

Rübel, A., et al (2009). *PAMINA Performance Assessment Methodologies in Application to Guide the Development of the Safety Case — PA Approaches Based on Different Geometric Complexity of Modeling for the Far-Field of a Repository in Salt*. Deliverable (D-N: D4.2.1), PAMINA Sixth Framework Programme, European Commission.

Sakakibara, N, Kyriakides, S. and Corona, E. (2008). "Collapse of partially corroded or worn pipe under external pressure," *International J. of Mechanical Sciences*, Vol. 50, pp. 1586-1597.

Sevougian, S. D., G. A. Freeze, M. B. Gross, J. Lee, C. D. Leigh, P. Mariner, R. J. MacKinnon, and P. Vaughn (2012). *TSPA Model Development and Sensitivity Analysis of Processes Affecting Performance of a Salt Repository for Disposal of Heat-Generating Nuclear Waste*. FCRD-USED-2012-000320 Rev. 0, U.S. Department of Energy Office of Used Fuel Disposition, September 2012.

Simpson, M. F. and Law J. D. (2010) *Nuclear Fuel Reprocessing*, INL/EXT-10-17753, Idaho National Laboratory, Idaho Falls, ID.

Simpson, M.F., M.N. Patterson, J. Lee, Y. Wang, J. Versey, and S. Phongikaroon (2013). "Management of Salt Waste from Electrochemical Processing of Used Nuclear Fuel," Proceedings of Global 2013: International Nuclear Fuel Cycle Conference, September 29-October 3, 2013, Salt Lake City, UT.

Smart, N. R., Blackwood, D. J. and Werme, L. (2002a). "Anaerobic corrosion of carbon steel and cast iron in artificial groundwaters: Part 1—electrochemical aspects," *Corrosion*, Vol. 58, pp. 547-559.

Smart, N. R., Blackwood, D. J. and Werme, L. (2002b). "Anaerobic corrosion of carbon steel and cast iron in artificial groundwaters: Part 2—Gas Generation," *Corrosion*, Vol. 58, pp. 627-637.

Telander, M. R. and Westerman, R. E. (1993) *Hydrogen generation by metal corrosion in simulated Waste Isolation Pilot Plant environments*. SAND92-7347, Albuquerque, NM: Sandia National Laboratories (July 1993).

Tien, P.L., F. Nimick, A. Muller, P. Davis, R. Guzowski, L. Duda, and R. Hunter 1983. *Repository Site Data and Information in Bedded Salt: Palo Duro Basin, Texas*. NUREG/CR-3129, SAND82-2223. Albuquerque, NM: Sandia National Laboratories.

Vaughn, P., G. Freeze, J. Lee, S. Chu, K.D. Huff, W.M. Nutt, T. Hadgu, R. Rogers, J. Prouty, E. Hardin, B. Arnold, E. Kalinina, W.P. Gardner, M. Bianchi, H.H. Liu, J. Birkholzer (2012). *Generic Disposal System Model: Architecture, Implementation, and Demonstration*, FCRD-USED-2012-000430, Fuel Cycle Research and Development; SAND2013-1539P, Sandia National Laboratories, Albuquerque, NM (November, 2012).

Wang, Y. and Lee, J. (2010). *Natural System Evaluation and Tool Development – FY10 Progress Report*, Report FCRD-UFD-2010-XXXXXX, Fuel Cycle Research and Development, DOE-NE Used Fuel Disposition, August 2010.

Wang, Y., M. Simpson, J. Rath, F. Hansen, J.H. Lee, C. Jove-Colon, K. McMahon, and P. Swift (2011a). *Closing the Nuclear Fuel Cycle with Salt*, Proceedings of the 13th International High-Level Radioactive Waste Management Conference (IHLRWMC), April 10-14, 2011, Albuquerque, NM.

Wang, Y., Simpson, M., Painter, S., Liu, H. H., and Annie B. Kersting, A. B. (2011b). *Natural System Evaluation and Tool Development – FY11 Progress Report*, FCRD-USED-2011-000223, Fuel Cycle Research and Development (July 15, 2011).

Wang, Y., A. Miller., H. Tellez, Y. Xiong, M. Simpson, and M. Shaltry (2012). *Feasibility Study of Direct Disposal of Electrorefining (ER) Salt Waste in a Salt Repository: Laboratory Tests*, FCRD-UFD-2012-000339, Fuel Cycle Research and Development.

Westerman, R. E., Nelson, J. L., Pitman, S. G., Kuhn, W. L., Basham, S. J. and Moak, D. P. (1984). "Evaluation of iron-base materials for waste package containers in a salt repository," *Scientific Basis for Nuclear Waste Management Symposium*, Vol. 26, Materials Research Society Proceedings, pp. 427-436.

Westerman, R. E. and Pitman, S. G. (1985). "Corrosion of Candidate Iron-Base Waste Package Structural Barrier Materials in Moist Salt Environments," *Scientific Basis for Nuclear Waste Management Symposium*, Vol. 44, Materials Research Society Proceedings, pp. 279-285.

Westerman, R. E., Haberman, J. H., Pitman, S. G., Pool, K. H., Rhoads, K. C. and Telander, M. R. (1988). *Salt repository project. Annual report—FY 1986. Corrosion behavior of A216 grade WCA mild steel and titanium grade 12 alloy in hydrothermal brines*. PNL/SRP-6221, Richland, WA: Pacific Northwest National Laboratory.

Wolery, T.W., and R.L. Jarek (2003). *EQ3/6, Version 8.0, Software User's Manual*. Las Vegas, NV: U.S. Department of Energy, Office of Civilian Radioactive Waste Management, Office of Repository Development.

Yeh, M. K. and Kyriakides, S. (1986). "On the Collapse of Inelastic Thick-Walled Tubes under External-Pressure," *Journal of Energy Resources Technology*, Vol. 108. Pp. 35-47.